December 2013

The Effectiveness of Silane and Siloxane Treatments on the Superhydrophobicity and Icephobicity of Concrete Surfaces

Sunil M. Rao
University of Wisconsin-Milwaukee

THE EFFECTIVENESS OF SILANE AND SILOXANE TREATMENTS ON THE SUPERHYDROPHOBICITY AND ICEPHOBICITY OF CONCRETE SURFACES

by

Sunil M. Rao

A Thesis Submitted in

Partial Fulfillment of the

Requirements for the Degree of

Master of Science

in Engineering

at

The University of Wisconsin-Milwaukee

December 2013

ABSTRACT

THE EFFECTIVENESS OF SILANE AND SILOXANE TREATMENTS ON THE SUPERHYDROPHOBICITY AND ICEPHOBICITY OF CONCRETE SURFACES

by

Sunil M. Rao

The University of Wisconsin-Milwaukee, 2013
Under the Supervision of Professor Konstantin Sobolev

Icy roads lead to treacherous driving conditions in regions of the U.S., leading to over 450 fatalities per year. De-icing chemicals, such as road salt, leave much to be desired. In this report, commercially available silane, siloxane, and related materials were evaluated as solutions, simple emulsions, and complex emulsions with incorporated particulates, for their effectiveness as superhydrophobic treatments. Through the development and use of a basic impact test, the ease of ice removal (icephobicity) was examined as an application of the targeted superhydrophobicity.

A general correlation was found between icephobicity and hydrophobicity, with the amount of ice removed on impact increasing with increasing contact angle. However,

the correlation was poor in the high performance region (high contact angle and high ice removal.)

Polymethylhydrogensiloxane was a top performer and was more effective when used as a “shell” type emulsion with silica fume particulates. An aqueous sodium methyl siliconate solution showed good performance for ice loss and contact angle, as did a commercial proprietary emulsion using a diethoxyoctylsilyl trimethylsilyl ester of silicic acid. These materials have sterically available functional groups that can react or associate with the concrete surface and are potentially film-forming. Materials with less reactive functional groups and a lower propensity to film-form did not perform as well.

TABLE OF CONTENTS

LIST OF FIGURES

LIST OF TABLES

LIST OF ABBREVIATIONS

ASTM	American Society for Testing and Materials
CMA	calcium magnesium acetate
DI	deionized
Et	ethyl
FHWA	Federal Highway Administration
GPa	giga Pascal
HDPE	high density polyethylene
IPA	isopropyl alcohol
KAc	potassium acetate
kPa	kilo Pascal
Me	methyl
MN	micro/nanostructured
MPa	mega Pascal
NCHRP	National Cooperative Highway Research Program

Pa	Pascal
PC	Portland cement
PCE/SP	polycarboxylate ether superplasticizer
PDMS	polydimethylsiloxane
PECVD	plasma enhanced chemical vapor deposition
PEHSO	polyethylhydrogensiloxane
PFC	polyfluorocarbon
PMHS	polymethylhydrogensiloxane
PTFE	polytetrafluoroethylene
PPE	personal protective equipment
PVA	polyvinyl alcohol
RPM	revolutions per minute
s/c	sand to cementitious material ratio
SADTE	silicic acid, diethoxyoctylsilyl trimethylsilyl ester
SAM	self-assembled monolayer

SEM	scanning electron microscope
SF	silica fume
SHRP	Strategic Highway Research Program
SMS	sodium methyl siliconate
SP	superplasticizer
Tg	glass transition temperature
VOC	volatile organic compound
w/c	water to cementitious material ratio
XRD	x-ray diffraction
µl	microliter

ACKNOWLEDGMENTS

I would like to thank Dr. Konstantin Sobolev for sharing his premise, for presenting me with the topic, for inviting me into his group, and for all the guidance, time, and interesting discussions. Dr. Ismael Flores-Vivian provided a great deal of guidance, time, and support, especially with respect to emulsion production and tile treatment - thanks Ismael! And many thanks to Dr. Michael Nosonovsky, Dr. Ben Church, and Dr. Hugo Lopez for being part of my defense committee and for the help, guidance, and instruction in the past few years.

I would also like to thank Marina Kozhukhova for all her emulsion and tile work; our projects ran in parallel and I could not have finished in a reasonable time without her help. Many thanks also to Reza Moini for help with the tile production, Scott Muzenski for his experience, tips and work on the CFIRE report, Brandon Bosch for help with the literature review, and to Dr. Steven Hardcastle for the AAF related instruction and help.

And a special thanks to my wife, Maribeth, for her support and for putting up this preoccupation.

1 Introduction

Adequate road conditions are vital for the performance of transportation infrastructure. There are on average 467 fatalities per year due to icy road conditions in the U.S. [1]. Even more injuries and substantial property losses occur each year as a result of primary and/or secondary effects from loss of vehicle control on ice. Figure 1 shows the number of fatalities by state and the icy road risk zones based on the 2009-2010 data [1][2]. The moderate and high risk zones primarily cover the Midwest and extend into Texas and Oklahoma.

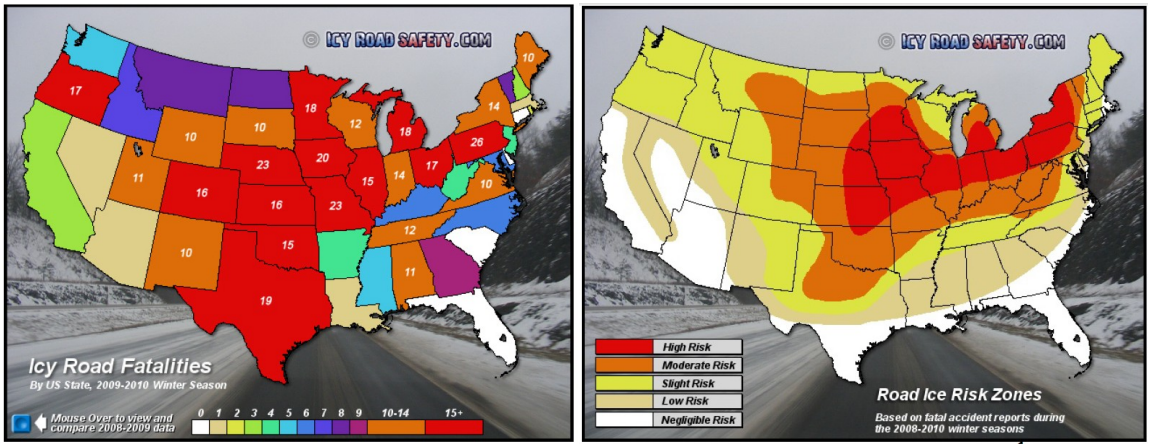

Figure 1 Number of US fatalities due to icy roads and risk zones (2009-2010 data) [1].

According to storm chaser Dan Robinson, the road ice hazard is defined by the conditions and situations where icing has the highest impact on life and property [1]. These factors are high-speed travel (above 45 mph, interstates, rural 2-lanes); the element of surprise (including bridges); subtle and intermittent icing (not visibly prominent); light winter precipitation (snow and freezing rain); and freezing rain, drizzle, and fog (invisible ice, Figure 2, left). In essence, the road ice hazard is primarily

highway-speed travel during light winter precipitation events, when driver awareness is low and visual indicators are few.

The majority of deaths and serious injuries occur during these conditions; however, the most accidents occur in the following critical areas [1]:

- Bridges, overpasses and elevated roadways (Figure 2, right)
- Steep hills
- High speed roadways
- Curves
- Deceleration spots
- Acceleration spots
- Low-traffic roads
- Trouble spots include highway exit ramps, driveways, parking lots, and rural roads
- Tunnels
- Cobblestone and brick pavement

Figure 2 Invisible "black ice" on a bridge (left) and crash due to icy bridge (right) [1].

In order to diminish the road ice hazard, different strategies have been used on roadways to remove snow and ice. The National Cooperative Highway Research Program (NCHRP) publishes the guidelines for materials and methods for their applications. The methods are classified as: a) anti-icing, b) deicing, c) mechanical removal of snow and ice together with friction enhancement, and d) mechanical removal [3]. These strategies involve the application of chemicals on roadways and the use of mechanical means to remove excessive snow accumulations.

Ketcham *et. al.* (1996), published recommendations for successful anti-icing practices for various combinations of precipitation, pavement temperature, traffic volumes, and mandated levels of service [4]. The guidance is based upon the results of 4 years of anti-icing field testing conducted by 15 State highway agencies and supported by the Strategic Highway Research Program (SHRP) and the Federal Highway Administration (FHWA). Recommended anti-icing practices were made for different anti-icing treatments based on the following chemicals: sodium chloride (NaCl), magnesium

chloride ($MgCl_2$), calcium chloride ($CaCl_2$), calcium magnesium acetate (CMA), and potassium acetate (KAc).

Eli Cuelho *et. al.* (2010), reported on commonly available anti-icing chemicals applied on concrete and asphalt pavements at four application rates and under three temperature scenarios [5]. Sodium chloride, magnesium chloride, calcium chloride, potassium acetate, and a chemical made from agricultural by-products were tested. Results from an ice adhesion test (Figure 3) demonstrated that the use of anti-icing chemicals reduced the bond strength and the temperature at which the bond between the snow and the pavement failed. Field tests demonstrated improvements in performance for most chemicals through the reduction or elimination of the snow–pavement bond. It was concluded that effective anti-icing chemicals can provide safe driving conditions during winter maintenance, reducing costs as well as impacts on the environment and infrastructure.

Storm Scenarios	Initial Conditions		
	Pavement Temperature °F (°C)	Snow Temperature °F (°C)	Air Temperature °F (°C)
I (P14–SA14)*	14 (-10)	14 (-10)	14 (-10)
II (P32–SA23)*	32 (0)	23 (-5)	23 (-5)
III (P32–SA30)*	32 (0)	30 (-1)	30 (-1)

*P = Pavement temperature and SA = snow and air temperature in degrees Fahrenheit

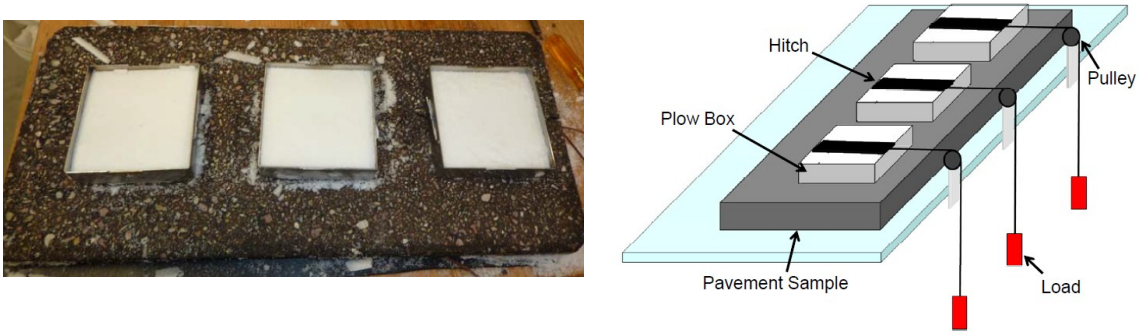

Figure 3 Test temperatures (top left), sample for shearing test (bottom left), and set up sketch for the shearing test (right) [5]

Most of these strategies rely on chemicals which act as a coat on the pavement surface (anti-icing) to prevent or to break the bond between snow or ice and the pavement surface (deicing). Ketcham *et. al.* (1996), present a table used to recommend the eutectic temperatures and concentrations of applicability of different anti-icing materials [4]. Due to temperature changes, traffic load, and pavement maintenance operations, these chemicals dissolve and disperse into the nature. Wisconsin Transportation Bulletin reported some cases where ground waters with deicing chemicals were found in wells used as drinking water sources [6]. These chemicals may cause deterioration in concrete and steel structures, as well as accelerate vehicle corrosion. Despite all these disadvantages, chemicals used to reduce the road ice hazard are in widespread use.

Table 1 Eutectic temperatures and concentrations [4]

Chemical	Eutectic temperature °C (°F)	Eutectic concentration %
calcium chloride ($CaCl_2$)	-51 (-60)	29.8
sodium chloride (NaCl)	-21 (-5.8)	23.3
magnesium chloride ($MgCl_2$)	-33 (-28)	21.6
calcium magnesium acetate (CMA)	-27.5 (-17.5)	32.5
potassium acetate (KAc)	-60 (-76)	49

Anti-icing materials with a physical or chemical bond to the pavement surface are more desirable than materials currently in use. Chemically attached anti-icing materials can have a higher durability at relatively small amounts of material use. In this respect, hydrophobic and superhydrophobic coatings are promising.

In this report, commercially available silanes, siloxanes, and related materials that would bond to concrete were evaluated as potential superhydrophobic treatments that would impart icephobic properties. Coating treatments were assessed as solutions, simple emulsions, and complex emulsions that incorporated the use of particulates.

In this and future work, the development of these coatings requires the evaluation of candidate components on a variety of substrates with differing surface morphologies. Considering the numerous combinations that may be of interest, a testing method that enables practical evaluation of multiple samples is desirable. To that end, a basic impact test for ice removal was developed.

The influence of surface roughness was considered by using different sanding grits for surface preparation. In addition, evaluations were performed on ten mortar mixes,

which included shifts in fiber, sand, and porosity (via w/c ratio), along with treatment particulates that allowed for roughness hierarchy contributions.

The concept was driven by the premise and work of Dr. Konstantin Sobolev on rendering concrete superhydrophobic, on both the exterior and the interior, using hydrophobic agents and particulates that impart roughness to the surface, and formulating superhydrophobic systems that function throughout the matrix. This premise considers the wear on road surfaces due to typical use. With the appropriate surface treatment and particulate profile within the concrete itself, a road can be made superhydrophobic. As the road surface wears, the coating deteriorates and a new surface from within the concrete is exposed, revealing new particulates (for roughness) from the interior. Periodic reapplication of the superhydrophobic surface treatment along with the steady exposure of the interior particulate matrix (that can include various particulates and fibers) can maintain the desired water-repellant and potentially icephobic properties.

2 Background and literature review

2.1 Portland cement

The typical composition of Portland cement (as received powder) is shown in Table 2. There are a number of hydration products and reactions, but an approximation for the calcium silicate hydration reactions is shown in Figure 4 [7]. Concrete chemists' notation is shown in both.

Table 2 a) Concrete chemists' abbreviations b) Typical composition of Portland cement. Adapted from K. Sobolev [7]

a)	
Compound	**Concrete chemist abbreviation**
CaO	C
SiO_2	S
Al_2O_3	A
Fe_2O_3	F
H_2O	H

b)		
Concrete chemist notation	**Compound**	**Example composition**
C_3S	Dicalcium silicate $(CaO)_2 \cdot SiO_2$	55%
C_2S	Tricalcium silicate $(CaO)_3 \cdot SiO_2$	20%
C_3A	Tricalcium aluminate $(CaO)_3 \cdot Al_2O_3$	10%
C_4AF	Tetracalcium aluminoferrite $(CaO)_4 \cdot Al_2O_3 \cdot Fe_2O_3$	8%
$CaSO_4 \cdot 2H_20$	Gypsum $CaSO_4 \cdot 2\,H_2O$	5%

$$0.75(CaO)_3 \cdot SiO_2 + 0.25\,(CaO)_2 \cdot SiO_2 + 10.5\,H_20 = (CaO)_3(SiO_2)_2(H_20)_8\ (apprx) + 2.5\,Ca(OH)_2 \quad \textbf{(a)}$$

$$0.75\,C_3S + 0.25\,C_2S + 10.5\,H = C_3S_2H_8\ (apprx) + 2.5\,CH \quad \textbf{(b)}$$

$$\text{calcium silicates } (C_3S + C_2S) + \text{water} = \text{calcium silicates hydrates} + \text{calcium hydroxide} \quad \textbf{(c)}$$

Figure 4 An approximation for the hydration reaction of Portland cement, a) in standard chemical notation, b) in concrete chemists' notation, c) in written form. Adapted from K. Sobolev [7]

Considering the surface of silica alone, by the late 1940's, using infrared spectroscopy, it had been shown to be hydroxylated [8][9][10][11]; a depiction is presented in Figure 5.

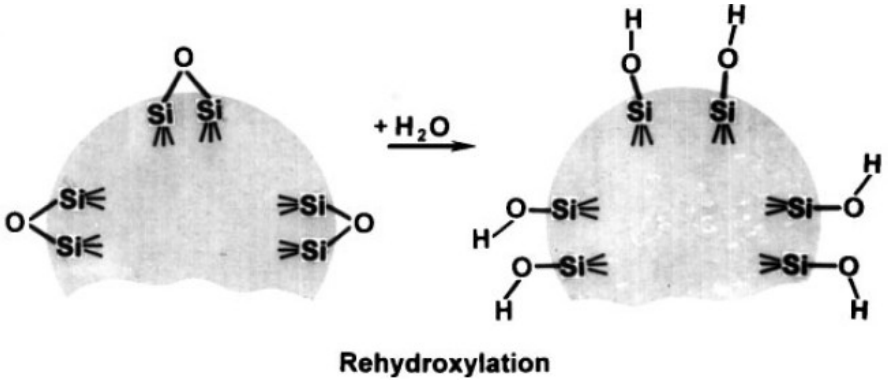

Figure 5 Hydroxylated silica surface [8]

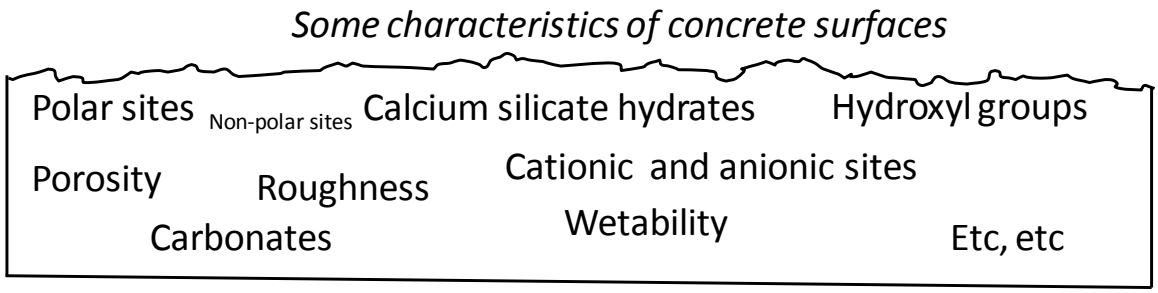

Figure 6 Considerations pertaining to concrete surfaces

2.2 Developing hydrophobic and superhydrophobic properties

The hydrophobicity of a material is defined as the ability of the material to repel water and depends on the surface chemical composition and the surface geometry (micro and nanostructural morphology) [12]. The contact angle between a drop of water and the surface is generally used as an indicator of hydrophobicity or wetability. When the contact angle is greater than 90°, it indicates hydrophobicity, while a contact angle less than 90° denotes hydrophilicity, which is the tendency of a surface to become wet or to absorb water, as shown in Figure 7. Common concrete is an example of a hydrophilic

mesoporous material which absorbs water. Superhydrophobicity corresponds to a contact angle between 150° and 180°. Surfaces with intermediate properties, with high contact angles between 120° and 150°, above typical values for hydrophobic materials, are called “overhydrophobic.” The water contact angle with a solid surface can be measured by goniometer or tensiometer [13].

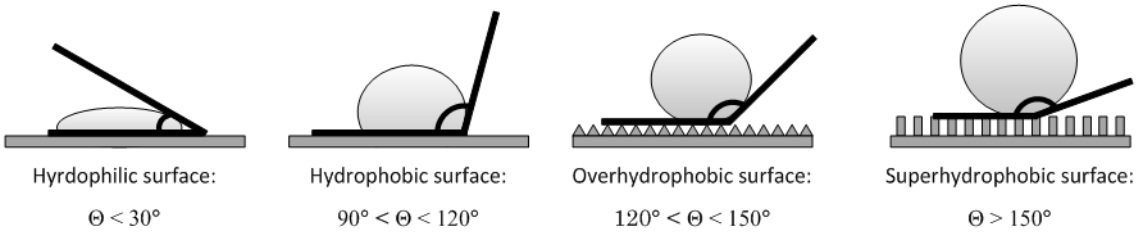

Figure 7 Hydrophillic, hydrophobic, overhydrophobic, superhydrophobic surfaces [14]

Superhydrophobic hierarchical surfaces with hierarchical roughness patterns (Figure 8) imposed over larger roughness patterns have generated interest due to their potential in industrial applications (mainly, for self-cleaning).

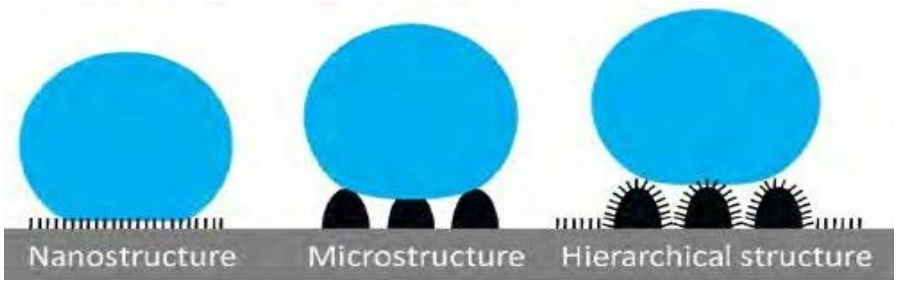

Figure 8 Surface morphologhies [15]

These surfaces mimic the Lotus leaf surface, which is well known for its superhydrophobicity and self-cleaning properties, (Lotus-effect). Mimicking living nature

for engineering applications is called “biomimetics,” and biomimetic approaches can be used to synthesize hydrophobic and superhydrophobic concrete [16][17][18][19][20].

2.2.1 Hydrophobic treatment of concrete based materials

Waterproofing and the incorporation of hydrophobic additives into the concrete matrix are two approaches used to improve the physical properties of concrete. The first approach consists of using hydrophobic materials on the surface of concrete to repel water [21], which also improves the freeze thaw durability of concrete. The type of material and quantity used affects its concrete protecting efficiency [22]. The second approach consists of creating a hydrophobic concrete or cement matrix using admixtures [17][23][24][25]. The addition of an admixture of a hydrophobic nature into the concrete mix is a viable option to achieve a good quality concrete.

2.2.2 Surface waterproofing treatments

Many admixture companies (e.g., Wacker, Kryton, Xypex) offer ready to use products for the surface waterproofing or sealing of concrete as protection against corrosion on reinforcing steel, cracking, frost damage, salt damage, lime leaching, fungal, moss, and stains, etc. [26]. Most of these products, and those found in the literature, are based on silanes and siloxanes, along with some variations, such as sodium silicate, silicone resin solution, silane/siloxane, silane/siloxane with an acrylic topcoat, alkylalkoxysilane, two component acrylics, silicone in turpentine, siloxane acrylic, thixotropic cream (based on octyltriethoxysilane), water based solutions of alkylalkoxysilane, and acrylic latex.

In contrast to other hydrophobic materials, such as epoxy and acrylic based treatments, silanes and siloxanes have smaller molecular sizes, which allow them to reach smaller pores, resulting in more effective surface treatments. Silane compounds are based on the silane structure (shown in Figure 9a). Figure 9b shows the general structure of silane derivatives, where R represents an alkyl, aryl, or other organofunctional group and OR' generally represents an alkoxy functional group, but can be a hydroxyl group (OH) or a salt, (ONa). Silane derivatives differ from siloxanes in their molecular size, with the latter generally being polymers or larger molecules with several silicon atoms (Figure 10.) Along with their smaller sizes relative to epoxies and acrylics, the silanes and siloxanes of interest have alkoxyl groups that can chemically bond to hydrated silicates, leaving a concrete surface modified with hydrophobic alkyl groups, as depicted in Figure 11 [27]. In addition to their hydrophobic effect, these substances reduce the bond between the ice and concrete [28].

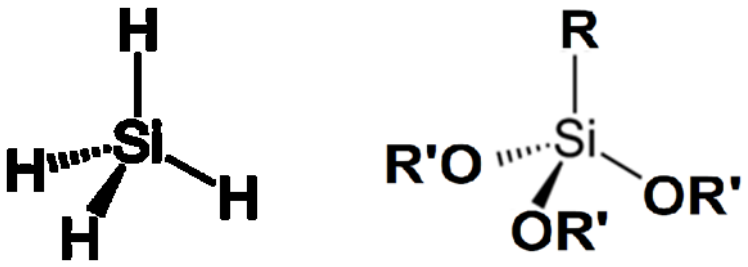

a) b)

Figure 9 a) silane b) the general structure of silane derivatives (R' = alkane or H)

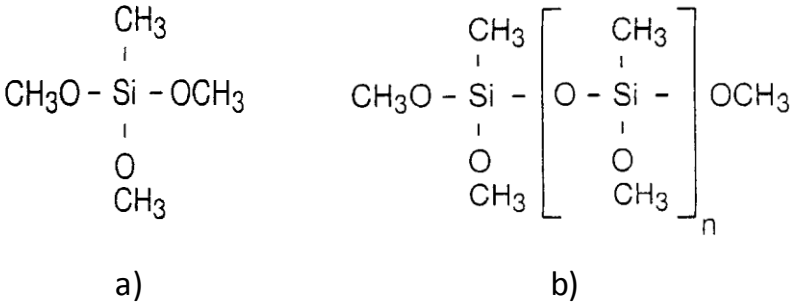

Figure 10 The chemical composition of (a) silane type methytrimethoxysilane and (b) siloxane type polymethylmethoxysiloxane [27] [29]

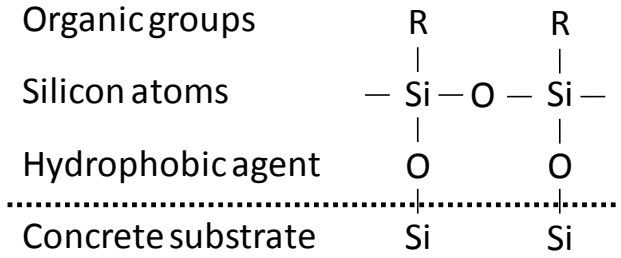

Figure 11 The nature of chemical bond of silane/siloxane to concrete substrate (based on De Vries and Polder [27])

The effectiveness of these materials depends on their molecular compositions along with their penetration depths into concrete, their resistance to adverse environments, and the ability of their chemical composition to limit the penetration of damaging species such as chloride ions and carbon dioxide into the material. Some simplified representations of coating/treatment morphology are shown in Figure 12; note that they that do not depict porous effects.

In *Modified Concrete Theory and Practice, 2nd Edition revised and expanded*, Batrakov presented some possible orientations for bonded and polymerized silane and siloxane

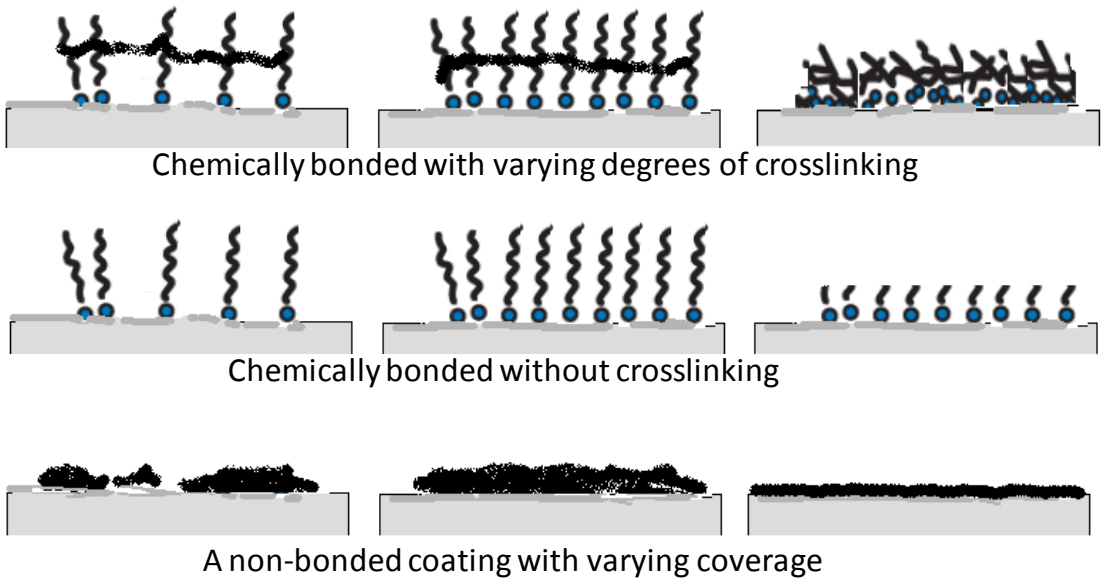

Figure 12 A simplified conceptual morphology of coatings

based materials on concrete (Figure 13) [29]. A furthering of the hydrophobic chemical effects by exploiting surface roughness with the incorporation of particulates was depicted by Flores-Vivian, et al (Figure 14) [14].

Silanes and siloxanes are generally not soluble in water. Dow Corning suggests using isopropanol as a solvent for a number of the silane chemistries [30]. Commercial products generally use volatile organic compounds (VOCs). For example, Rust-Oleum's Neverwet™ base coat contains aliphatic hydrocarbons, n-butyl acetate, methyl isobutyl ketone, methyl acetate, and ethyl acetate[31]. However, Cabot® Waterproofing Crystal Clear #1000, a silicone treatment for concrete, masonry, and wood, is essentially a waterbased silicone emulsion with a relatively low VOC content of 100 grams per liter

[32], or approximately 10% by weight. Zero VOC, minimized odor, cost effective materials would be preferred for treatment of large public areas, such as roads. Flores-Vivian et al, used siloxane emulsions, with and without particulates, as non-VOC coatings for concrete [14] [33] [34][35]. Figure 15 schematically depicts these emulsions.

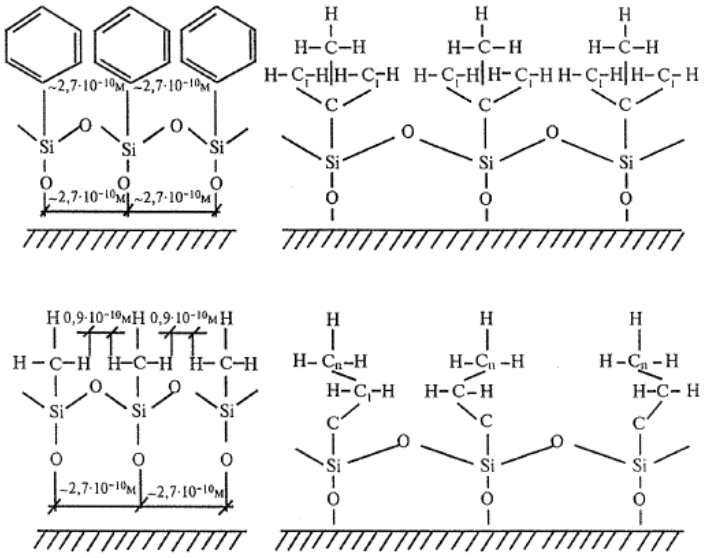

Figure 13 Silane/siloxane bonding to concrete from Batrakov [29]

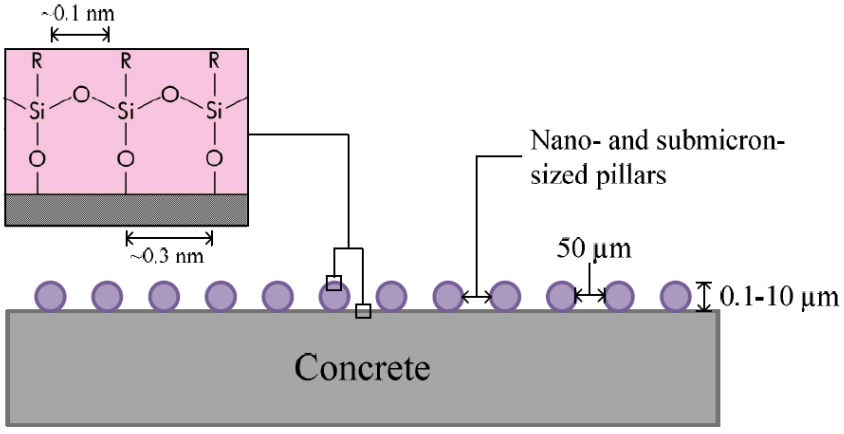

Figure 14 Hydrophobic siloxane bonding to concrete with added particulate roughness [14]

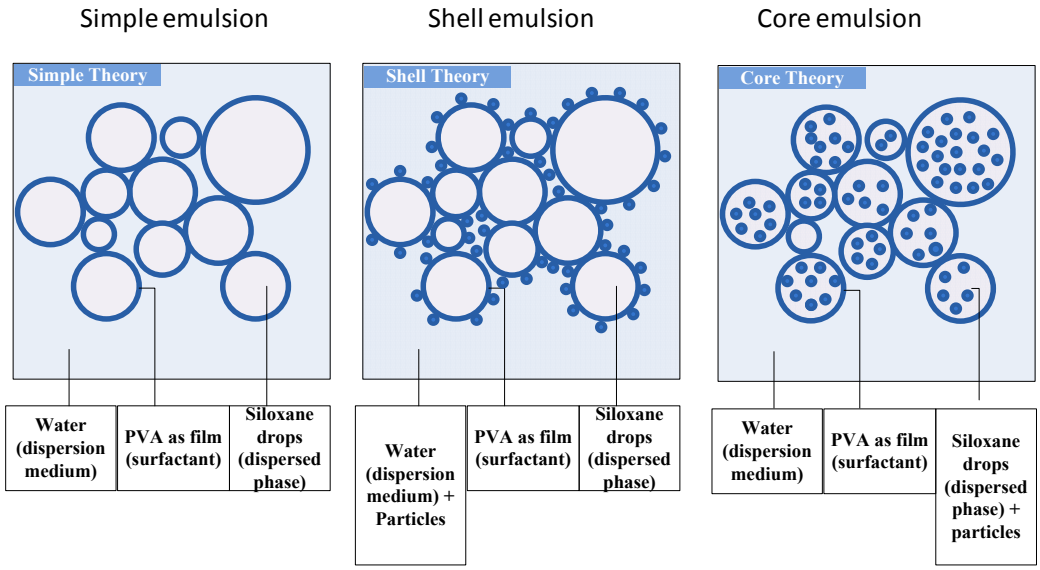

Figure 15 Emulsion types [34]

2.2.3 Evaluating the effectiveness of hydrophobic surface treatments

Basheer et al. (1997) presented a comprehensive list of the methods used to assess the efficiency of different surface treatments for water and ion penetration into concrete [36]. The tests generally assessed transport processes in treated substrates in terms of water vapor permeability diffusion (breathability) and water absorption. The resistance offered by the hydrophobic surface to water penetration can be measured by exposing the treated surface to water after sealing the other surfaces, or by submerging the entire sample in water, and measuring the change in weight of the samples over a specific amount of time. The National Cooperative Highway Research Program (NCHRP) report 244, recommends that, to be accepted, any surface treatment should reduce water intake at least by 75% compared to untreated surfaces [37]. However, highly porous materials, such as concrete and masonry, were not considered in this report. The

German Committee for Reinforced Concrete considered porous materials and recommended a limit for water absorption of 2.5% by mass and a reduction of 50% compared to untreated surfaces[38].

The most effective coating chemicals were found to be some epoxies, along with silane and siloxane based materials. Basher et al., (1997) also reported the effectiveness of a second coat and the use of undiluted silane materials [36]. Xiaojian (2011) reported on the effect of silane surface treatment on water absorption [28]. Silane treated specimens absorbed water quicker in the first hour, but over time the percent of water adsorption tended to stabilize, while for non-treated concrete the adsorption continued. Air-entrained samples demonstrated higher water adsorption than non-air-entrained. Also reported was that high strength concrete and surface treated concrete withstood freeze and thaw cycling better than their lower strength and untreated counterparts.

An important and practical application of surface hydrophobicity, reported by Ibrahim and Al-Gahtani (1999), pertained to the effects of surface treatments on the degradation of reinforcing steel when exposed to detrimental conditions [39]. The effects of chloride-induced corrosion, carbonation, and sulfate attack were studied by measuring the reduction in compressive strength of concrete specimens (w/c = 0.45) protected by 6 different surface treatments: sodium silicate, silicon resin solution, silane/siloxane, silane/siloxane with an acrylic topcoat, alkylalkoxy silane, and a two component acrylic coating. These sealers were not able to prevent sulfate attack, carbonation or chloride ingress. However, they did reduce the chloride concentration in

specimens exposed to chloride solutions for 3 months and reduce the carbonation depths after 5 weeks of exposure compared to uncoated or untreated concrete. After 330 days of immersion in sulfate solution, the specimens had a lower reduction in compressive strength than uncoated specimens. The most effective chemicals were the combinations of silane and siloxane with an acrylic topcoat.

The fact that hydrophobic treatments do not completely protect concrete may be explained by the work of Tittarelli, et al., (2000) related to oxygen diffusion through hydrophobic matrices [40]. The oxygen reduction current under at a steady potential was measured on samples of a steel plate reinforced concrete with w/c of 0.45 and 0.8 and coated with a siloxane based commercial product. The current level was proportional to the presence of oxygen in the matrix. After casting, all the specimens demonstrated a high content of oxygen which probably lodged in the air voids. However, when non-hydrophobic specimens were immersed in water, the current dropped as a result of the decrease of oxygen diffusion into the matrix. The presence of water in the voids blocked the diffusion of oxygen into the concrete. In contrast, for hydrophobic concrete, the lack of water in the voids allowed a continuous supply of oxygen. This research also reported the correlation between the tests on mortars and concrete. At the same w/c, the diffusion of oxygen is higher in concrete than in mortars, probably due to the porous interfacial zone between the aggregate and cement paste.

2.2.4 Hydrophobic admixture treatments

Hydrophobic admixtures added during cement milling have been used to preserve the powdered cement from humidity in the environment. The addition of these chemicals to stored cement prevents early hydration. However, the hydrophobic protection fades during the concrete mixing process (Popovics, 1982); consequently, this type of hydrophobic admixture is not designed to protect concrete from freezing and thawing [23].

The type of hydrophobic admixtures that may affect the freeze-thaw resistance of concrete would have to be incorporated into the fresh mix. The chemicals reported to add hydrophobicity to bulk of concrete include mineral oil, vegetable oil, paraffin waxes, calcium stearate, hydroxynaphthenic acids, sucrose mono-palmitate, sucrose distearate, zinc stearate, silicon sucrose trioleate, hydrocarbon resins and bitumen [24][25], aqueous emulsions of alkyltriethoxysilane [41], and an aqueous emulsion of butylethoxysilane [40]. The complete classification of silico-organic compounds used for concrete hydrophobization was proposed by Batrakov, (1990) [29]. Most of these chemicals have some negative effects on concrete mix, e.g.,oleates affect the monosulfate reaction, stearates decrease the setting time of cement pastes, acids may alter the pH of concrete, and almost all were reported to lower the compressive strength of concrete or mortars. Only samples containing corn oil at relatively low dosages, 0.25% by weight of cement added to mortar as an emulsion, demonstrated higher values of compressive strength than the control samples [24].

Tests performed on mortars with a water-to-cement ratio of 0.3 and incorporating corn oil and stearic acids at different dosages, indicate that these hydrophobic admixtures act as retardants and also act as densifying agents by reducing porosity (initial and long-term). These samples were also soak-tested for water absorption at different curing ages. All mortars with hydrophobic agents yielded reduced water absorption compared to reference samples [24][25].

Tittarelli et al. (2000) reported on the effects of hydrophobic concrete on the corrosion of steel in the presence or absence of cracks in concrete [40]. Specimens with water-to-cement ratios of 0.45 and 0.8 were immersed in a sodium chloride solution, examined visually, and tested for electrochemical potentials and weight loss. It was concluded that the use of silane blocks the corrosion process in uncracked concrete, but worsens the damage in cracked concrete.

Sobolev and Batrakov (2007) reported that concrete's resistance to freezing and thawing was improved by the application of siloxane-based emulsion used as an admixture [17]. The high reactivity of the siloxane (polyethylhydrogensiloxane, PEHSO) is due to the large number of (-Si-H) sites that react with the hydroxyl groups of cement (or portlandite), resulting in the generation of hydrogen and formation of a stable hydrophobic pore structure. The use of the emulsion at 0.065% in the concrete mix creates up to 2-3% of hydrogen formed within the volume (while air-entraining agents are commonly used at 0.1-0.5% to create 5% of air voids, according to specifications). The size of the pores within the paste can be manipulated by varying the droplet size of

the siloxane in the emulsion. Optimal performance in concrete can be achieved when more than 70% of the droplets are less than 1 micron. The emulsion used contained 50% siloxane and a polyvinyl alcohol emulsifying agent. It was mentioned that the hydrogen released caused a slight expansion of the concrete during the first hours of hydration due to internal pressures of up to 0.05 MPa.

2.3 Developing icephobic properties

Icephobicity investigations have been extensive for metallic, ceramic, and polymeric materials but have been limited with respect to concrete [42]. For these materials icephobic coatings are commonly used to help prevent ice formation. It has been demonstrated that superhydrophobic coatings have a limited ability to prevent ice formation on metallic surfaces thus leading to an interest in examining concrete icephobicity, coating chemicals, and testing methodology.

2.3.1 Chemical composition of treatments

Coatings and solutions consisting of a wide range of micro/nano materials with different surface chemistries and topographies have been tested for icephobicity. They can be divided into four categories; low surface energy coatings, heterogeneous and composite coatings, superhydrophobic and porous materials, and use of other methods [43].

Low surface energy coatings can use polydimethylsiloxane (PDMS or silicone) or Teflon® (polytetrafluoroethylene, PTFE). In their review, Menini *et al*. (2011) summarized that the relatively low adhesion between ice and siloxane-based polymers is due to their

dissimilar rheological-mechanical properties; with the polymers having low Tg values, they tend to be flexible or lubricating at the interface. Additionally, imparting low surface energy and hydrophobic properties to a surface, disrupts the water film ("liquid like layer") at the ice-surface interface, reducing ice adhesion [43]. Mulherein and Haehnel (2003) tested 16 different commercial materials claiming to be 'icephobic' and concluded that these products were successful in reducing the amount of energy to remove ice, but had limited ability to prevent the build-up of ice[44]. Sarshar et al. (2012) demonstrated that nano-structured superhydrophobic powder can be produced by bonding a low surface energy coating (tridecafluoro-tetrahydroctyltrichlorosilane) to commercially available powdered silica nanoparticles (99.9 % SiO2, 10–100 nm particle size) using a fluorination procedure. The silica nanoparticle powder was mixed with a commercial product polyurethane clear coat using an ethanol acetone solvent mixture [45].

The formation of heterogeneous chemistries on a surface using two or more hydrophobic agents, disrupts the water film ("liquid like layer") at the ice-surface interface, reducing ice adhesion [43]. Heterogeneous and composite coatings that are a mix of polysiloxane and fluorocarbon materials can lower ice adhesion better than homogeneous coatings with either PDMS or the polyfluorocarbon (PFC) type of structures. Farhadi *et al*. (2011), Kulinich *et al*. (2010) and He *et al*. (2010) tested coatings of organosilane, fluoropolymer and silicone rubber on rough surfaced aluminum[46][47][48]. Results demonstrate that the aluminum surfaces coated with

hydrophobic room temperature vulcanized silicone rubber resists ice formation. They showed the coating can largely prevent ice formation on the surface, except for a few ice growth spots at a working temperature of −6 °C. However, the coating was covered by a layer of ice after 30 min of spraying super cooled water. [46][47][48].

Superhydrophobic or porous coatings reduce the surface area of a material thus leading to less bond and stress concentrations. Surface roughness can have a significant influence on hydrophobicity. Menini et al. (2011) reviewed multiple methods used to enhance surface roughness and porous structure, such as etching a substrate, depositing nanoparticles, utilizing nanolithography, electroplating polymers, or attaching ZnO 'nano-towers' as shown in Figure 16 [43]. The addition of a low surface energy thin film has been used, employing various techniques such as plasma enhanced chemical vapor deposition (PECVD), deposition of self-assembled monolayers (SAM) and passivation with stearic acid. This allows the frozen droplets to slide off with minimal force and has many characteristics for icephobicity in aluminum [43].

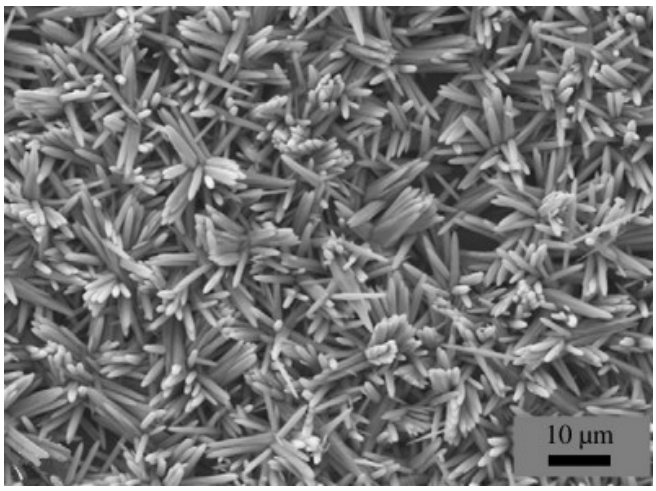

Figure 16 SEM image of ZnO Nanotowers [43].

Other methods were described by Guo *et al*. (2012) who tested a micro/nanostructured surface (MN-surface) composed of micro scratches combined with nanohairs on a metal substrate. It was found that the MN-surface has a robust icephobic property relative to that of nanostructured and microstructured surfaces and smooth surfaces without any structure [49].

2.3.2 Application methods

Some common methods of application include spinning, dipping, spraying, or combinations of these. The amount and uniformity of coverage, surface roughness, porosity or absorbency, among other physical properties are desirable criteria to quantify.

Kulinich and Farzaneh (2009) used multiple coating methods [50]. A summary of the coating process is given in Figure 17. Before coating, the samples were polished with emery paper and cleaned in organic solvents. Centrifugated particles (7.0 g) were mixed with 80 ml of deionized water. Suspensions were sonicated for 30 minutes, and then 6.0 ml Zonal 8740, a perfluoroalkyl methacrylic copolymer product was added and mixed for 3 hours. The first group of samples was sprayed 10 cm from the surface until the surface was fully covered. The second group of samples was spin-coated at a spinning speed of 200 rpm for 5 seconds and 3000 rpm for 10 seconds. Samples were produced with and without nanoparticles. After coating, the specimens were heat treated at 120°C in air for 3 h to remove the residual solvents [50].

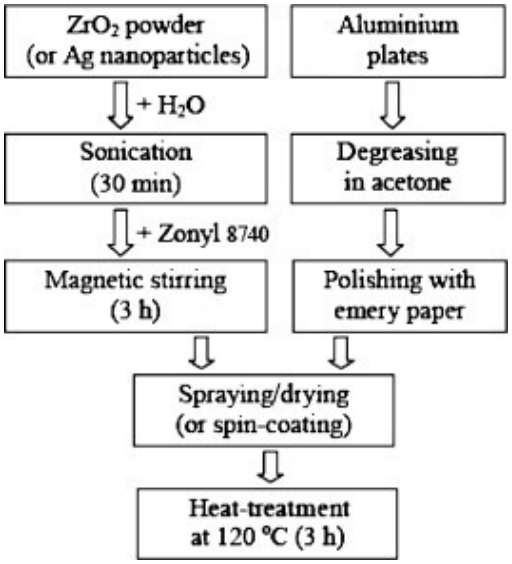

Figure 17 Schematic representation of coating procedure [50]

Cao *et al*. (2009) prepared a sample of aluminum by first mixing 2.5 g of the organosilane-modified silica particles of various diameters (20 nm, 50 nm, 100 nm, 1 µ m, 10 µ m, and 20 µ m) with 5 g of the polymer binder, 75 g of toluene, and 15 g of acetone. They applied the particle – polymer composite by using a spray gun at a pressure of 20 psi and then cured it at room temperature for 12 hours [51]

Sarshar *et al*. (2012) evaluated aluminum samples with icephobic coatings. To create a rough surface, samples were lightly sanded with 900 grit wet-or-dry sandpaper using acetone and isopropyl alcohol. The coating was spray deposited with varying thicknesses of 15–20 µm and 25–30 µm [45].

2.3.3 Testing for icephobicity

Apart from the shear test shown above in Figure 3, from Cuelho et al [5], there are multiple techniques and apparatuses used to test ice adhesion. The most common

methods utilize wind tunnels as well as centrifugal force and shear force devices. Each test is used to determine the performance of an icephobic coating by calculating the force to remove the ice from the material.

Kulinich *et al*. (2010) performed their testing by spraying super cooled micro droplets of water in a wind tunnel at subzero temperature to simulate freezing rain. Samples were iced in a wind tunnel and sprayed with super cooled droplets with an average size of 80 µm. They were then spun in a centrifuge apparatus at constantly increasing speed. A Peltier device, supplied with the goniometer used, kept the droplets frozen. The contact angle and contact angle hysteresis were measured by standard procedures [4] . The centrifuge apparatus also evaluated the adhesion and shear stress of ice detachment.

Laforte *et al*. (2005) performed a similar test using centrifugal force to detach the ice layer (Figure 18)[52]. The ice detaches as the centrifugal force just overcomes the adhesion of the ice. When detachment occurs two piezoelectric cells fixed to the sides of the apparatus relay the time to a computer and the rotation speed is determined. Depending on the coating, the test runs from 2 -20 seconds and is repeated for accuracy [52].

Figure 18 Sample beam in the centrifugal apparatus [52]

Zou et al. (2011) built a custom apparatus to test for ice adhesion by measuring the shear stress at which ice detaches from a specimen [53]. A 4 µl water droplet with a radius of 0.985 mm is placed on the surface to be tested The conical tip is then aligned with the water droplet and lowered down to the sample surface until the contact force is zero. The conical tip and water droplet are then cooled to ≤−10° C. During the test, the temperature and time are recorded and monitored. The apparatus is then nitrogen purged in an isolation box to avoid condensation. Digital images are taken during the test to determine the contact of the water droplet to the specimen. Once the droplet is completely frozen, the conical tip applies force on the water droplet, advancing at a rate of 1 mm/s. As the droplet becomes detached, the two horizontal load cells record the average force to shear the frozen droplet. The shear stress can be calculated using the surface area from the digital images and the shear force to detach the frozen droplet [53].

Hejazi *et al*. (2013) used a PASCO CI – 6746 stress-strain apparatus to test for the adhesion strength of ice by applying horizontal shear force until an ice column was

separated from its substrate [42]. The testing equipment can be seen in Figure 19. Before testing, thin plastic tubes were placed vertically on the substrate surface and filled with water and kept in a freezing room at −20°C until the water was entirely frozen. It was then demolded and transferred to another freezing room with the temperature of −3 ± 2°C where the stress-strain apparatus was used. The horizontal shear force was applied to the base of the ice column until it separated from the material. Measurements were recorded using DataStudio software [42].

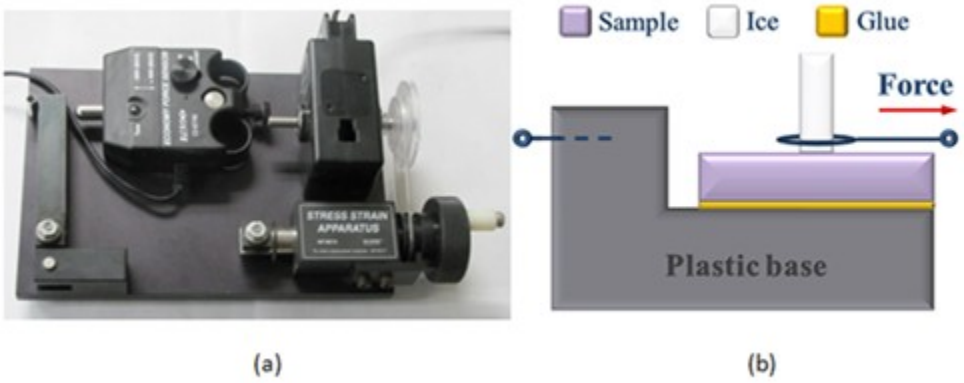

Figure 19 Schematic of the apparatus (a) PASCO stress/strain apparatus (b) Horizontal force applied to the ice column [42]

3 Materials

3.1 Mortar tile materials

A standard set of mortar tiles with s/c = 2.75 and w/c = 0.5 tiles was used in the preliminary screening and the roughness work. Subsequently, a variety of mortar mixes were used with differing s/c, w/c, and fiber contents (M series tiles.)

3.1.1 Portland cement used in all mortar mixes

All mortar specimens were prepared using commercial Type I Portland cement (PC) from Lafarge. The chemical composition and physical properties of cement are presented in Table 3, along with the requirements of ASTM Standard Specification for Portland Cement (ASTM C150) [42].

3.1.2 Sand used in all mortar mixes

ASTM C778 graded standard quartz sand [54]with an average particle size of 425 μm was used.

3.1.3 PVA fibers used in M series concrete fiber/sand mixtures

Polyvinyl alcohol (PVA) fibers (RECS 15x12 mm Kuralon K-II) with a diameter of 0.04 mm and length of 12 mm were used in this study. These fibers had a Young's modulus of 40 GPa and a tensile strength of 1.6 GPa. The PVA structure is shown in Figure 25.

Table 3 Chemical composition and physical properties of Portland cement

CHEMICAL			PHYSICAL		
	ASTMC150	Test		ASTMC150	Test
Item	Limit	Result	Item	Limit	Result
SiO_2, %	--------	19.8	Density, g/cm^3	--------	3.20
			Time of setting,		
Al_2O_3, %	--------	4.9	minutes		
Fe_2O_3, %	--------	2.8	Initial	45 min	165
CaO, %	--------	63.2	Final	375 max	257
			Compressive strength,		
MgO, %	6.0 max	2.3	MPa		
SO_3, %	3.0 max	2.9	1 day	--------	12.1
Ignition loss, %	3.0 max	2.8	3 days	12.0 MPa	21.7
Na_2O, %	--------	0.2	7 days	19.0 MPa	28.3
K_2O, %	--------	0.5	28 days	28.0 MPa	36.5
CO_2, %	--------	1.3			
Potential, %					
C_3S	--------	54.7			
C_2S	--------	15.5			
C_3A	--------	8.4			
C_4AF	--------	8.4			
$C_4AF+2(C_3A)$	--------	25.1			
$C_3S+4.75(C_3A)$	--------	94.5			
Na_2O_{equi}	0.6 max	0.57			

3.1.4 Superplasticizer used in concrete fiber/sand mixtures

The high-range water-reducing admixture used was commercially available polycarboxylate ether superplasticizer (PCE/SP) with a 31% solids concentration.

3.1.5 Preparation of substrate tile specimens: Standard and M series

The relevant ASTM standards were used for mixing (ASTM C 305) [55], casting, demolding, and storage (ASTM C 109) [56] of mortar specimens. Table 4 shows the compositions of the tiles used.

Standard mortar tiles

The standard mortar tiles (15 mm x 15 mm x 8mm thick) were prepared with a water to cement ratio (w/c) of 0.5 and a sand to cement ratio (s/c) of 2.75. The mortar paste was poured into a grid-like mold and leveled on shaker table. The tiles were allowed to set and harden for 24 hours at ambient room conditions and were demolded and placed in a curing chamber at 25 ± 1.5 ºC and 100% relative humidity for 72 hours. The tiles were then dried for 24 hours at 100-110 deg C and allowed to cool for 3 hours at ambient room conditions. These “finished” tiles were stored in isopropyl alcohol – when needed, the tiles were removed and allowed to dry in room conditions for approximately 1-2 hours before sanding.

M series mortar tiles with varied water/sand/fiber content

Tiles M1-M10 had varying water, sand, and fiber content; these tiles were also 15 mm x 15 mm x 8mm. For the mortars used, the water to cementitious material (w/c) ratio, sand to cementitious material (s/c) ratio, superplasticizer dosage (% by weight of cement solids), and PVA fiber (% by volume) are shown in Table 4. The superplasticizer

dosage was adjusted to achieve a workable mortar. After casting, the tiles were allowed to harden for 24 hours at 23±3 °C and at least 90% of relative humidity. Specimens were demolded 24 hours after the mixing procedure, allowed to cure in tap water for 72 hours, then dried for 36 hours at 60-70 °C.

Table 4 Mortar mix design

	Standard mortar tiles	Tiles with fibers					Tiles without fibers				
Mixture ID =>		**M1**	**M2**	**M3**	**M4**	**M5**	**M6**	**M7**	**M8**	**M9**	**M10**
w/c ratio	0.5	0.25	0.3	0.4	0.45	0.5	0.25	0.3	0.4	0.45	0.5
s/c ratio	2.75	0	1	2	2.5	3	0	1	2	2.5	3
SP, % solid	0	0.14	0.1	0.1	0.1	0.1	0.42	0.045	0.04	0.02	0.01
PVA fibers % by Vol	0	1	1	1	1	1	0	0	0	0	0

3.2 Materials used in tile treatments

There were four categories of treatments evaluated, solutions, simple emulsions, core emulsions, and shell emulsions. The emulsions are described in CFIRE report 04-09 and Flores-Vivian et. al. (2013) [14][33] explained in detail the differences between these three emulsion concepts. To summarize the treatments:

- **Solutions:** isopropyl alcohol or aqueous solutions of the active materials were used, depending on the solubility of the silane or siloxane
- **Simple emulsions:** the basic emulsions were comprised of a continuous aqueous phase with an emulsifier and an insoluble silane/siloxane droplet phase
- **Core type emulsions:** equivalent to a basic emulsion, with particulate material residing in the insoluble droplet phase

- **Shell type emulsions:** particulates reside in the continuous phase surrounding the droplets sometimes near the droplet interface

3.2.1 Silane materials

Silane compounds, based on the silane structure shown in Figure 9b, were selected in order to encompass a variety of modified silane chemical functionalities. The materials selected were commercially available products; their abbreviated structures are shown in Figure 20 below [57]. Six of these materials were first examined in pre-work testing for contact angle on ceramic tile; that list was expanded for this study.

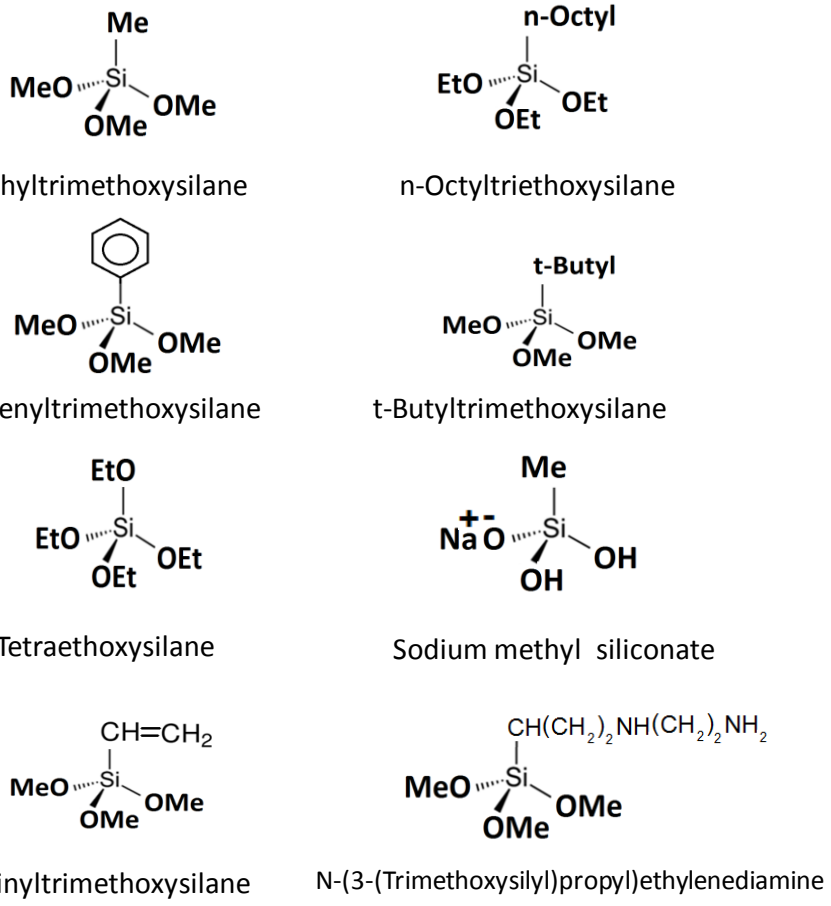

Figure 20 Structures of silane derivatives evaluated

3.2.2 Siloxane materials

Siloxane and materials that resemble siloxane or have structures that are derived from siloxane were also evaluated. Polydimethylsiloxane (PDMS), shown in Figure 21a, was used in preliminary screening as a solution in isopropanol, and is a non-reactive waterproofing agent. Polymethylhydrogensiloxane (PMHS), shown in Figure 21b, was used in isopropanol solution and also in a variety of emulsion forms. The Si-H hydrogen in PMHS is reactive.

a) b)

Figure 21 Siloxane based materials evaluated a) Polydimethylsiloxane (PDMS) a non-reactive waterproofing agent, b) Polymethylhydrogensiloxane (PMHS) [58]

3.2.3 Hexamethyldisilazane

Hexamethyldisilazane has been used to render silica and other polar surfaces hydrophobic. The S-N bond in hexamethyldisilazane is more reactive than Si-O; its structure and reaction with silica surface silanol groups (Si-OH) is shown in Figure 21. $SiMe_3$ groups are transferred from nitrogen to oxygen, in this case, or can transfer to another nitrogen [59][60][61].

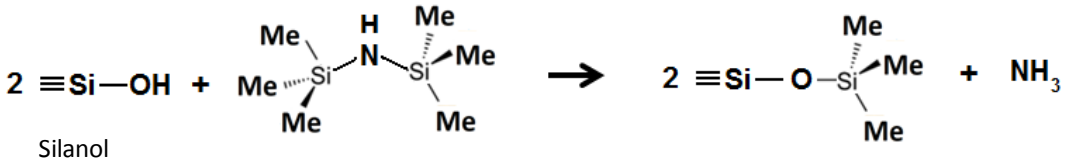

Figure 22 Hexamethyldisilazane and the silanizing reaction with silica

3.2.4 Methoxy-terminated aminosilsesquioxanes

This is the main component in as-received Dow Corning® 1-6184 Water Repellent, the composition range of which is given in Table 5 [30].

Table 5 Dow Corning® 1-6184 Water Repellent, 65-85% active, as received

Component	Wt %
Aminosilsesquioxanes, methoxy-terminated	70.0 - 90.0
Methyl alcohol	15.0 - 35.0
Aminoethylaminopropyltrimethoxysilane	5.0 - 10.0
Methyltrimethoxysilane	1.0 - 5.0

The structure of methoxy-terminated aminosilsesquioxanes is difficult to discern. Dow Corning technical support stated that a structure was not available. These materials are derived from silsesquioxane, which has an empirical formula $RSiO_{1.5.}$ According to Brooks, the silsesquioxane structure depends on method of preparation [62]. Possible structures silsesquioxane and the methoxy-terminated aminosilsesquioxane derivatives are shown in Figure 23; existence of the ladder structure has not gained complete acceptance [62].

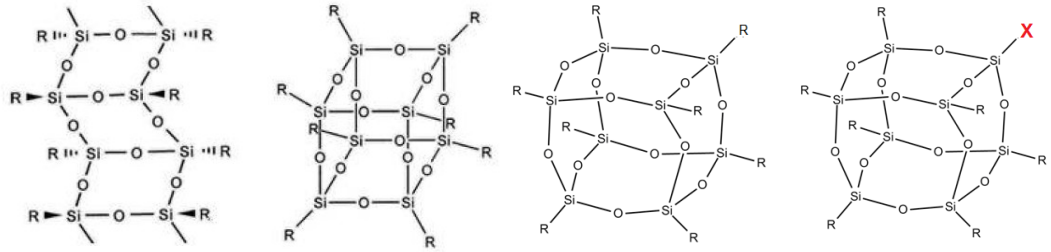

Possible structure, **X**: Amino: -NH2, -NHR , -NRR'
Methoxy: - Me

Figure 23 Possible structures for silsesquioxane and substituted derivatives [63][62]

3.2.5 Dow Corning® IE-6683 emulsion

Dow Corning® IE-6683 emulsion is a commercial product, which, as received, is a 40% active emulsion intended for use as a water repellent treatment for porous cementitious materials The approximate composition of IE6683 is shown in Table 6 [30]. Dow does not provide the exact composition. The structures of main components, silicic acid, diethoxyoctylsilyl trimethylsilyl ester (SADTE) and octyltriethoxysilane are shown in Figure 24.

Table 6 Dow Corning® IE-6683 Water Repellent Emulsion 40% active, as received

Component	Wt %
Silicic acid, diethoxyoctylsilyl trimethylsilyl ester	15.0 - 35.0
Triethoxyoctylsilane	10.0 - 30.0
Polyethylene oxide lauryl ether	<=2.0
Aminofunctional siloxane	1.0 - 5.0
Ethoxylated C12-C13 alcohol	<=1.0

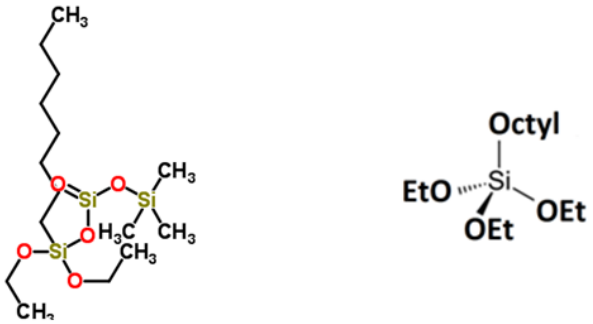

Figure 24 Structure of IE-6683 components a) silicic acid, diethoxyoctylsilyl trimethylsilyl ester [64] and b) octyltriethoxysilane

3.2.6 Polyvinyl alcohol (PVA) emulsifier

For emulsion stabilization, water soluble polyvinyl alcohol (PVA) was selected because of its nonionic character and excellent compatibility with concrete materials [65]. A highly hydrolyzed (98%) PVA with molecular weight of 16,000 from Acros Organics was used, as it minimizes the tendency of foam. Deionized water (DI water) was used as the dispersion medium for the emulsions. The PVA structure is shown in Figure 25.

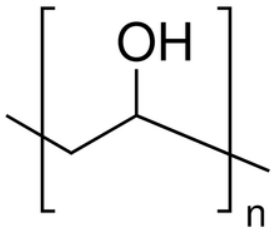

$n_{fiber} >> n_{emulsifier}$

Figure 25 Polyvinyl alcohol (PVA) structure for emulsifier, fibers (Adapted from [66]

3.2.7 Surfactants emulsifiers

Tergitol NP6, Tergitol TMN6, Tergitol TMN10 surfactants from Dow were also used as emulsifiers.

3.2.8 Particulate additive

Silica fume (SF) from Elkem was used to stabilize [48-50] and modify the emulsion. It was used as a particulate additive that would impart roughness and also have reactive (bonding) properties with Portland cement. The SF was analyzed by the X-ray powder diffraction (XRD) and scanning electron microscope (SEM) techniques. An X-ray diffractogram and microscope image (Figure 26) shows that silica fume particles are amorphous and spherical [35].

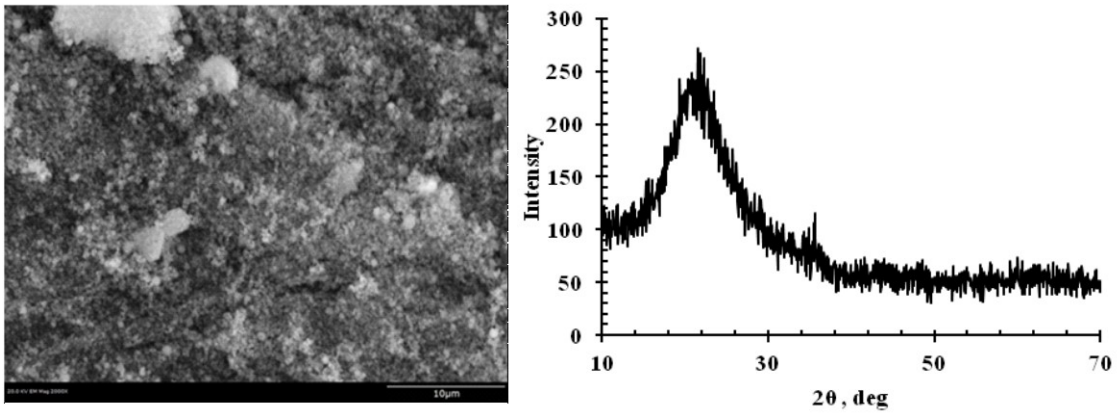

Figure 26 Silica fume SEM images (left) and X-Ray Diffractogram pattern (right) [67]

3.2.9 Biocide

Acticide G was used to prevent mold, mildew, and bacterial growth in the emulsions

3.2.10 Emulsion compositions

The emulsion formulas are listed Table 7. For their production methods, see section 4.6 Emulsion preparation.

Table 7 Emulsion formulas

Emulsion ID	**E_0**	**E_{0R}**	**E_{1C}**	**E_{1S}**	**E_{1SR}**
Emulsion type	Simple	Simple	Core	Shell	Shell
Emulsion comment	25% PMHS PVA	5% PMHS PVA, diluted E_0			diluted E_{1S}
Composition					
Water, deionized	71.215	71.215	66.215	66.215	80
PVA	3.485	3.485	3.485	3.485	0.697
Siloxane, PMHS	25	25	25	25	5
Silica Fume	0	0	5	5	1
Biocide	0.3	0.3	0.3	0.3	0.06
Total	100	100	100	100	100

4 Methods

4.1 Mixing and casting of mortar tiles

See 3.1.5 Preparation of substrate tile specimens.

4.2 Pre-treatment surface preparation for standard mortar tiles

The as-cast cured and dried tiles had concave and irregular surfaces that first had to be flattened and then finish sanded. For both wet and dry sanding, this was done in two steps, the first to flatten surface the tile surface and the second to sand the flat surface.

4.2.1 Belt sanding

Belt sanding to flatten surface

Belt sanding was used to remove the concave surface and the top layer of tile. A 1HP Craftsman belt sander (3”x21” belt) was used with 40 grit aluminum oxide belt. The sander was held in position, belt side up, on a bench. The tile was held and sanded to remove the concavity and an additional thin layer of approximately 0.5 mm. With the sander on and the belt in motion, the tile was pressed against the belt with a force of approximately 5lb. The tile was held against the belt with its edge approximately parallel to the machine direction and moved back and forth perpendicular to the belt direction 5 times with the tile always in contact with belt for a total of approximately 3 seconds. Then, while off the belt, the tile was then rotated 90 degrees, and the sanding process was repeated (5 times back and forth perpendicular to the belt direction, tile always in contact with belt, approximately 3 seconds total). The tile was visually examined after

each sanding to confirm that material removal was uniform and the surface was visually flat.

Finish belt sanding

After belt sanding to flatten the surface, finish sanding was done using a fresh 40, 80, or 120 grit aluminum oxide belt and performed as follows: with the sander on and the belt in motion, the tile was pressed against the belt with a force of approximately 5 lb and moved back and forth perpendicular to the belt direction 5 times for approximately 3 seconds; the tile was rotated 90 degrees and the process repeated. The tile was visually examined after each sanding to confirm that material removal was uniform. All sanding was done outdoors using the appropriate PPE.

4.2.2 Manual wet sanding

This sanding method was manual with the 60 grit silicon carbide wet-or-dry self-adhesive abrasive disc glued to a rigid countertop and the tile sample wet sanded in a circular motion using approximately 10 lb of downward force.

For wet sanding to flatten the surface, each tile was manually wet sanded ten times in 3” circles. The tile was turned 90 deg and again wet sanded ten times in 3” circles. The tiles were then examined to confirm flatness and then rinsed in tap water. For finish sanding, the same wet sanding procedure was repeated using a fresh disc.

4.2.3 Tile cleaning

After sanding, tiles were rinsed in tap water, ultrasonically cleaned in tap water 5 min, again rinsed in tap water, again ultrasonically cleaned in tap water 5 min, rinsed in distilled water, dried at 110 deg C for 3 hours, and allowed to cool at room temp for 24 hours.

4.3 Pre-treatment surface preparation for M series tiles

In order to expose a fresh surface and sand aggregates, the M series tiles were wet sanded with 60 grit silicon carbide wet-or-dry paper for 30 seconds and rinsed with tap water.

Then, to remove any loose particles, the rinsed tiles were immersed in an excess of tap water and ultrasonically cleaned using a Hielscher model UIP1000hd ultrasonic homogenizer, a probe style sonicator, for 60 seconds at 50% of maximum power. The specimens were then dried in an oven at 40 °C for 24 hours.

4.4 Solution preparation

When screening for active materials effectiveness, solutions were used rather than emulsions. 25% active ingredient solutions were produced for all treatment materials, with most being dissolved in isopropyl alcohol and sodium methyl siliconate and potassium methyl siliconate salts being dissolved in water. All mixes were made by gravimetrically adding active compound to solvent in an HDPE bottle and manually

shaking for approximately 1 minute. Materials that did well in the screening were selected to move on as candidates for emulsions.

4.5 Emulsion aqueous phase preparation

Emulsions first required the production of the continuous aqueous phase with emulsifier, followed by emulsion production by adding silane/siloxane to the aqueous phase under high speed mixing.

4.5.1 Surfactant emulsifier aqueous phase

Tergitol surfactant and biocide was added to a beaker of de-ionized (DI) water room at temperature and stirred with a stir bar for approximately 5 minutes.

4.5.2 PVA emulsifier aqueous phase

The water-soluble PVA swells quickly in water and has a tendency to clump together. To avoid clumping, PVA powder was gradually added to de-ionized water and stirred for 10 minutes at 23±3°C, using a magnetic stirrer on a hot plate. Then, to achieve complete dissolution, the temperature was increased to 95±2.5°C and kept constant for 40 minutes while stirring; biocide was added near the end of this stirring time. The solution was allowed to cool in a water bath until a temperature of 23±3°C was achieved.

4.6 Emulsion preparation

A high speed mixer (HSM, model L5M-A from Silverson) was used to prepare the emulsions. The mixing procedure for PMHS and silica fume in PVA solution is diagramed

in Figure 27. In order to stabilize the plain emulsions (without particles), high speed/shear mixing at 10,000 rpm was used to produce very small droplet sizes. Medium speed (5000 rpm) was used only when particles were added.

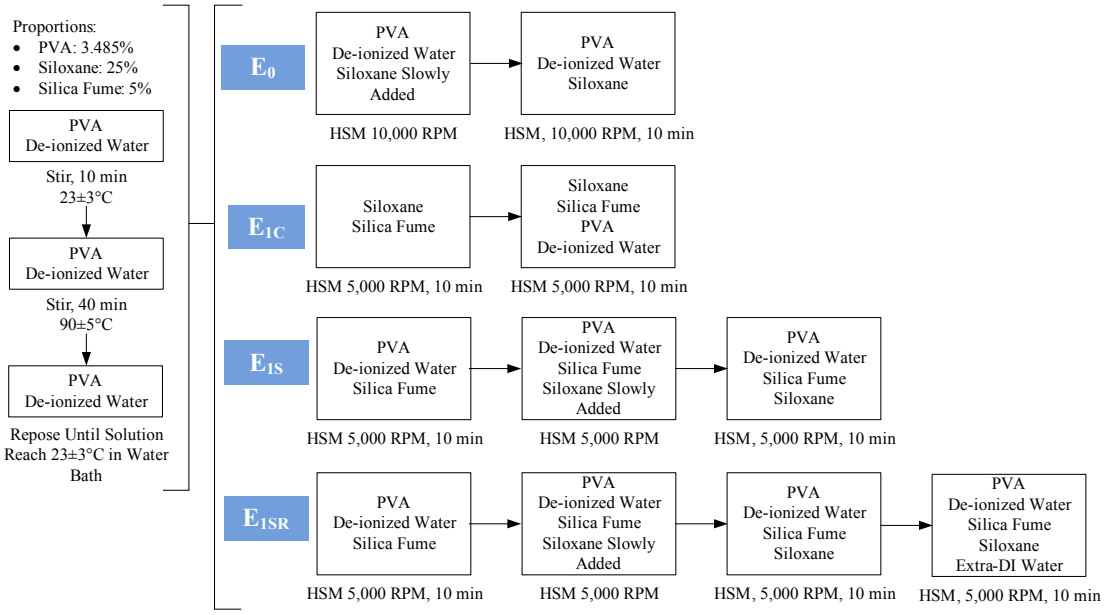

Figure 27 The procedure for preparation of emulsions

4.6.1 Simple emulsion preparation

The pre-produced surfactant or PVA aqueous phase was mixed in a large beaker at 10,000 RPM and silane/siloxane was gradually added. After addition was complete, mixing was continued for 10 minutes and the resulting emulsion was allowed to cool at room temperature.

The 25% PMHS PVA emulsion was produced in this manner. 5% PMHS emulsion was made by gravimetrically adding a 25% PMHS PVA simple emulsion to water in a HDPE bottle and manually shaking for approximately 1 minute. 5% IE-6683 emulsion was

made by gravimetrically adding the 40% IE-6683 as received emulsion to water in a HDPE bottle and manually shaking for approximately 1 minute.

4.6.2 Core type emulsion preparation

Silica fume was gradually added to a beaker of PHMS mixing at 5,000 RPM then mixed for an additional 10 minutes. The resulting SF/PHMS suspension was gradually added to a beaker of PVA aqueous phase solution mixing at 5,000 RPM, mixed for an additional 10 minutes, and allowed to cool at room temperature.

4.6.3 Shell type emulsion preparation

Silica fume was gradually added to a beaker of PVA aqueous phase solution mixing at 5,000 RPM and mixed for an additional 10 minutes, producing an aqueous suspension. Mixing continued at 5,000 RPM and PHMS was gradually added. The emulsion was mixed for an additional 10 minutes, and allowed to cool at room temperature. For the diluted shell type emulsion, additional DI water was added and mixed for another 10 minutes at 5,000 RPM.

4.7 Treatment methods

4.7.1 Immersion treatment

In this method, used for the preliminary studies, tiles were individually soaked in a single solution for 30 minutes. When removed, excess solution was manually shaken off and the tile set on a flat surface. All tiles were allowed to dry and potentially cure at ambient

room conditions for a minimum of 24 hours before contact angle measurements were made.

4.7.2 Surface dosage treatment

Instead of complete immersion, an aliquot of treatment can be dosed onto a surface and evenly spread. For **volumetric dosage method,** treatment liquid was carefully delivered onto a tile using a micropipette set at desired amount and then manually spread as needed using the disposable plastic pipette tip so that the coating was visually uniform. The **gravimetric dosage** was the same as the volumetric, but additionally, the tiles were weighed before and after application and the coverage computed. All tiles were allowed to dry at ambient room conditions for a minimum of 24 hours before contact angle measurements were made.

4.8 Visual roughness via scanning electron microscopy

In pre-work, it was determined that quantifying roughness was not possible: the profilometer was not able to read even sanded surfaces and the 3D scanner did not allow for practical testing times. Tiles were examined on a JEOL JSM-6610LV scanning electron microscope (SEM) The tiles were examined without sputtering, so the SEM work was done at 70 Pa (low vacuum) to minimize charging. Unsputtered tiles were also examined at 16-18x under high vacuum using a 45 degree aspect, with tile mountings as shown in Figure 28.

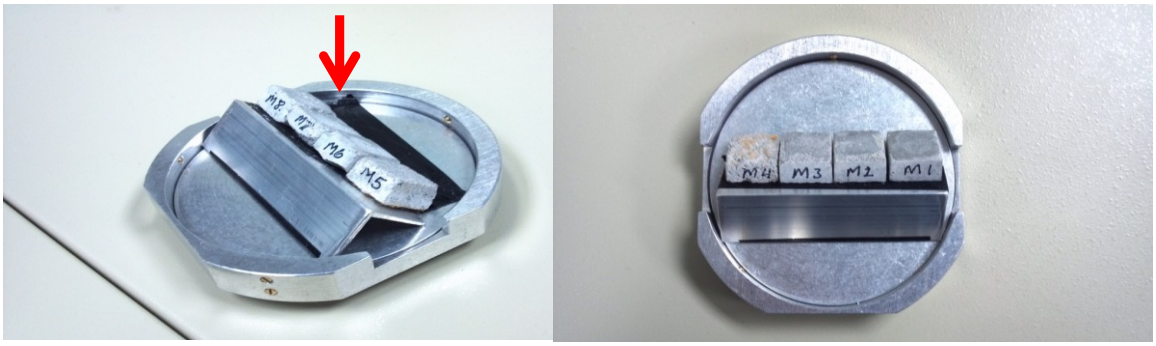

Figure 28 SEM tile mounting with 45 degree aspect

4.9 Hydrophobicity experimental method

4.9.1 Sessile drop contact angle

A Krüss DSA100 "Drop Shape Analysis System" goniometer was used for sessile drop contact angle measurements. Deionized water was used as the liquid phase: 20 microliters of water was dosed onto the tile surface at 800 microliters/min from a distance of 2 mm above the tile surface using the instrument's automatic syringe. The drop was allowed to stabilize for 22 seconds and the contact angle (based on the drop image) was measured using the Krüss DSA4 Drop Shape Analysis software. Each of the tile repetitions was tested and the average value reported. In the later M series mortar mix phase of the project, the dosage rate was adjusted to 200 microliters/min.

Contact angle determinations were made using the Krüss DSA software using the pertinent fits shown in Table 8.

Table 8 Krüss contact angle fit models. Image examples from this work. Table information from Krüss DSA4 software manual [68]

Kruss abbreviation	T-1	T-2	CIR	L-Y
Kruss fit name	Tangent-1	Tangent-2	Circle and Height-Width	Laplace-Young
Assumed contour shape	Eliptical arc	Localized polynomial fit	Circular arc	Gravity flattened curve
Recommended measuring range	10-120	10-180	0-20	20-180
Dynamic measurement possible	yes	yes	no	no
Symmetrical drop shape required	no	no	yes	yes

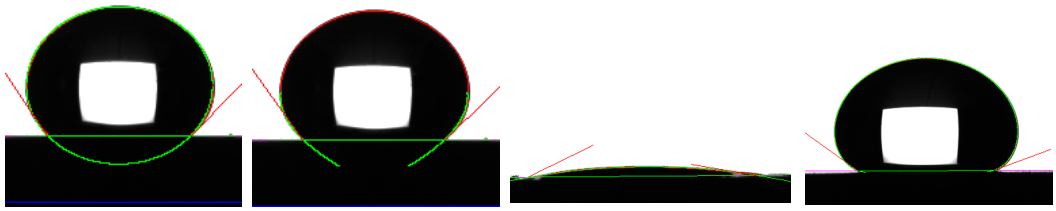

4.9.2 Roll off angle (tilt table)

After level sessile drop video capture was complete, the tilt table routine was initiated. Tilt table angle was ramped from 0 to 90 degrees at a rate of 1.23 deg/sec, with video capture on. The roll off angle was determined by selecting the tilt table angle at which the drop's receding angle contact let loose.

4.10 Falling rod impact test - % ice loss

The falling rod test was developed for quantification of ice removal via physical impact. For this test, a water droplet was applied to a small tile. The tile and water were held in a chilled environment, generating a frozen ice droplet. A falling mass striking the ice

droplet provided the means of ice removal (Figure 29), with the amount of ice removed being a measure of icephobicity.

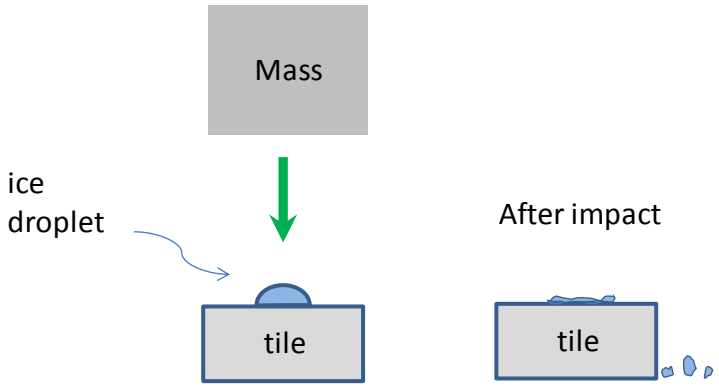

Figure 29 Ice loss on physical impact concept

4.10.1 Laray falling rod apparatus

The apparatus used for falling rod impact was a Laray falling rod viscometer, shown in Figure 30.

Figure 30 Laray falling rod viscometer apparatus with timer

The Laray viscometer is normally used to measure the viscosity of paste-like inks and fluids and comes equipped with a two photoelectric switches spaced 10 cm apart to enable the calculation of rod speed.

For the ice impact application of the falling rod, the rod drop time consistently measured 0.1 sec for 0.1m at freezer temperatures of -10 deg C and -20 deg C, corresponding to 1.0 m/sec rod velocity. See Figure 31

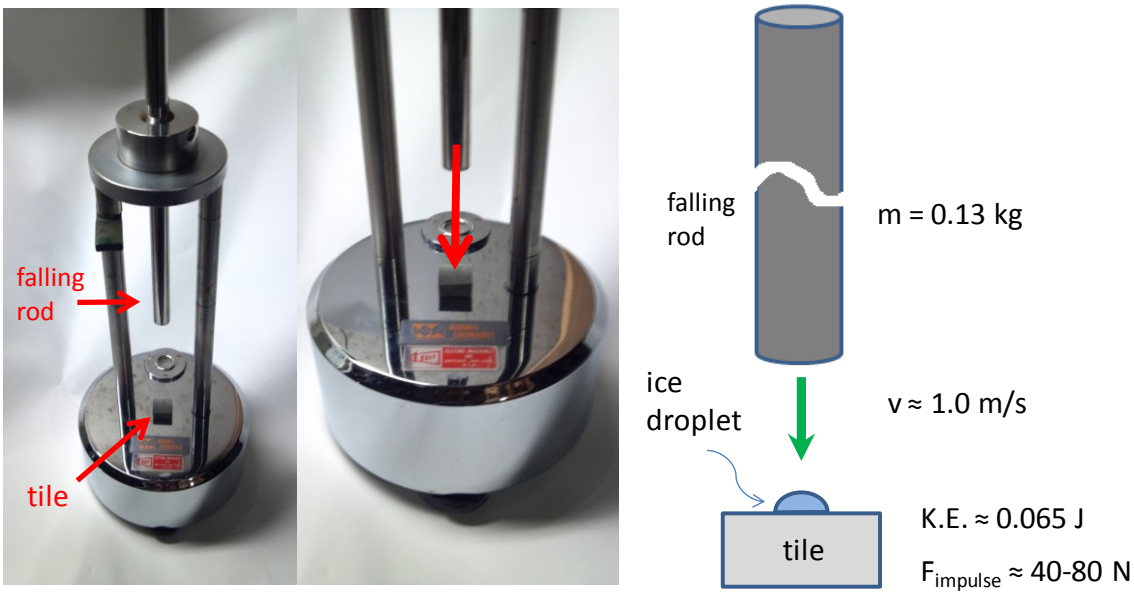

Figure 31 Ice removal via physical impact of falling rod

4.10.2 Pre-chilling of tiles

The 15mm x 15mm x 8mm tiles used for contact angle measurement were also used for the falling rod impact test.

The tile samples were placed in a freezer with an air temperature of -20 ± 3 ºC. After being freezer chilled for a minimum of 45 min, each tile was weighed on an analytical

balance, with 0.0001g readout. All weighing was done in a buffer room immediately outside the freezer and at a temperature of +10 ± 3 ºC; the analytical balance was allowed to equilibrate to this temperature for a minimum of 1 hour. The weighing was done by removing no more than six tiles at a time from freezer. The tiles were placed back in the freezer for a minimum of 15 min before dosing water on top.

(Note that in preliminary/screening work, mortar tile samples were chilled to a -10 ± 3 ºC as compared to -20ºC in the final method. 150 microliters of icy distilled water was placed on the tiles while in the freezer (vs. +10ºC deionized water in final method). Samples were chilled for another 30 min then impact testing performed at ambient room conditions (vs. +10ºC in final method). The tiles were pulled individually from the freezer for impact testing and the falling rod was placed in ice water for approximately 1 min between tests and dried before the impact.)

4.10.3 Casting of ice on tile

The deionized water used for ice casting and the micropipette were allowed to equilibrate to +10 ± 3 ºC for a minimum of 1 hour in the buffer room. Before dosing water, the micropipette was set for 150 microliters and adjusted if needed so that its dosage, as weighed on the analytical balance, was 0.150 +/-0.010 g of water at +10 ± 3 ºC.

In the freezer, nominally 150 microliters of water was dosed on each pre-equilibrated and leveled tile using the preset micropipette (Figure 32.) In order to prevent

micropipette icing and contraction, no more than 6 droplets at a time were dosed. The water and micropipette were returned to the buffer room for 1-2 minutes before dosing water again. The tiles with ice droplets were allowed to chill for a minimum of 15 minutes before being weighed. Again, the weighing was done in the buffer room by removing no more than six tiles at a time from freezer.

150 µl water

15 mm x 15 mm x 8mm tile

Figure 32 Water droplet dosed on tile

After weighing, the tiles with ice droplets were returned to the freezer and allowed to chill for another 15 minute minimum before impact testing.

4.10.4 Falling rod ice impact tests

The Laray falling rod apparatus was placed in the freezer, leveled, and allowed to equilibrate for a minimum of 1 hour before impact testing was performed. Each tile was tested individually by placing the tile with ice on the Laray base and visually aligning the droplet with center of the rod. The rod was then raised to its starting position. The lever holding the rod was tripped to allow the rod to fall on tile with ice. The rod was wiped with a dry paper towel and returned to its raised position.

The tile with remaining impacted ice was lifted off the base and any loose ice was removed by holding the tile vertically and lightly tapping the tile twice on the Laray base, which was subsequently wiped with a dry paper towel. The final tile weights were recorded, again by removing no more than six tiles at a time from freezer. Calculations for each tile included ice drop weight, ice drop weight loss, and % ice loss.

5 Preliminary research results

The preliminary work, which included a screening of a relatively large list of materials and the establishment of the falling rod impact test for icephobicity, utilized the standard mortar tiles and solution versions of the treatment materials.

5.1 Screening study of siloxane and silane compounds as hydrophobic and icephobic surface treatments for concrete

Expanding on the list of treatments from pre-work done on ceramic tile, this preliminary study continued the evaluation of commercially available silane and siloxane compounds not only as hydrophobic treatments, but also as icephobic treatments for concrete. Standard mortar tiles (40 grit dry belt sanded and cleaned) were examined with a variety of treatment materials used at 25% in isopropanol or aqueous solution. Table 9 lists these materials and their abbreviated structures are shown above in section 3.2 Materials used in tile treatments. The experimental work had the following objectives:

- Quantify the hydrophobicity of treated tiles using sessile drop contact angle measurements of deionized water on the treated tiles
- Develop an impact test for icephobicity, characterize the tile treatments for icephobicity and provide an assessment of the test itself.

Emulsions were not used, since this was a screening for effectiveness of the active materials and selected materials would move on as candidates for emulsions. Each tile

was individually treated using the 30 minute soak method described in section 4.7.1 Immersion treatment. The impact test used was the preliminary version of the final test method, as detailed in the section 4.10 Falling rod impact test. Two tiles were produced for each treatment, with one tile being tested for contact angle and one tile being tested for ice loss, i.e., one "repetition" for each test.

Table 9 Screening study list of siloxane/silane treatment materials with tilenames

Tile sample name	Siloxane/silane active treatment	Percent active as applied	Solvent
A00	Untreated		
A01	Polymethylhydrogensiloxane	25%	isopropanol
A02	Polydimethylsiloxane, 200 cSt	25%	isopropanol
A03	Polydimethylsiloxane, 300 cSt	25%	isopropanol
A04	t-Butyltrimethoxysilane	25%	isopropanol
A05	N-(3-(Trimethoxysilyl)propyl)ethylenediamine *	25%	isopropanol
A06	Methyltrimethoxysilane	25%	isopropanol
A07	Hexamethyldisilazane	25%	isopropanol
A08	Phenyltrimethoxysilane	25%	isopropanol
A09	Aminosilsesquioxanes. methoxy-terminated *	25%	isopropanol
A10	Vinyltrimethoxysilane	25%	isopropanol
A11	n-Octyltriethoxysilane	25%	isopropanol
A12	Tetraethoxysilane	25%	isopropanol
A13	Sodium methyl siliconate	25%	water
A14	Potassium methyl siliconate	25%	water

* Primary component in alkoxysilane blend

Results for both contact angle (theta mean) and % ice loss are shown in Table 10 below. The best results for contact angle came from the use of polymethylhydrogensiloxane and n-octyltriethoxysilane treatments with 131 and 124 degrees, respectively. Octyltriethoxysilane also had the highest % ice loss. The sodium and potassium methyl

siliconate salts remain compelling, since they enable water-based treatment composition.

The plot of % Ice Loss on impact vs. Contact angle is shown in Figure 33.

Table 10 Contact angle and ice loss results

Tile sample name	Siloxane/silane active treatment	Ice drop weight	% Ice loss	Contact angle theta mean [deg]
A00	Untreated	0.117	47%	8
A01	Polymethylhydrogensiloxane	0.136	77%	131
A02	Polydimethylsiloxane, 200 cSt	0.141	60%	85
A03	Polydimethylsiloxane, 300 cSt	0.134	70%	121
A04	t-Butyltrimethoxysilane	0.135	78%	124
A05	N-(3-(Trimethoxysilyl)propyl)ethylenediamine *	0.135	57%	85
A06	Methyltrimethoxysilane	0.134	69%	121
A07	Hexamethyldisilazane	0.138	28%	65
A08	Phenyltrimethoxysilane	0.136	69%	114
A09	Aminosilsesquioxanes. methoxy-terminated *	0.139	60%	72
A10	Vinyltrimethoxysilane	0.141	78%	123
A11	n-Octyltriethoxysilane	0.134	94%	124
A12	Tetraethoxysilane	0.140	65%	70
A13	Sodium methyl siliconate	0.135	84%	111
A14	Potassium methyl siliconate	0.133	46%	113

* Primary component in alkoxysilane blend

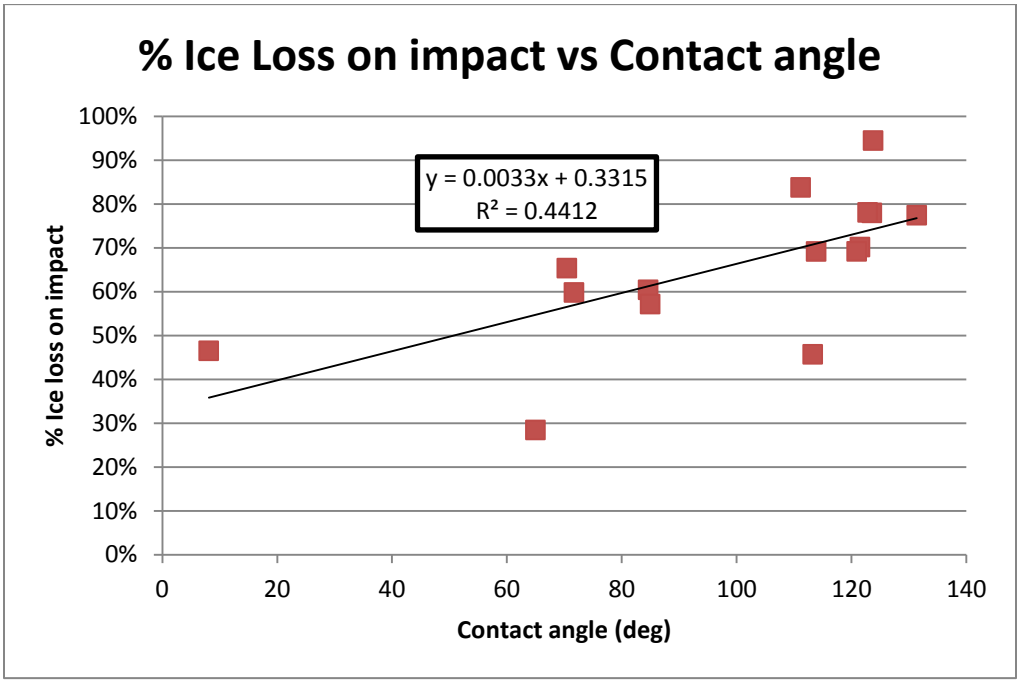

Figure 33 The relationship between icephobicity and contact angle

In terms of contact angle, the best performers were polymethylhydrogensiloxane at 131 degrees and n-octyltriethoxysilane at 124 degrees. n-Octyltriethoxysilane also had the highest % ice loss at 94%, followed by sodium methyl siliconate at 84%. Though it did not give the very best contact angle value (111 deg), sodium methyl siliconate remains compelling, since it is water soluble and it was still a good performer in the group. One would have expected potassium methyl siliconate to behave similarly to the sodium salt, and it did in terms of contact angle; % ice loss was much less, however, at 46% vs. 84% for the sodium salt. This may say more about the preliminary version of the falling rod ice removal test than the material itself, particularly since one repetition was done. Though the correlation coefficient was 0.44, there was a general trend with icephobicity (via % ice loss) increasing with hydrophobicity (via contact angle.) The test itself gave

some compelling results, which warranted further work as detailed in the following section.

5.2 Falling rod impact test assessment and further material screening

The screening study of commercially available silane and siloxane compounds utilized a preliminary or proof-of-concept version of the falling rod impact test that warranted further work. This subsequent preliminary work was intended to assess and refine and the preliminary falling rod impact test for icephobicity. The experimental work had the following objectives:

- Develop a standard procedure for the falling rod impact icephobicity test
- Evaluate the consistency of results using five repetitions per tile
- Reassess the correlation between icephobicity and hydrophobicity
- Narrow the treatment material list

Again, standard mortar tiles (15 mm x 15 mm x 8mm thick, 40 grit dry belt sanded and cleaned) were used. See section 3.1 Mortar tile for detail. The treatment materials were selected based on the results from the previous section. This work showed a linear correlation between % ice loss on impact and contact angle with an R^2 of 0.44. Examination of the plot allowed material selection for this next iteration of the falling rod test. Figure 34 depicts this selection of material. As can be seen, some extremes were selected, along with materials near the trendline as well as outliers. Table 11

summarizes the six treatment materials selected and the reasoning behind their selection.

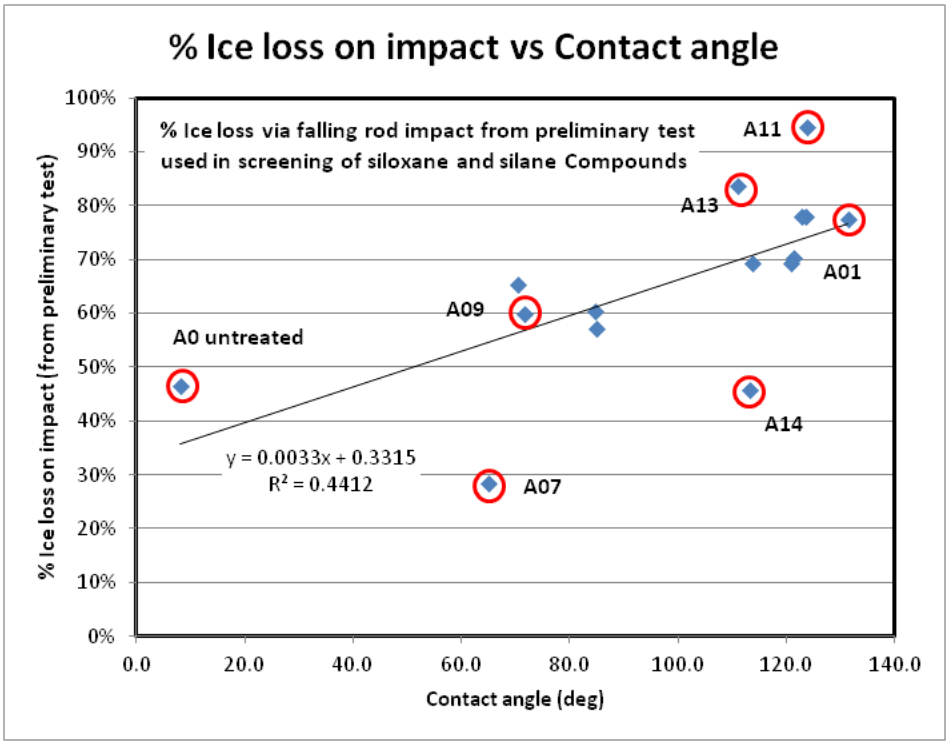

Figure 34 Selected treatment materials (circled and labeled) from the preliminary falling rod test used in the screening of siloxane and silane compounds. A0, A01, A07, A09, A11, A13 and A14 are the original tilenames.

Table 11 Treatment materials and the reasoning behind their selection

Tilename from plot	Siloxane/silane active treatment	Ice drop weight	% Ice loss	Contact angle theta mean [deg]	Reason for selection
A00	Untreated	0.117	47%	8	reference, low CA
A01	Polymethylhydrogensiloxane	0.136	77%	131	highest CA, on trendline
A07	Hexamethyldisilazane	0.138	28%	65	midrange CA, outlier low % Ice loss
A09	Aminosilsesquioxanes. methoxy-terminated *	0.139	60%	72	midrange CA, on trendline
A11	n-Octyltriethoxysilane	0.134	94%	124	highest % ice loss, high CA
A13	Sodium methyl siliconate	0.135	84%	111	high % ice loss
A14	Potassium methyl siliconate	0.133	46%	113	high end CA, low % Ice loss, similar chemistry to A14

* Primary component in alkoxysilane blend

25% active solutions in isopropyl alcohol were produced for most treatment materials, while 25% active aqueous solutions used for the water soluble sodium methyl siliconate and potassium methyl siliconate. Straight isopropyl alcohol was used for the untreated control tile. Each tile was individually treated using the 30 minute soak method described in section 4.7.1 Immersion treatment, the same procedure as used in the above siloxane/silane screening. Ten tile repetitions were produced for each treatment (see Table 12) with five to be used for falling rod ice impact testing and the other five to be used for contact angle testing. The falling rod ice impact method used was the standard procedure described in section 4.10 Falling rod impact test except that the freezer air temperature was -10 ± 3 ºC (rather than -20 ºC ± 3 ºC) and all weighing was done in the freezer (rather than in the buffer room at +10 ºC)

Table 12 Summary of tilenames and treatments

Tile sample name	Reps	Treatment	% Active	Solvent	Treatment
F00	10	Isopropyl alcohol	0%	IPA	30 min soak
F01	10	Polymethylhydrogensiloxane	25%	IPA	30 min soak
F07	10	Hexamethyldisilazane	25%	IPA	30 min soak
F09	10	Aminosilsesquioxanes, methoxy-terminated *	25%	IPA	30 min soak
F11	10	n-Octyltriethoxysilane	25%	IPA	30 min soak
F13	10	Sodium methyl siliconate	25%	water	30 min soak
F14	10	Potassium methyl siliconate	25%	water	30 min soak

* Primary component in alkoxysilane blend

Table 13 shows the results for ice drop mass, % ice loss, and contact angle. The values shown are the average and standard deviation of 5 repetitions. Ten tiles were made for each tilename: tiles 1-5 were used for ice drop mass and % ice loss; tiles 6-10 were used for contact angle testing.

Table 13 Summary of results: ice drop mass, % ice loss, contact angle for Tileset F

Tile sample name	Treatment	Average Ice drop mass g	Std dev Ice drop mass g	Average % Ice Loss	Std dev % Ice Loss	Average Contact angle (deg)	Std dev Contact angle (deg)
F00	Isopropyl alcohol	0.1446	0.0019	25%	16%	14	5.3
F01	Polymethylhydrogensiloxane	0.1466	0.0005	82%	5%	135	2.8
F07	Hexamethyldisilazane	0.1507	0.0027	28%	9%	18	6.6
F09	Aminosilsesquioxanes. methoxy-terminated *	0.1415	0.0122	74%	5%	105	10.8
F11	n-Octyltriethoxysilane	0.1336	0.0147	45%	14%	64	14.6
F13	Sodium methyl siliconate	0.1339	0.0051	69%	6%	124	4.8
F14	Potassium methyl siliconate	0.1426	0.0072	64%	11%	124	5.8

* Primary component in alkoxysilane blend

5.2.1 Weight measurements and consistency of ice drop mass

Before any weighing was done, the analytical balance was allowed to equilibrate to the freezer temperature of -10ºC. This took approximately 90 minutes, as determined by the frequency of the scale automatically going into calibration mode. The LCD display

was readable, but it did dim significantly in freezer conditions. Before proceeding, a 10g calibration weight was used to check that the scale was reading accurately at the equilibrated freezer temperature.

The micropipette used to deliver the water to the tile is typically used at room temperature. While dosing at -10ºC, there was some icing observed in the disposable pipette tip. When icing was observed, the tip was replaced, and though icing could have influenced the delivered amount prior to replacement, this did not appear to be a significant problem. The ice drop mass values (average and standard deviation of repetitions 1-5) are shown in Table 13 and Figure 35.

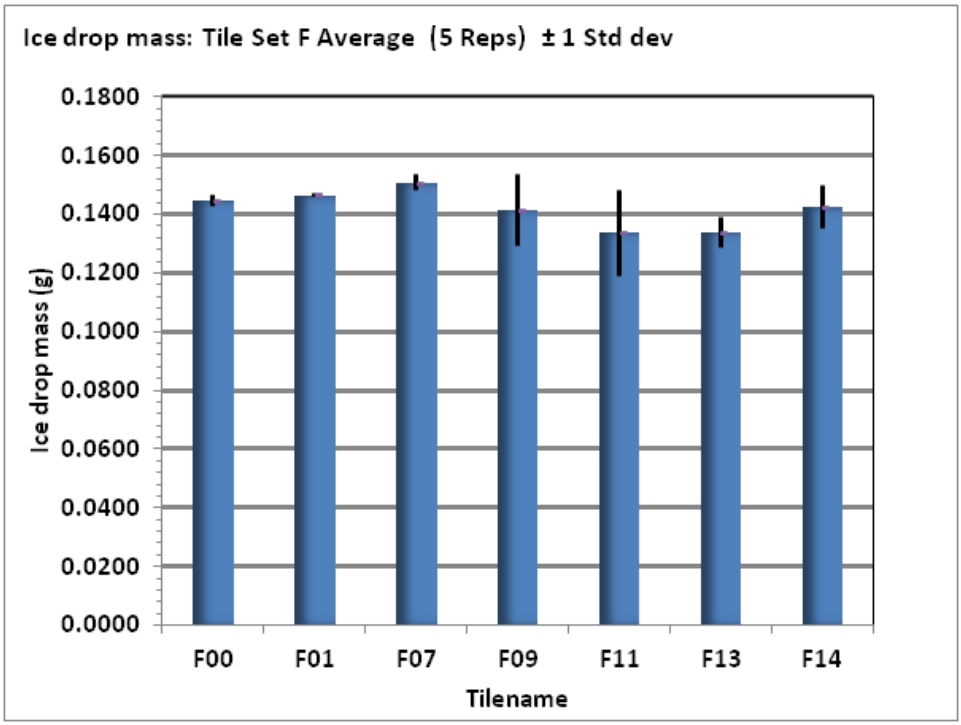

Figure 35 Chart of ice drop masses (averages and standard deviations of tiles 1-5)

5.2.2 % Ice loss via falling rod impact

The values for % ice loss ranged from a low of 25% for the untreated tiles to a high of 82% for tiles F01 (polymethylhydrogensiloxane treatment), as shown graphically in Figure 36. Tiles F09, treated with methoxy-terminated aminosilsesquioxanes (primary component) also performed well, with 74% ice loss. The aqueous solutions of sodium methyl siliconate and potassium methyl siliconate gave good results at 69% and 64% ice loss, respectively. Hexamethyldisilazane (F07) did not differ significantly from the untreated tiles and n-octyltriethoxysilane (F11) was uninteresting at 45% ice loss. On average, the standard deviation was a reasonable 10% ice loss, with higher variation in the poorer performing tiles and lower variation in the better performing tiles: the top 3 tiles had an average 75% ice loss and an average standard deviation of 6% ice loss; the bottom 3 had an average 33% ice loss and an average standard deviation of 13% ice loss.

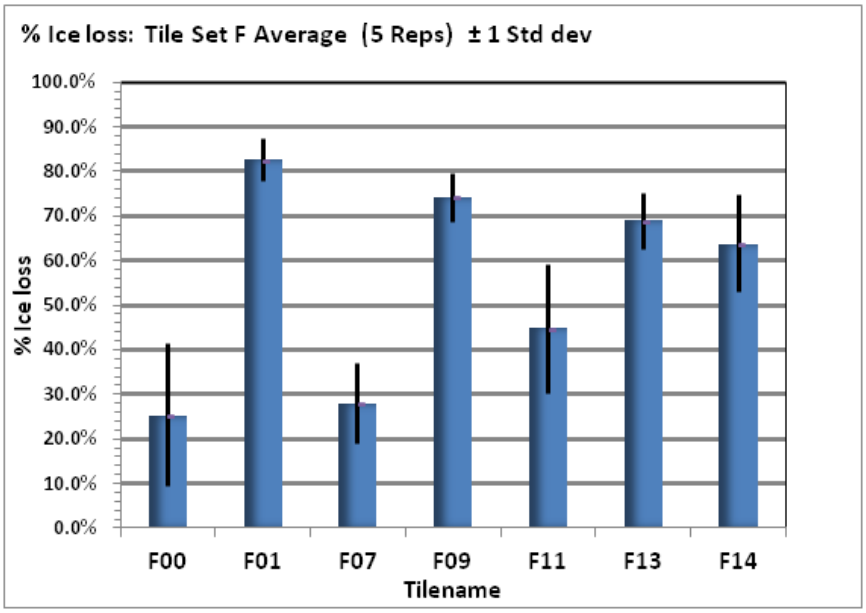

Figure 36 Chart of % ice loss (averages and standard deviations of tiles 1-5)

So the results were quite consistent and the test was compelling enough to pursue. And while the procedure used worked quite well, with future testing, the scale was positioned in a warmer area so that the display would be easier to read. To this end, subsequent testing was done with the scale placed in a buffer room immediately outside the freezer at +10 ºC.

5.2.3 Contact angle

Contact angle testing was done on repetitions 6-10 of the ten treatment repetitions produced. The contact angle values and images are shown in Figure 37. The relative performance of the tiles was generally similar to the % ice loss rankings. The exception to this was the methyl siliconate salts (F13, F14) which had higher contact angles, both at 124 degrees, than methoxy-terminated aminosilsesquioxane (F09) at 105 degrees.

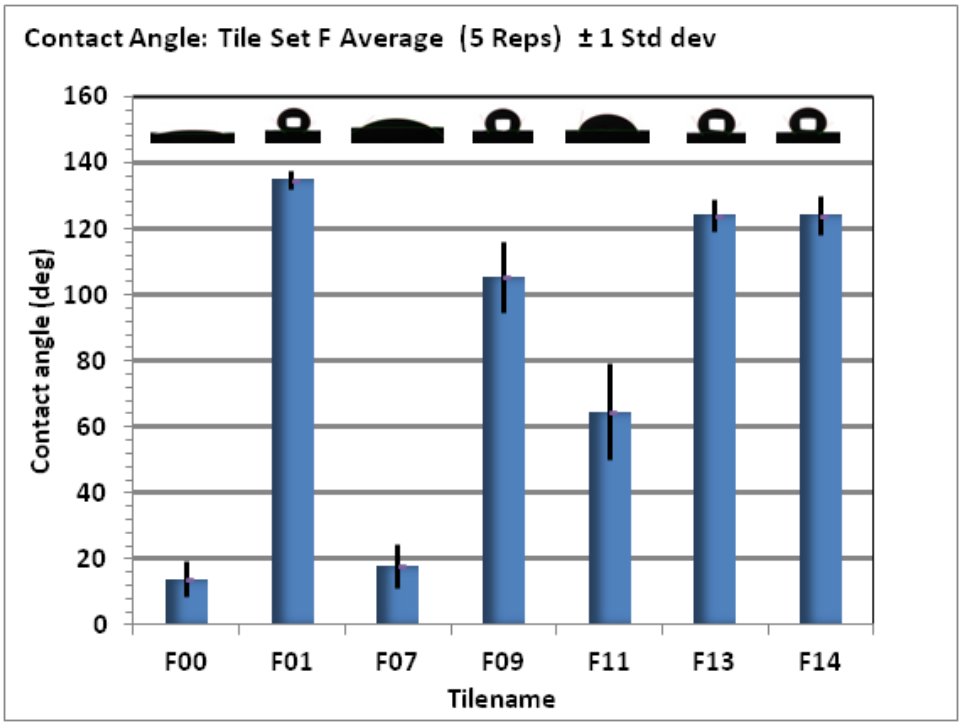

Figure 37 Chart of contact angles (averages and standard deviations of tiles 6-10)

5.2.4 Contact angle and % ice loss

The % ice loss on impact and contact angle results from Table 13 are plotted in Figure 38, which shows a strong general relationship between icephobicity and hydrophobicity, with a correlation coefficient of 0.93 for the materials used.

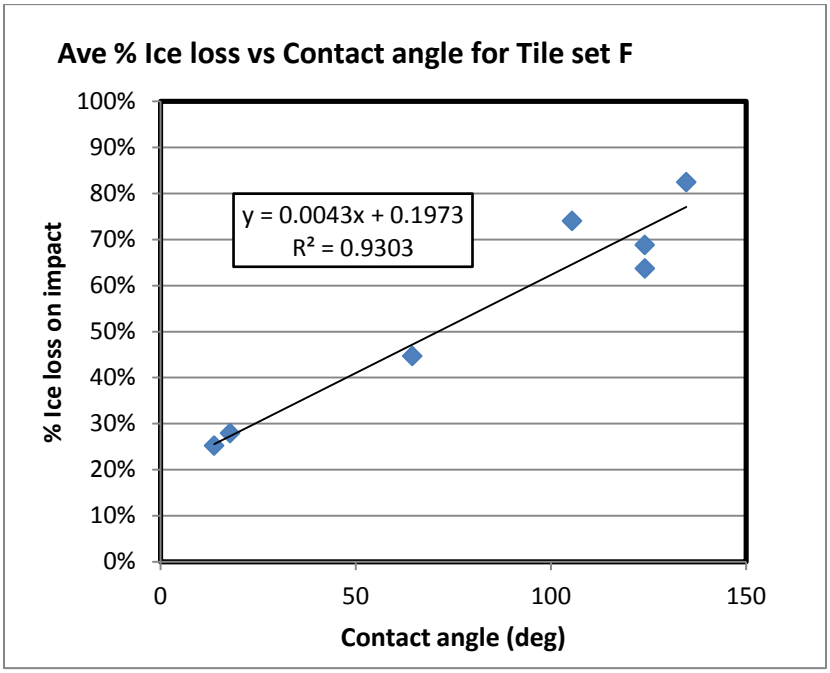

Figure 38 Chart of contact angle averages and standard deviation

This indicates that hydrophobicity can be predictor for icephobicity, at least for concrete. However, examination of the data for contact angles greater than 100 degrees revealed a cluster of points that did not show any trend, indicating a lack of sensitivity in the test or the influence of other factors, and warranting scrutiny in further tests.

In agreement with the siloxane/silane screening, the water-insoluble polymethylhydrogensiloxane continued to be a top performer, giving both high contact angle and % ice loss. Also a water-insoluble siloxane oil, the methoxy-terminated aminosilsesquioxanes treatment (primary component in the Dow Corning® 1-6184 Water Repellent used) had a compelling % ice loss and an intermediate contact angle. Less compelling is that the overall composition of the Dow Corning® 1-6184, as received,

is not clear, nor is its % active material content, which can range from 65-85% (see Table 5.) The water soluble sodium and potassium methyl siliconates were good performers, with compelling % ice loss and high end contact angles. Of particular interest with the siliconates is that along with their similar chemistries, they gave similar % ice loss and contact angle results.

It was prudent to narrow the number of treatments and, based on these results, one water-insoluble material for emulsions, polymethylhydrogensiloxane, and one water-soluble material for solutions, sodium methyl siliconate, were selected.

5.3 Emulsifier selection

Tergitol based emulsions, depending on the process used, were stable. They were stable when mixed at 20,000 RPM on an IKA T25 Ultra-Turrax mixer, but at 10,000 on the Silverson, they were not stable and use of the Silverson was required to allow incorporation of particulates. As a result, the Tergitol surfactants were dropped and PVA emulsifier was selected for further work.

6 The effect of sanding imparted roughness

In addition to treatments and coatings, the roughness of the mortar surface in tested tiles and in the field, has the potential to affect hydrophobicity and icephobicity. The surfaces of small tiles have curvature that would not appear in bulk castings. In addition, surface irregularities and variation in as-cast tiles, requires a consistent flattening and finishing procedure that enables comparison of the tiles. Sanding has been selected as a practical means to accomplish this. The preliminary studies utilized standard mortar tiles that were 40 grit dry belt sanded and cleaned. The objectives in this study were as follows:

- Examine the effect of tile sanding on hydrophobicity and icephobicity of standard mortar tiles using contact angle and % ice loss via falling rod impact
- For treatments, utilize the screened and selected materials from the preliminary studies, but in aqueous solution and emulsion form, and include a commercially available emulsion from Dow Corning®

6.1 Substrate tile material

Four versions of sanding standard mortar tiles were used: 60 grit manual wet sanding with silicon carbide and 40 grit, 80 grit, and 120 grit aluminum oxide dry belt sanding. The flattening and sanding steps are detailed in section 4.2 Pre-treatment surface preparation for standard mortar tiles and summarized in Table 14.

Table 14 Flattening and sanding steps for tiles

	60 grit tiles	40 grit tiles	80 grit tiles	120 grit tiles
Manual wet sanding to flatten: 60 grit	Step 1			
Manual wet sanding: 60 grit	Step 2			
Belt sanding to flatten: 40 grit		Step 1	Step 1	Step 1
Finish belt sanding: 40 grit		Step 2	Step 2	Step 2
Finish belt sanding: 80 grit			Step 3	Step 3
Finish belt sanding: 120 grit				Step 4
Tile cleaning	Step 3	Step 3	Step 4	Step 5

6.2 Scanning electron micrographs of untreated tiles

The images of untreated tiles are shown in Figure 39. The 40, 80, and 120 grit sanded can be seen as getting sequentially smoother, with the 120 grit tile exhibiting the highest degree of polished sand grains. On visual assessment, the 60 grit wet tile looks quite coarse relative to the grit size. It is plausible that, despite being ultrasonically cleaned, the dry belt sanded tiles retained fine dust in their voids and crevices, packed-in by the sanding process, while with manual wet sanding the fines were systematically flushed away, leaving an apparently coarser surface.

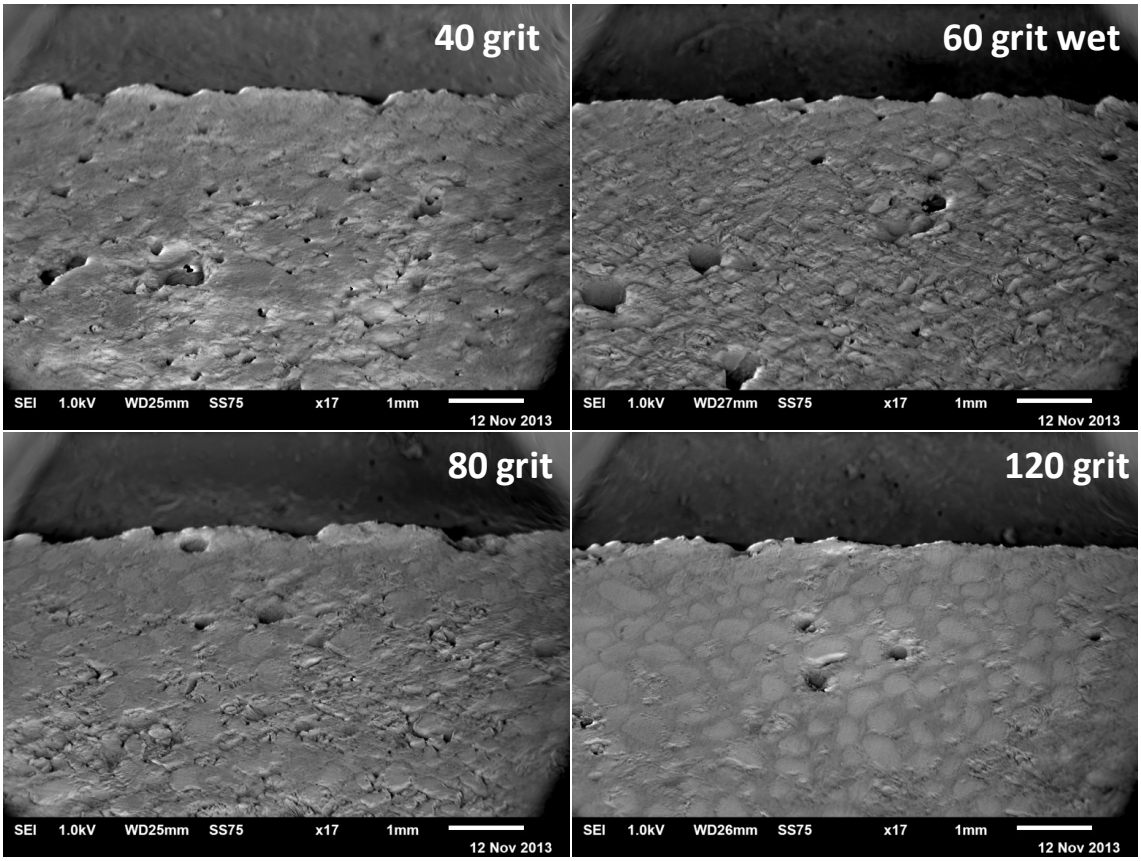

Figure 39 Scanning electron micrographs of untreated tiles at 17x, 1.0 kV

6.3 Treatment materials and application method

Treatments in this study were applied to the surface of the tiles. In pre-work, it was determined that the dosage should be no more than on the order of 60 microliters of 5% active for surface application on a 15mm x 15mm tiles, resulting in coating treatment coverage on the order of 270 g/m^2 and active material coverage of approximately 13 g/m^2. Utilizing the screened and selected materials from the preliminary work, PMHS and SMS, along with commercially available Dow Corning® IE-6683 emulsion, the treatments used were as follows:

- 5% PMHS isopropanol solution, used as a reference
- 5% PMHS PVA emulsion (see E_{0R}, Table 7 above)
- 5% sodium methyl siliconate in water
- 5% IE-6683 emulsion (see Table 6 above)

The PMHS PVA emulsion was produced at 25% active as described in section 4.6.1 Simple emulsion preparation, while the Dow Corning® IE-6683 was a 40% emulsion, as received. Both were diluted to 5% concentrations by weight.

All tiles were surface treated using the gravimetric dosage method as described in section 4.7.2 Surface dosage treatment, with 60 microliters of 5% active treatment per tile. Two tile repetitions were produced for each treatment/sanding combination. Table 15 shows the results for coating coverage, % ice loss, and contact angle. An examination of the results for untreated tiles confirmed that they all had typically low values for ice loss and contact angle.

Figure 40 shows that treatment coverage was quite consistent, with an overall average of 263 g/m^2 and a standard deviation of 6.0 g/m^2. This corresponded to 13.2 g/m^2 of active material applied to the tiles on average.

Table 15 Tabulation of results: coating coverage, % ice loss, and contact angle

Tilenames Rep1 Rep2	Surface sanding grit	Treatment	Treatment type	Average Coating coverage g/m2	Std dev Coating coverage g/m2	Active coverage g/m2	Average % Ice Loss	Std dev % Ice Loss	Average Contact angle (deg)	Std dev Contact angle (deg)
H01 H02	40	Untreated		0	0.0	0.0	28%	11%	14.4	5.4
I01 I02	60	Untreated		0	0.0	0.0	48%	7%	10.8	5.3
H05 H06	80	Untreated		0	0.0	0.0	52%	7%	9.7	3.0
H09 H10	120	Untreated		0	0.0	0.0	42%	16%	10.1	5.5
H13 H14	40	Polymethylhydrogensiloxane	Isopropanol	242	9.4	12.1	79%	4%	133.9	3.3
I05 I06	60	Polymethylhydrogensiloxane	Isopropanol	258	9.1	12.9	77%	6%	129.9	1.6
H17 H18	80	Polymethylhydrogensiloxane	Isopropanol	247	9.1	12.4	76%	11%	128.4	5.4
H21 H22	120	Polymethylhydrogensiloxane	Isopropanol	246	0.0	12.3	79%	11%	132.4	2.8
H25 H26	40	Polymethylhydrogensiloxane	Emulsion	251	20.1	12.5	85%	0%	117.6	1.7
I13 I14	60	Polymethylhydrogensiloxane	Emulsion	273	0.9	13.7	79%	3%	108.5	4.9
H29 H30	80	Polymethylhydrogensiloxane	Emulsion	268	8.2	13.4	83%	5%	108.8	2.9
H33 H34	120	Polymethylhydrogensiloxane	Emulsion	262	6.6	13.1	80%	6%	122.0	4.9
H37 H38	40	Sodium methyl siliconate	Aqueous	265	5.0	13.2	78%	10%	124.3	2.9
I21 I22	60	Sodium methyl siliconate	Aqueous	278	1.6	13.9	86%	1%	127.5	1.3
H41 H42	80	Sodium methyl siliconate	Aqueous	264	6.3	13.2	87%	4%	115.4	4.5
H45 H46	120	Sodium methyl siliconate	Aqueous	276	2.2	13.8	78%	3%	107.2	10.5
H49 H50	40	Dow Corning® IE-6683	Emulsion	265	2.5	13.3	89%	4%	112.9	1.8
I29 I30	60	Dow Corning® IE-6683	Emulsion	271	7.5	13.5	86%	3%	119.9	4.4
H53 H54	80	Dow Corning® IE-6683	Emulsion	275	6.6	13.7	80%	3%	110.9	4.1
H57 H58	120	Dow Corning® IE-6683	Emulsion	271	0.3	13.6	78%	0%	110.9	18.4

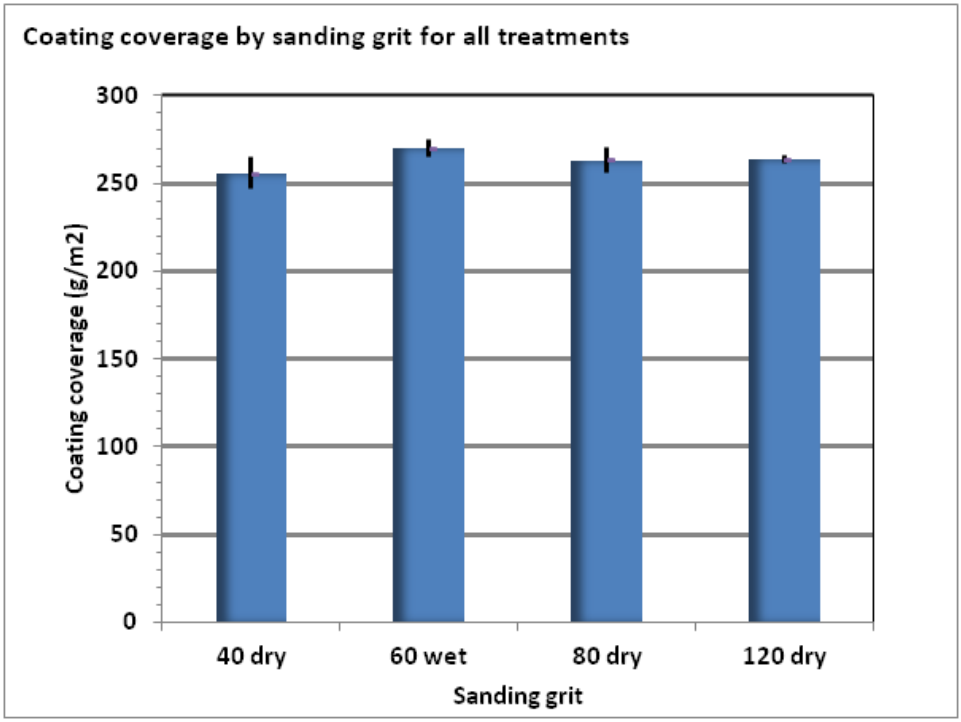

Figure 40 Coating coverage by sanding grit

6.4 The overall effect of sanding type

The charts in Figure 41 and Figure 42 show that the sanding method did not give any significant differences in contact angle or % ice loss.

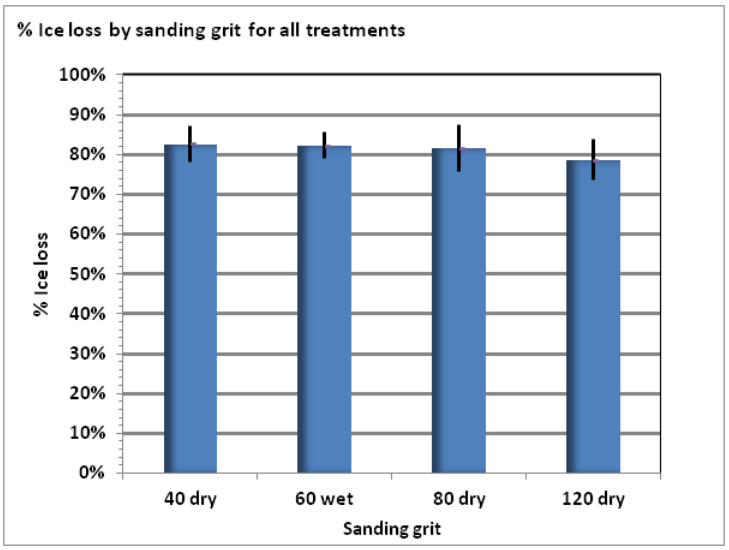

Figure 41 % Ice loss by sanding grit

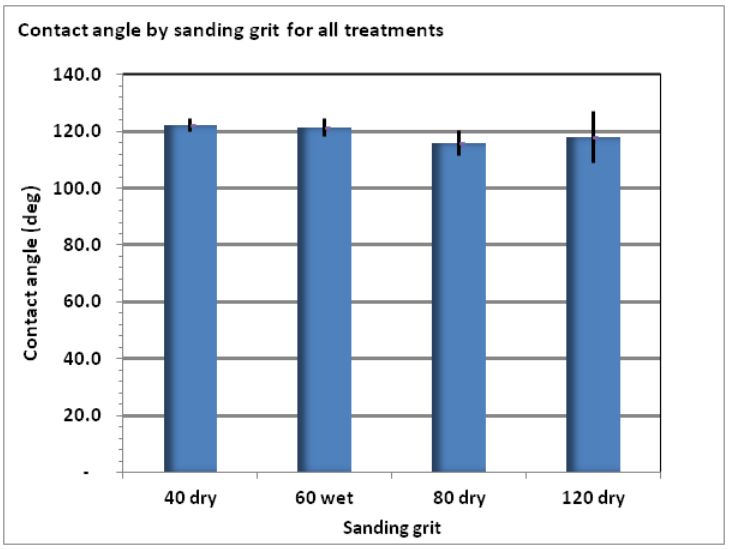

Figure 42 Contact angle by sanding grit

6.5 The overall effect of treatment type

Table 16 shows values averaged by treatment type with the corresponding standard deviations. All three materials performed quite well.

Table 16 Results by treatment type averaged for all sanding grits

Treatment	Treatment type	Surface sanding grit	Average % Ice Loss	Std dev % Ice Loss	Average Contact angle (deg)	Std dev Contact angle (deg)
Untreated		Averaged	42%	11%	11.2	4.8
Polymethylhydrogensiloxane	Isopropanol	Averaged	78%	2%	131.1	3.3
Polymethylhydrogensiloxane	Emulsion	Averaged	82%	3%	114.2	3.6
Sodium methyl siliconate	Aqueous	Averaged	82%	5%	118.6	4.8
Dow Corning® IE-6683	Emulsion	Averaged	83%	5%	113.6	7.2

The charts in Figure 43 and Figure 44 show % ice loss on the order of 80% with contact angles around 115 degrees for the emulsions and aqueous solution. The impractical PMHS isopropanol solution, which has been used as a reference starting from the preliminary screening aspects of this report, gave the highest contact angle of 131 degrees on average for the various sandings, but did not have a correspondingly high % ice loss value.

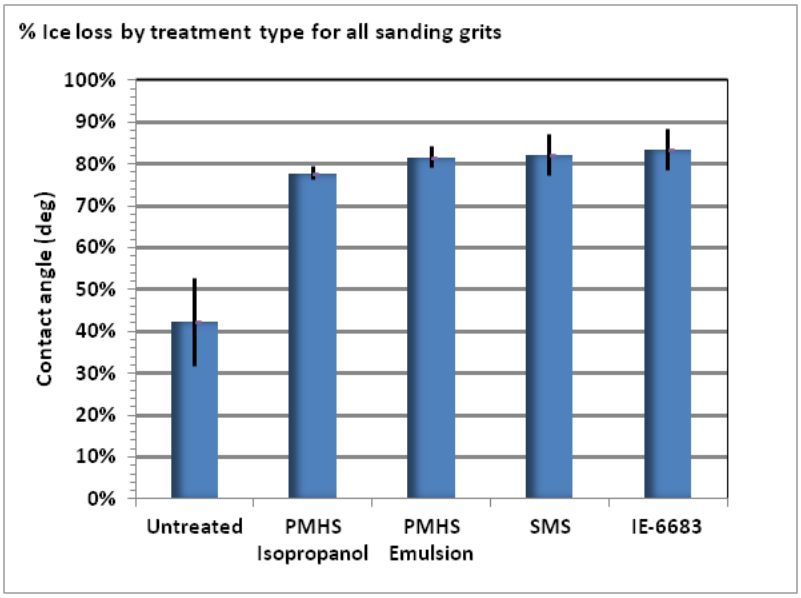

Figure 43 % Ice loss by treatment type

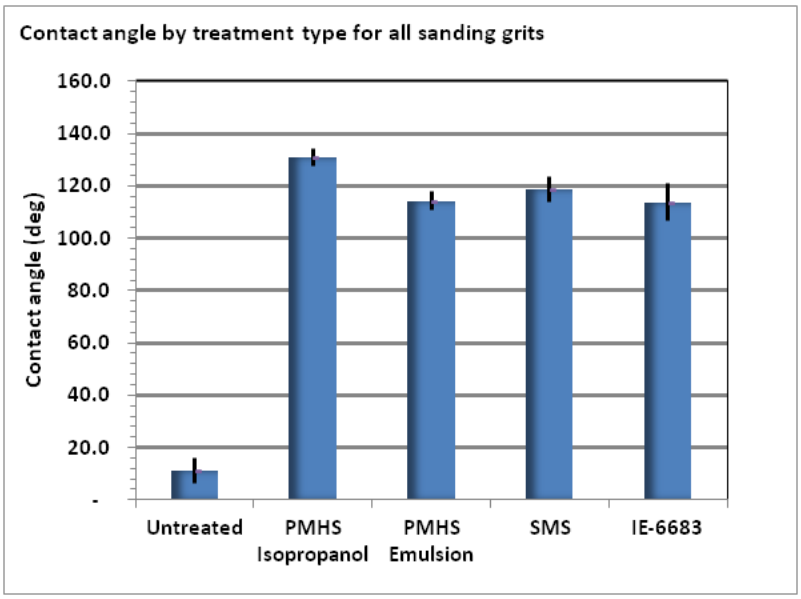

Figure 44 Contact angle by treatment type

6.6 The coating specific effect of sanding type

Table 17 and Table 18, along with their corresponding charts, Figure 45 and Figure 46, show the effects of sanding by treatment-type on ice loss and contact angle. The Ice loss results show that the rankings for the various treatments can differ depending on what grit is selected, though the values tended to converge for the 120 grit tiles (Figure 45.) And although PMHS in isopropanol shows contact angle values approx 15 degrees higher than its PMHS PVA emulsion counterpart (Figure 46), its % ice loss values were marginally lower and not advantageous.

Table 17 % Ice loss by sanding grit and treatment

Sanding grit	% Ice loss			
	PMHS isopropanol solution	PMHS emulsion	SMS aqueous solution	IE6683 emulsion
40	79%	85%	78%	89%
60	77%	79%	86%	86%
80	76%	83%	87%	80%
120	79%	80%	78%	78%

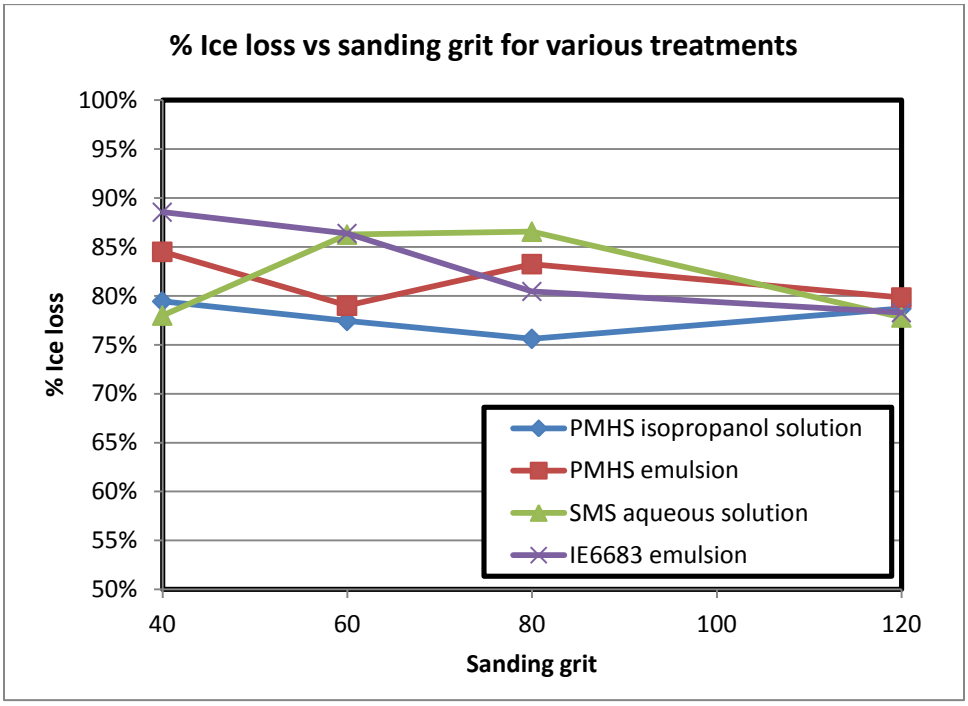

Figure 45 The relationship between % ice loss and sanding grit for various treatments

Table 18 Contact angle by sanding grit and treatment

Sanding grit	Contact angle			
	PMHS isopropanol solution	PMHS emulsion	SMS aqueous solution	IE6683 emulsion
40	134	118	124	113
60	130	109	127	120
80	128	109	115	111
120	132	122	107	111

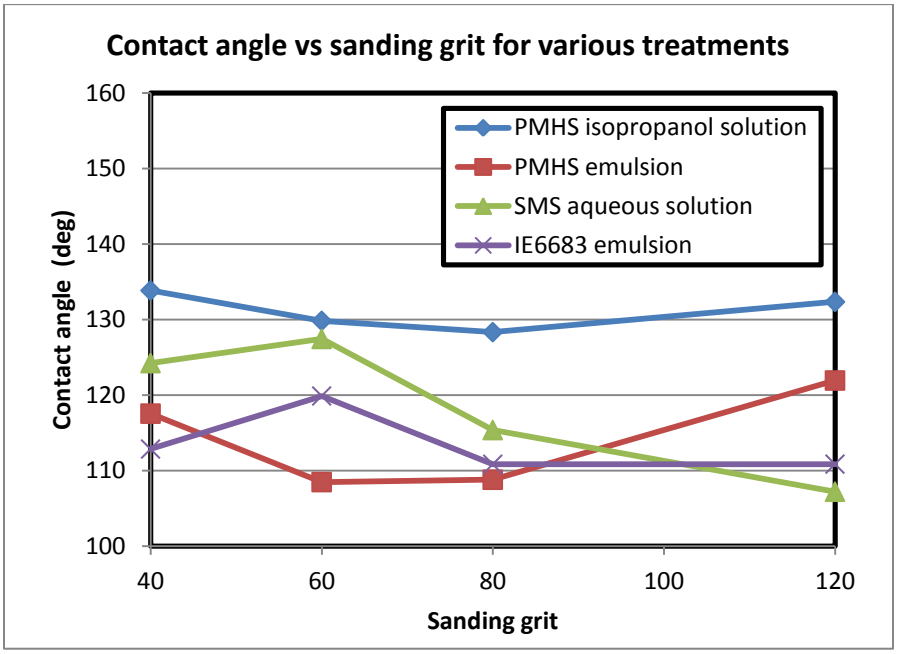

Figure 46 The relationship between contact angle and sanding grit for various treatments

6.7 Correlation of ice loss to contact angle

Plots b through f in Figure 47 scrutinize the high performance region (high contact angle, high ice loss) that in the preliminary studies showed poor correlation between the parameters. As before, the data show that overall, % ice loss was essentially independent of contact angle in this region (Figure 47b). Separating the data by grit shows either a lack of correlation or a decrease in ice loss with increasing contact angle; again, this is in agreement with the preliminary work, showing clustered, poorly correlated data for contact angles greater than 100 degrees. The data for 40 grit and 80 grit sanded tiles had slight negative slopes for ice loss vs. contact angle, with correlation coefficients of 0.70 and 0.46, respectively. Only on the plot that includes all data with

untreated tiles is there a positive slope (Figure 47a), indicating that % ice loss increases with contact angle on a general basis.

There was no sanding method used that stood out as being more or less enlightening than another with the coatings used in this study. Furthermore, the coating specific plots did not show any significant synergistic effects between treatment and sanding method. Manual wet sanding with 60 grit silicon carbide paper is less constrained (no equipment) and, being less dusty, it would be the method of choice for laboratory work; if the equipment is available, sanding can be done on a rotary wet polishing device (commonly used in metallurgical sample preparation.) Since the 120 grit belt sanded surface appeared to be very smooth, its use may pertain better to wear-smoothened surfaces than fresh surfaces and may still have a place in general coating evaluation.

In terms of treatments to pursue, the Dow Corning® IE-6683 was a good performer, but did not have any compelling properties over and above PMHS PVA emulsion and sodium methyl siliconate, which continued to show good performance for ice loss and contact angle and nothing in the results refutes their selection. And as with Dow Corning® 1-6184, the composition of IE-6683 is not clear (see Table 6), making it problematic for furthering an understanding of the interaction between treatment and surface chemistries.

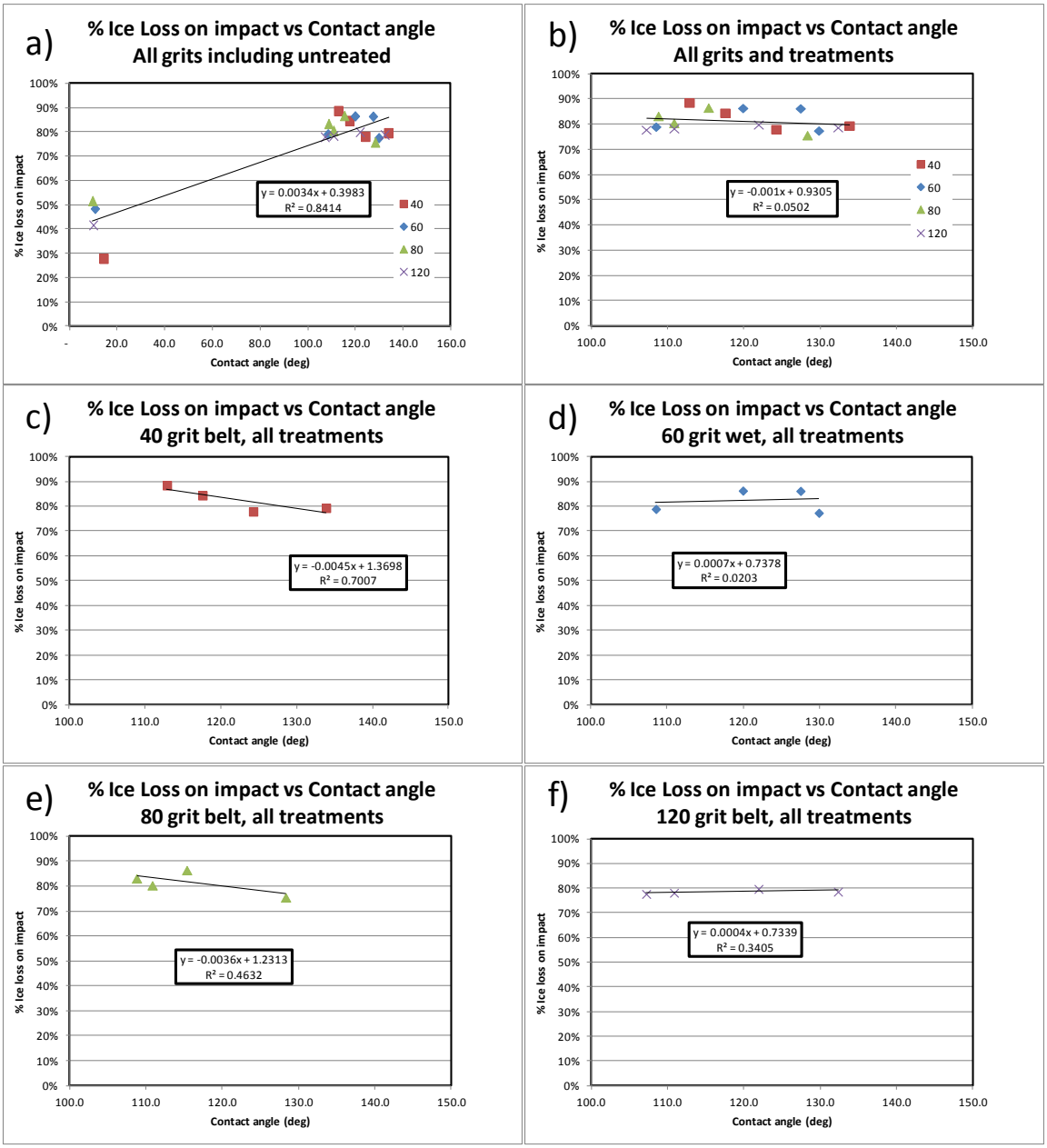

Figure 47 Relationship between Ice loss and contact angle for overall data and by grit

7 The effect of two step water-based treatments on contact angle

Double treatment combinations of PMHS emulsion, IE-6683 emulsion, and SMS aqueous solution and were evaluated without particles for any synergistic effects on hydrophobicity. These were the compelling materials used in section 6 The effect of sanding imparted roughness. The three coatings were used in combinations shown in Table 19, with the indicated dwell times between coating application.

Table 19 Two step coating combinations

Coating 1	Dwell time between coatings (hours)	Coating 2
SMS 3% aqueous solution	1	PMHS 5% PVA emulsion
SMS 3% aqueous solution	24	PMHS 5% PVA emulsion
SMS 3% aqueous solution	1	IE6683 5% emulsion
SMS 3% aqueous solution	24	IE6683 5% emulsion
PMHS 5% PVA emulsion	1	SMS 3% aqueous solution
PMHS 5% PVA emulsion	24	SMS 3% aqueous solution
IE6683 5% emulsion	1	SMS 3% aqueous solution
IE6683 5% emulsion	24	SMS 3% aqueous solution
PMHS 5% PVA emulsion	1	IE6683 5% emulsion
PMHS 5% PVA emulsion	24	IE6683 5% emulsion
IE6683 5% emulsion	1	PMHS 5% PVA emulsion
IE6683 5% emulsion	24	PMHS 5% PVA emulsion

60 grit wet sanded standard mortar tiles were used as the substrate and coatings were applied using the gravimetric surface dose method. In pre-work, it was determined that the 5% sodium methyl siliconate aqueous solution applied as a second coating to a relatively non-porous surface left a white residue, which according to Dow literature is a carbonate precipitate [30]. So a 3% sodium methyl siliconate aqueous solution was

used. Comparisons were first made to examine the effect of this concentration change relative to the previous treatments using 5% concentrations at 60 µl liquid applications. 3% SMS was used various doses, 60 µl, 50 µl, and 40 µl, and compared to the 5% PMHS and IE-6683 results, all on 60 grit wet sanded tiles. These results are shown in Table 20 and Figure 48.

Table 20 Summary of contact angle effects of 3% SMS at various surface dosages

Tilenames Rep1 Rep2	Treatment	Treatment type	Percent active in treatment	Treatment method	Average Coating coverage g/m2	Active coverage g/m2	Average Contact angle (deg)	Std dev Contact angle (deg)
I01 I02	Untreated				0	0.0	10.8	5.3
I05 I06	Polymethylhydrogensiloxane	Isopropanol	5%	60 µl applied	258	12.9	129.9	1.6
I13 I14	Polymethylhydrogensiloxane	Emulsion	5%	60 µl applied	273	13.7	108.5	4.9
I29 I30	Dow Corning® IE-6683	Emulsion	5%	60 µl applied	271	13.5	119.9	4.4
I21 I22	Sodium methyl siliconate	Aqueous	5%	60 µl applied	278	13.9	127.5	1.3
J01 J02	Sodium methyl siliconate	Aqueous	3%	40 µl applied	187	5.6	122.0	3.0
J03 J04	Sodium methyl siliconate	Aqueous	3%	50 µl applied	224	6.7	123.1	0.3
J07 J08	Sodium methyl siliconate	Aqueous	3%	60 µl applied	273	8.2	125.4	3.4

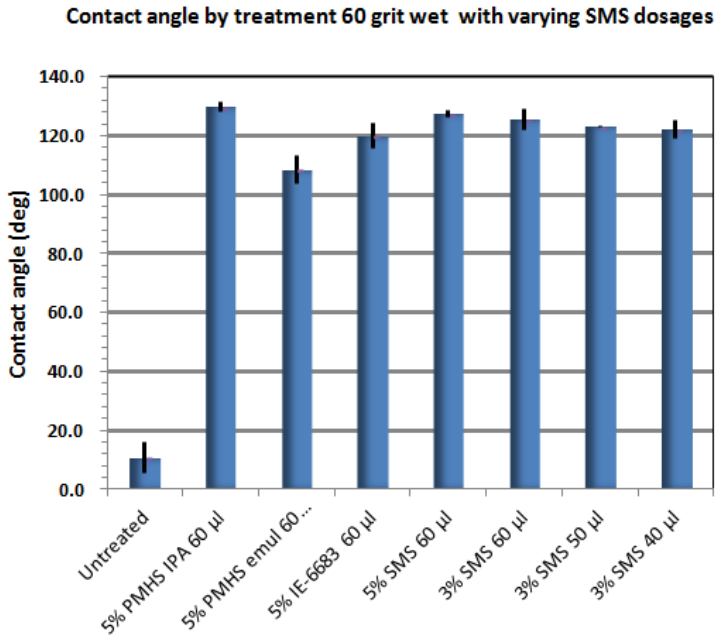

Figure 48 Contact angle effects of 3% SMS at various surface dosages

Spreading the second treatment was somewhat challenging, since even 1 hour after a first coating was applied, the second coating had a fairly high contact angle. Also, the 3% SMS coating used as a second coating still left a slight carbonate residue, which was not removed. The results of two step treatments of 50 µl + 50 µl are shown in Figure 49. Within these results, tiles with 1 hr delay time between coating 1 and coating 2 always gave a higher contact angle than 24 hr delay time.

Table 21 Two step coating coverages and contact angles

Sample (tiles averaged)		Coating sequence	Coating 1 coverage g/m2	Coating 2 coverage g/m2	Contact angle (deg)	
					1 hr	24 hr
J05 J06	J09 J10	SMS, PMHS	226	221	113.5	107.7
J11 J12	J13 J14	PMHS, SMS	231	228	111.8	107.7
J15 J16	J17 J18	SMS, IE-6683	229	222	112.2	103.0
J19 J20	J21 J22	IE-6683, SMS	224	231	113.9	104.9
J23 J24	J25 J26	PMHS, IE-6683	224	228	111.8	108.3
J27 J28	J29 J30	IE-6683, PMHS	224	229	104.7	101.4

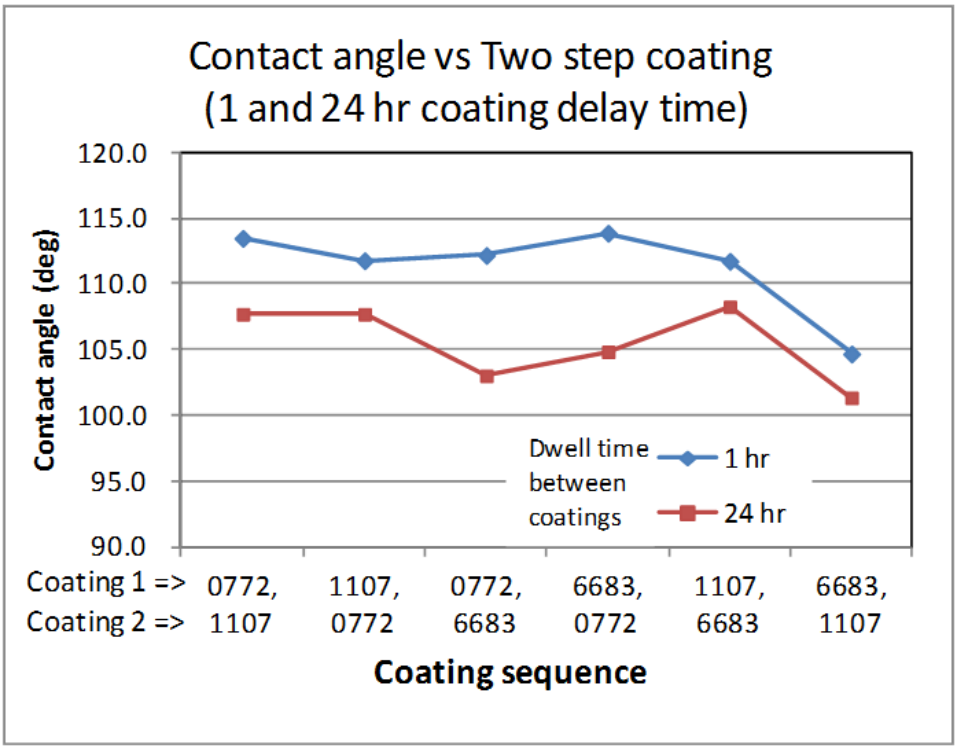

Figure 49 Two step coating results on 60 grit wet sanded standard mortar tiles

SMS and IE-6683 at all single doses examined gave contact angle values on the order of 120 to 127 degrees, while the PMHS single dose gave 109 degrees. For two step treatments, the maximum CA was 113.9. There was nothing compelling in the two step treatment results, especially considering the complexity involved, and PMHS, SMS, and IE-6883 continue to be of interest in terms of contact angle for single step treatments.

8 The effect of mortar mixture and fiber content

Previous examinations in this report used varying treatments on substrate tiles of single composition. In this study, the substrate tiles were varied and the treatment composition fixed, but applied at differing concentrations. The treatment used was a PMHS silica fume particulate shell emulsion, a composition selected from separate hydrophobicity screening. In this screening using standard mortar tiles, emulsion E_{1SR} ,a 5% siloxane shell emulsion (described in section 3.2.10 Emulsion compositions), increased the average contact angle by 10° over E_0, E_{1S}, and E_{1C} emulsions and a similar advantageous effect was observed for the roll-off angle.

This mortar mix study had the following objectives:

- Examine the effects of varying mortar composition and fiber content, and the resulting imparted roughness using PMHS/silica fume emulsion on superhydrophobicity and icephobicity
- Examine the effect of high/low concentrations of active PMHS/silica fume in the treatment emulsion on superhydrophobicity and icephobicity

8.1 Substrate M-series tiles

Adding sand and fibers to Portland cement, a fine powder, imparts two morphologies of roughness. Increasing the water to cement ratio tends to increase the porosity of the resulting mortar [7]. In this study, the M series tiles were used: M1-M5 all had a PVA fiber content of 1% by volume with w/c ratios ranging from 0.25 to 0.5 and s/c ratios

from 0 to 3; M6-M10 were a complementary set that had the same composition as M1-M5 , but without fibers. The mortar mix formulations are shown in above in Table 4 (section 3.1.5 Preparation of substrate tile specimens: Standard and M series)

8.2 Emulsion materials

In separate work, it was determined that shell type emulsions were the more compelling particulate bearing treatments; factors in this selection included emulsion stability and contact angle hydrophobicity. In this study, the shell emulsions E1S and E1SR with 25 and 5% of PMHS, respectively, were used, with aqueous PVA solution as the continuous phase, and silica fume (SF) as the particulate. (For details, see 3.2.10 Emulsion compositions and 4.6.3 Shell type emulsion preparation). For application of the treatment, the volumetric surface dosage method was used with 10 µl of treatment. The specimens were allowed to dry at a room temperature for 48 hours before contact angle measurements were made. % Ice loss measurements were made on separate replicated sets of tiles.

8.3 Contact angle and % ice loss

Due to the high water absorption, the contact angles for uncoated specimens were very small, generally less than 15 degrees. Uncoated specimens absorbed most of the water since Portland cement based materials are hydrophilic, so the roll off angle could not be measured for these tiles. The contact angles were comparable to the preliminary results on plain mortars without fibers.

The ice loss on impact and contact angle results are shown in detail and summary form below in Table 22, Table 23, Table 24, and Figure 50. Images of the tiles after impact are shown in Figure 51 and Figure 52. The full set of before and after images is presented in Appendix: Images for ice loss on impact for M series tiles.

Table 22 % ice loss on impact with contact angle data

Tile	Theta mean Untreated [deg]	% Ice Loss Untreated Ave	% Ice Loss Untreated Std Dev	Ave Theta mean 5% treatment [deg]	% Ice Loss 5% treatment Ave	% Ice Loss 5% treatment Std Dev	Ave Theta mean 25% treatment [deg]	% Ice Loss 25% treatment Ave	% Ice Loss 25% treatment Std Dev
	Untreated	Untreated	Untreated	5% Treatment	5% Treatment	5% Treatment	25% Treatment	25% Treatment	25% Treatment
M01	8.5	52%	14%	143.7	86%	6%	120.3	74%	13%
M02	9.8	46%	6%	145.4	84%	4%	118.6	59%	18%
M03	0.0	50%	8%	141.4	83%	5%	121.7	76%	13%
M04	0.0	21%	9%	123.6	75%	13%	128.2	79%	3%
M05	25.5	76%	2%	132.7	80%	10%	128.4	75%	7%
M06	10.0	32%	13%	141.4	88%	7%	110.3	64%	8%
M07	14.2	70%	2%	141.0	88%	4%	115.6	76%	4%
M08	5.3	77%	1%	141.3	83%	1%	129.9	71%	3%
M09	0.0	48%	8%	140.0	87%	1%	123.8	72%	12%
M10	0.0	65%	5%	136.3	77%	12%	127.0	68%	12%
Average	7.3	54%	7%	138.7	83%	6%	122.4	71%	9%

Table 23 Summary of compositions with roll off angle

				Roll-off angle (deg)	
Tile	**Fiber content (Vol %)**	**Sand content (s/c)**	**Water content (w/c)**	**5% Treatment**	**25% Treatment**
M01	1%	0	0.25	2.4	90.0
M02	1%	1	0.3	1.0	81.2
M03	1%	2	0.4	5.9	66.0
M04	1%	2.5	0.45	7.9	58.5
M05	1%	3	0.5	11.7	62.4
M06	0%	0	0.25	4.1	56.5
M07	0%	1	0.3	7.5	61.3
M08	0%	2	0.4	4.4	63.0
M09	0%	2.5	0.45	14.4	57.6

Table 24 Overall average table and plot

Tile	Theta mean Untreated [deg]	% Ice Loss Untreated Ave
Untreated average	7.3	54%
5% Treatment average	138.7	83%
25% Treatment average	122.4	71%

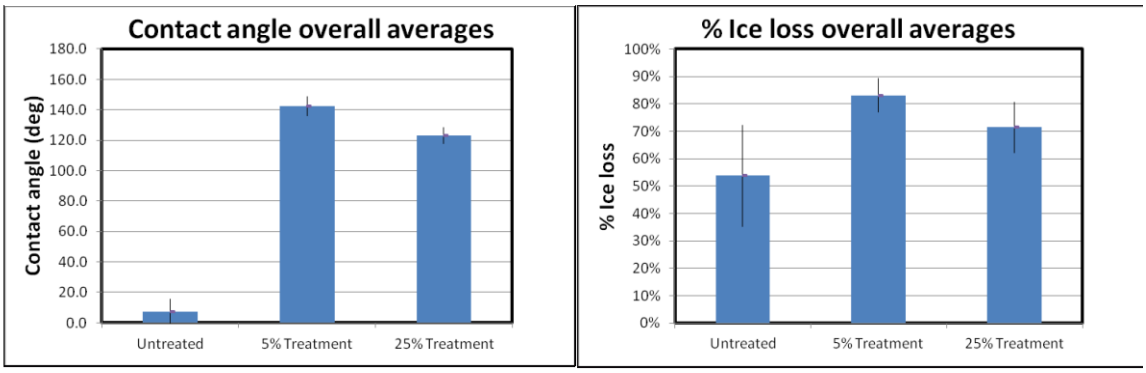

Figure 50 Overall contact angle and % ice loss

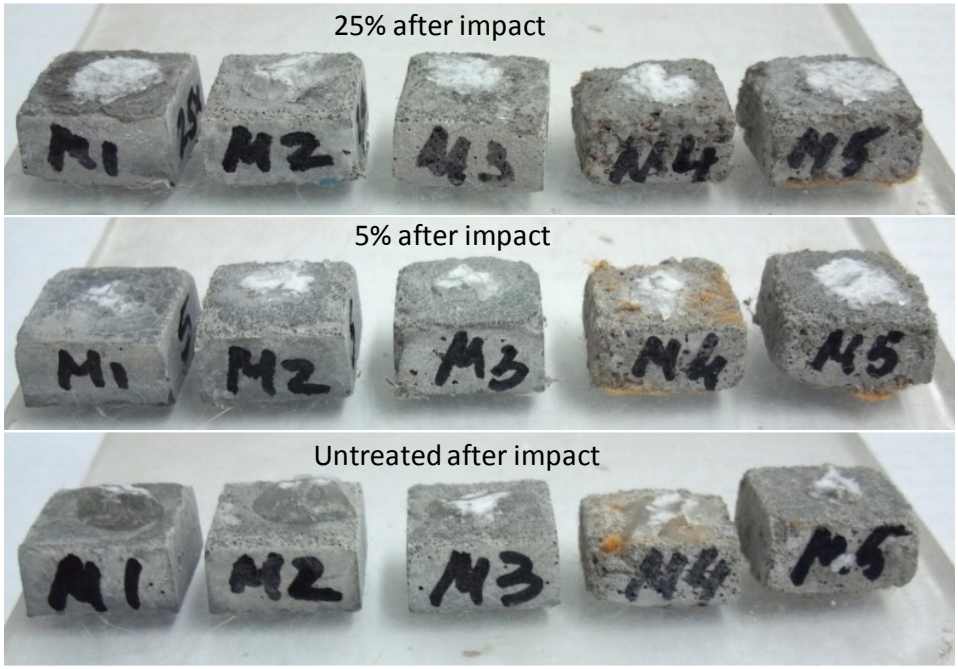

Figure 51 After ice impact M01-M05 with fibers

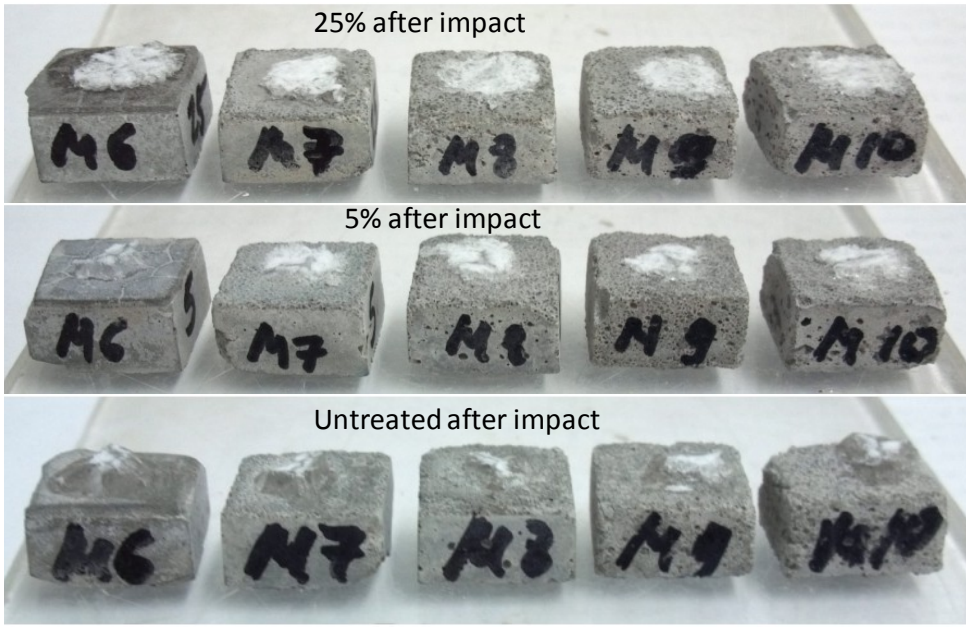

Figure 52 After ice impact M06-M10

8.4 The relationship between % ice loss on impact, contact angle, and roll-off angle

As mentioned, when conducting contact angle measurements on untreated tiles, there is an absorption effect during drop equilibration with the surface, not only surface wetting is taking place. One might question the validity of any contact angle result when most of the drop has “disappeared” into the pores rather than spread on the surface. So while Figure 53 shows the full set of data with central tendencies, the untreated data were highly influenced by porosity, while the treated tile results were not, making the argument to examine the treated data alone.

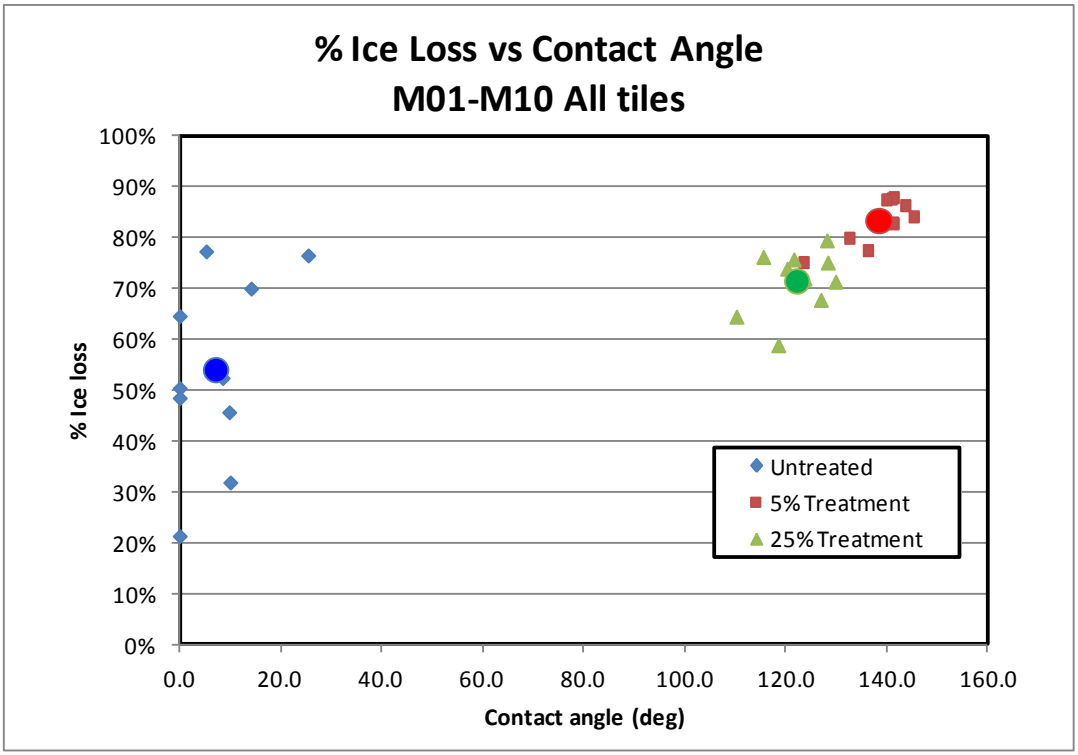

Figure 53 % Ice loss vs. contact angle for all tiles

Examining the treated tile results (Figure 54) a correlation can be seen between icephobicity and contact angle. Decomposing the overall plot into data with and without fibers (Figure 55) shows that, overall, this relationship is essentially unaffected by fiber content, with small shifts as discussed below. Icephobicity also increases with decreasing roll off angle (Figure 56). Linear fits have correlation coefficients of 0.68 for % ice loss vs. contact angle and 0.58 for % ice loss vs. sin(roll off angle).

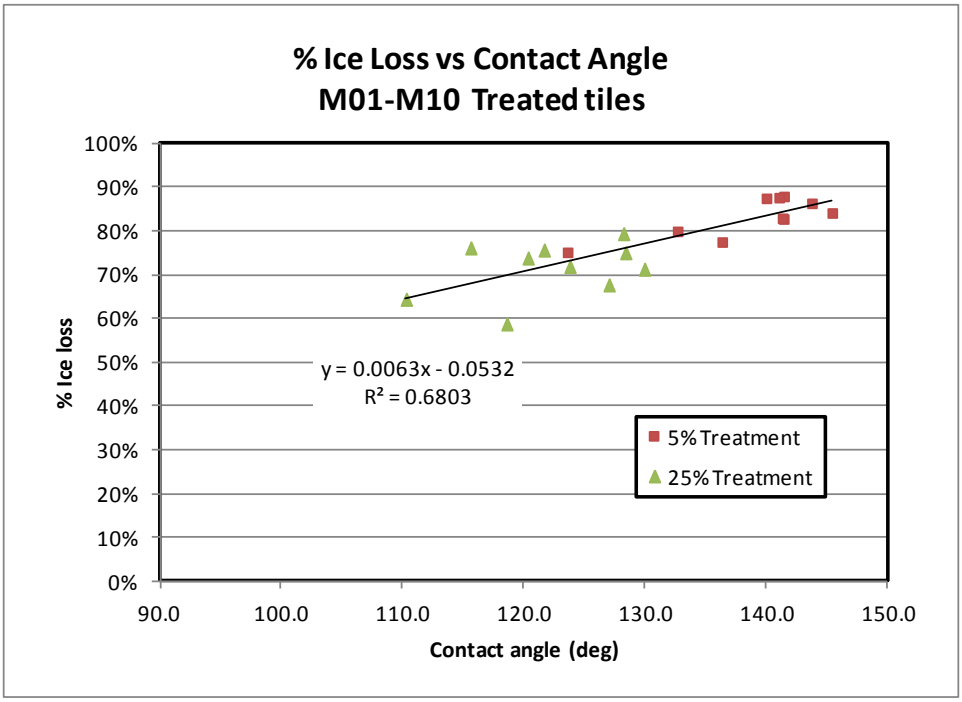

Figure 54 A comparison of % ice loss for all treated tiles vs. contact angle

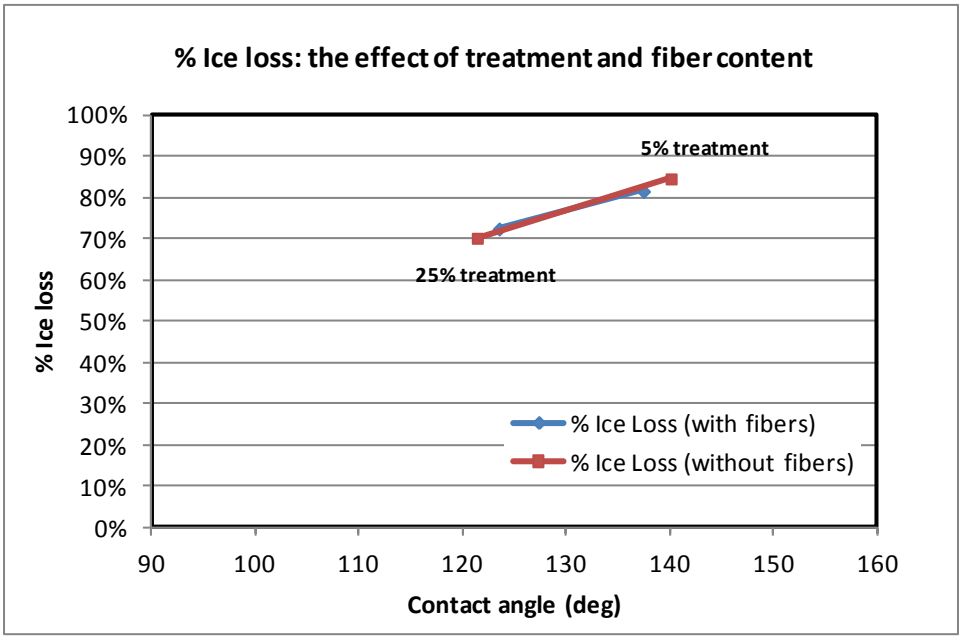

Figure 55 The effect of fiber content and treatment level on ice loss

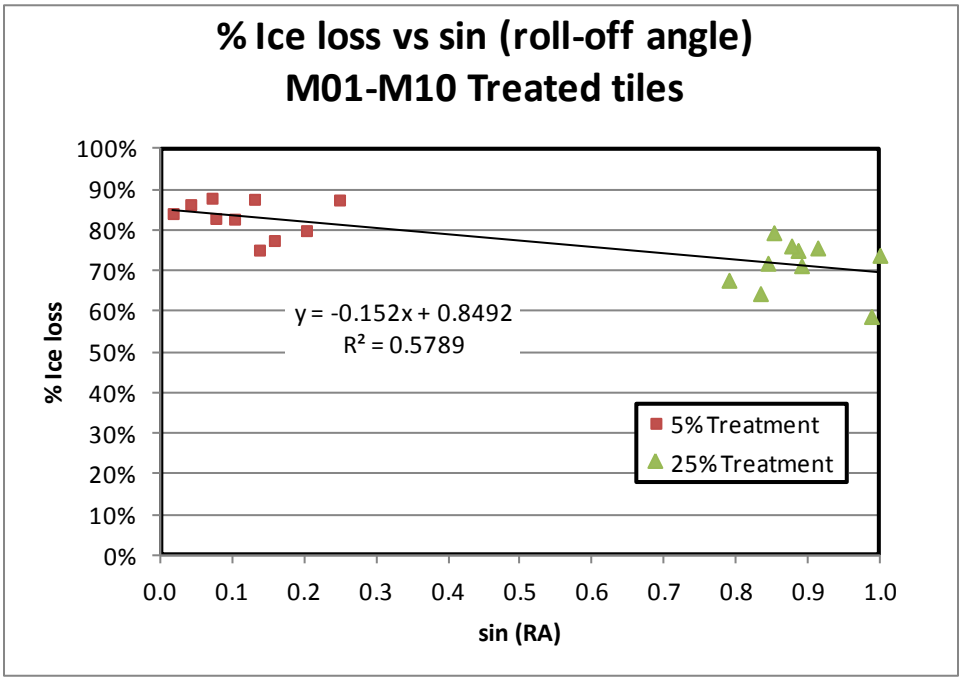

Figure 56 The relationship between % ice loss and roll off angle

8.5 The effect of fibers

The effects of fiber along with sand content are charted in Figure 57. With the addition of fibers, both contact angle and % ice loss decreased slightly for 5% treatment and increased slightly for 25% treatment (Table 25). The amount of active treatment material itself had a larger influence than fiber content, with the 5% treatment having on average 11-15% ice loss higher than 25% treatment.

Fibers had a small effect on roll off angle hydrophobicity, with values 2 degrees lower on average when fibers were present with 5% treatment (Figure 59.) (Though there was

an average 14 degrees worsening of roll off angle with 25% treatment, none of these tiles had good roll off angles.)

Table 25 Results summary, with and without fibers

	with fibers			without fibers		
Tile treament	**Theta mean [deg]**	**Roll-off angle (deg)**	**% Ice Loss**	**Theta mean [deg]**	**Roll-off angle (deg)**	**% Ice Loss**
Untreated	8.8		49%	5.9		58%
25% Treatment	123.9	71.6	73%	122.4	58.1	70%
5% Treatment	141.5	5.8	82%	143.4	7.9	85%
25% Treatment	1.5	13.5	2%	**<< deltas when fibers were used**		
5% Treatment	-1.9	-2.1	-3%			

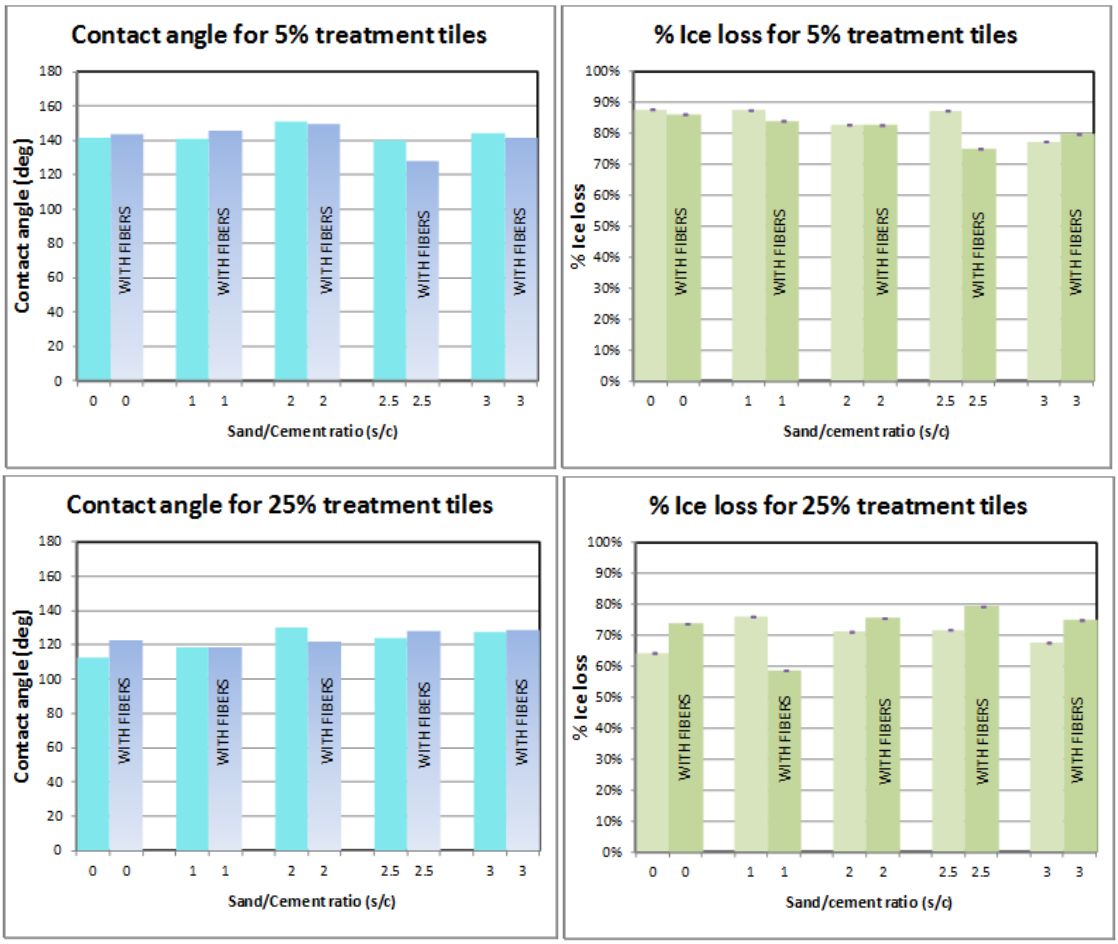

Figure 57 Effect of fibers and sand on contact angle and % Ice loss

8.6 The effect of sand content

Contact angle was essentially independent of sand content, as shown in Table 26 and Figure 58. The effect of sand content also had a statistically insignificant effect on % ice loss for treated tiles; increasing s/c from 0 to 3% for 5% treated samples gave an 8% drop in % ice loss, which was essentially similar to the standard deviation, which ranged from 3 to 11% for the various sand contents. Untreated tiles showed larger shifts in % ice loss as s/c is varied; the 2.5 s/c untreated tiles had markedly reduced % ice loss

possibly explained by their visually apparent higher porosity. It could then be said that the treatments tended to both increase and stabilize % ice loss relative to untreated tiles.

Table 26 Data averaged by sand content

Tile	Sand content (s/c)	Water content (w/c)	Theta mean [deg]	% Ice Loss Ave	% Ice Loss Std Dev	Theta mean [deg]	% Ice Loss Ave	% Ice Loss Std Dev	Theta mean [deg]	% Ice Loss Ave	% Ice Loss Std Dev
			Untreated	Untreated	Untreated	5% Treatment	5% Treatment	5% Treatment	25% Treatment	25% Treatment	25% Treatment
M01/M06	0	0.25	9.3	42%	14%	142.6	87%	7%	117.7	69%	10%
M02/M07	1	0.3	12.0	58%	4%	143.2	86%	4%	118.6	67%	11%
M03/M08	2	0.4	2.6	64%	4%	150.1	83%	3%	125.8	73%	8%
M04/M09	2.5	0.45	0.0	35%	8%	133.9	81%	7%	126.0	76%	7%
M05/M10	3	0.5	12.7	70%	4%	142.7	79%	11%	127.7	71%	10%

Charts for hydrophobicity as measured by roll-off angle are shown in Figure 59. Sand content had a smaller effect on the roll-off angle than the emulsion concentration. Roll-off angles of specimens with 25% emulsion were in the range of 50 to 65 degrees, while 5% emulsion values were dramatically lower, in the range of 4 to 15 degrees. For 25% treated tiles, at s/c = 0, it appears that the presence of fibers increased the roll-off angle hydrophobicity by over 30 degrees, but with the addition of sand the values decreased dramatically back to the fiber-free levels. Sand and fiber showed the opposite behavior for the 5% treatments, where the addition of sand had a marginally detrimental effect and fibers had a similarly marginal beneficial effect.

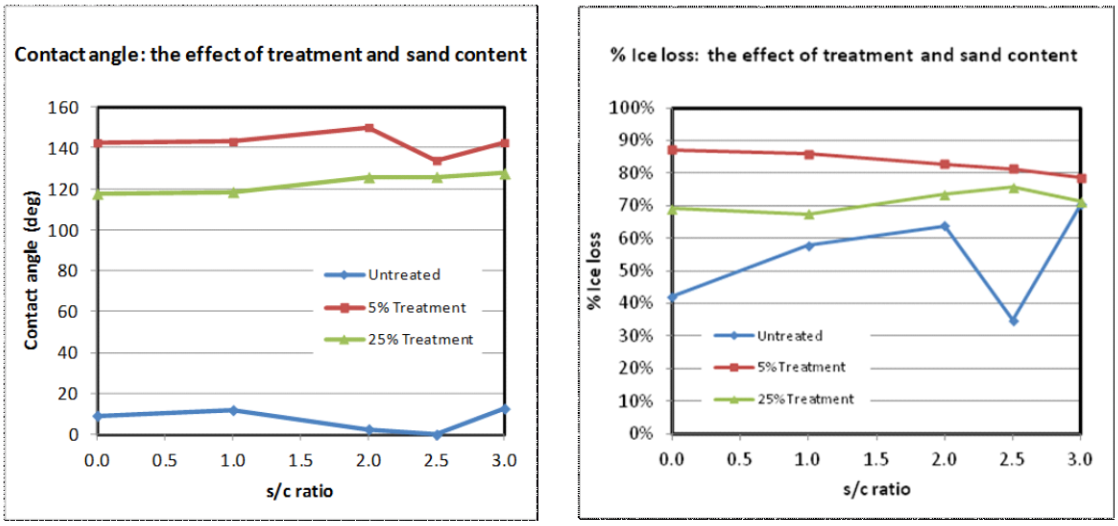

Figure 58 Contact angle and % Ice loss vs. sand to cement ratio

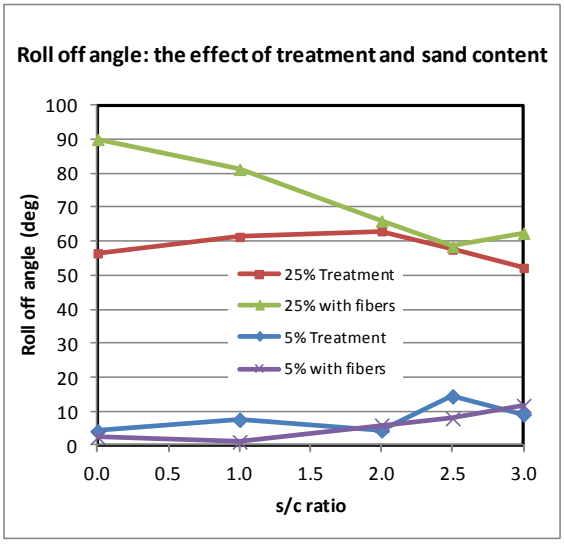

Figure 59 Roll off angle vs. sand to cement ratio

8.7 Tile surfaces - scanning electron micrographs

The SEM images give indications as to why the 25% treated tiles did not perform as well as the 5% treated tile. As before, the images are of unsputtered tiles, and the effects of charging can be seen; in some cases, due to the significant charging after focusing, the

SEM chamber had to be vented to allow dissipation of charge, evacuated again, the beam turned back on, and an image quickly captured. This was required generally in the 25% treatment tiles and the M4 fiber-bearing tile with 5% treatment. The fibers and high levels of coating, being essentially non-conductive, led to the most charging.

In all images, it can be seen that for the 25% treatments, there was a significant coating layer on the tiles that essentially eliminating any roughness advantages (depicted schematically in Figure 7 and Figure 8 above) and reducing hydrophobic properties. In this case, the reduction in hydrophobicity corresponded with a reduction in % ice loss.

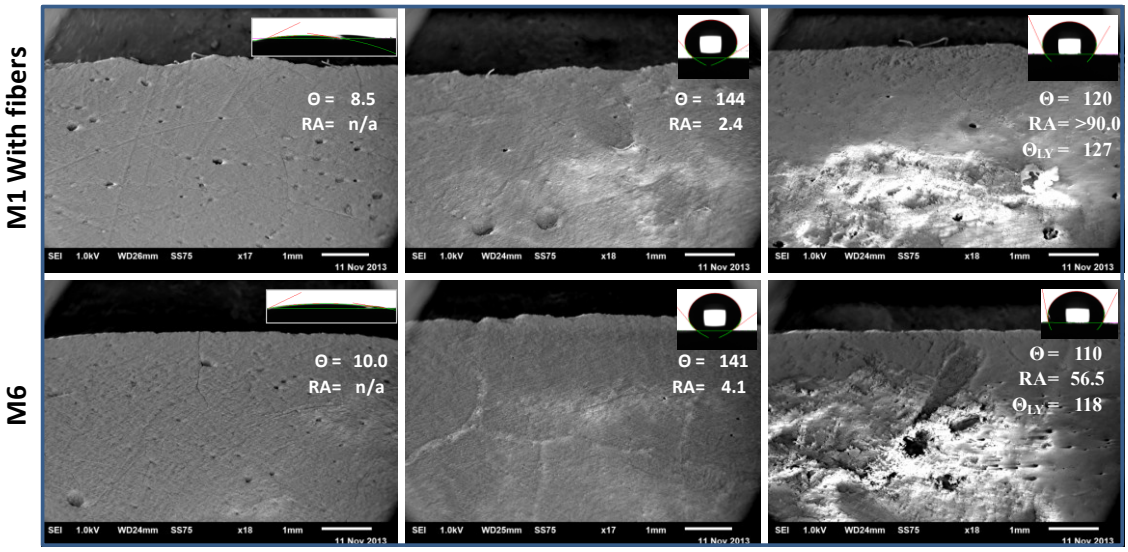

Figure 60 SEM: Sand and fiber effect s/c = 0

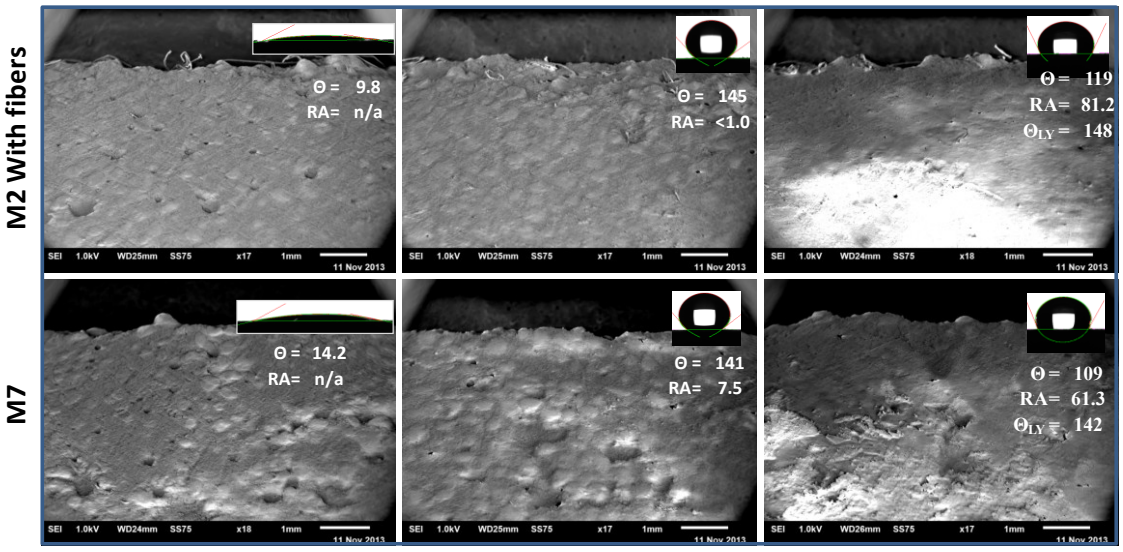

Uncoated 5% Treatment 25% Treatment

Figure 61 SEM: Sand and fiber effect s/c = 1.0

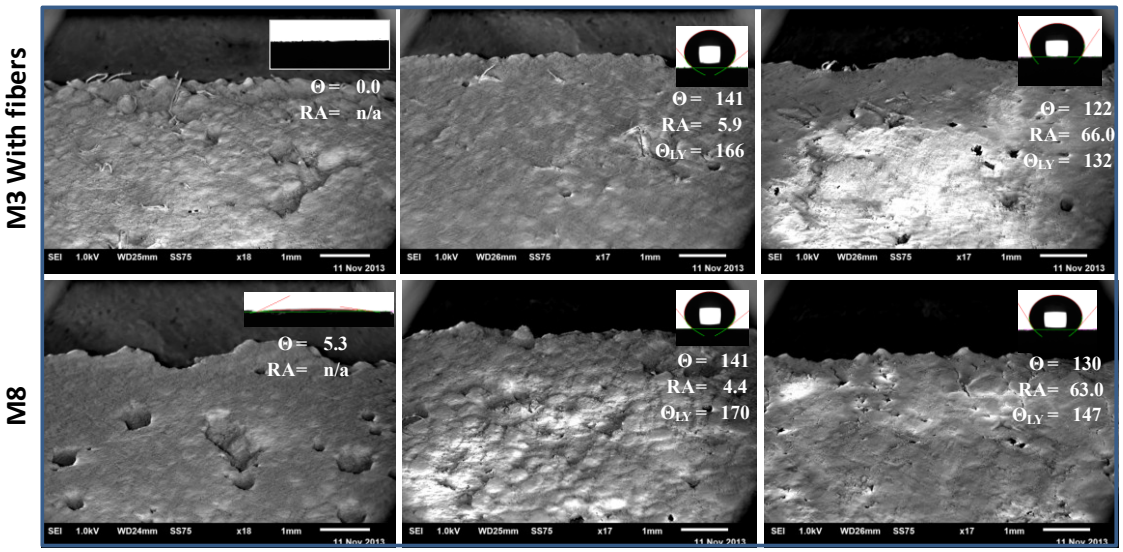

Uncoated 5% Treatment 25% Treatment

Figure 62 SEM: Sand and fiber effect s/c = 2.0

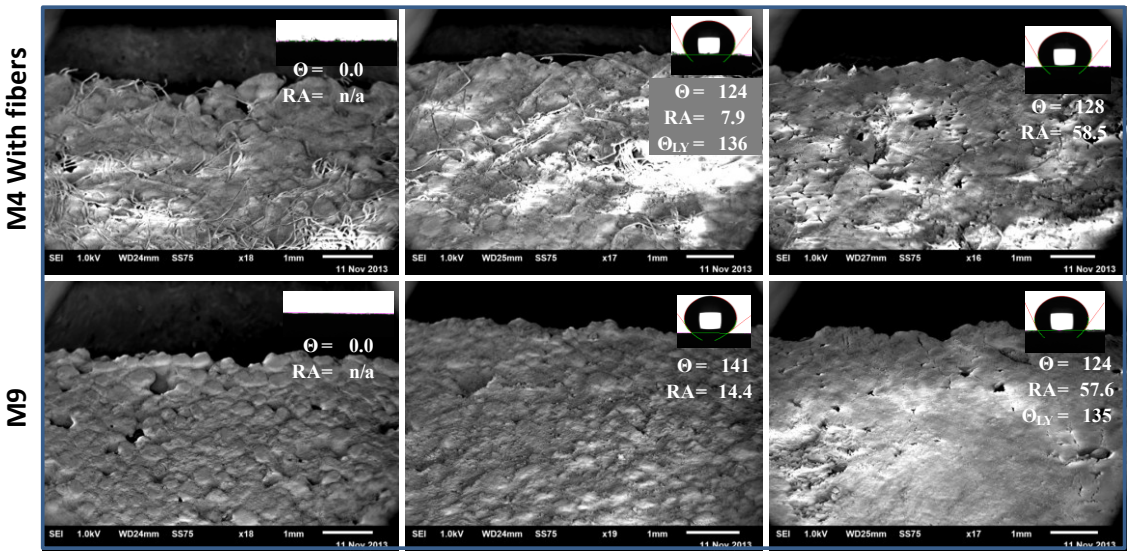

Uncoated 5% Treatment 25% Treatment

Figure 63 SEM: Sand and fiber effect s/c = 2.5

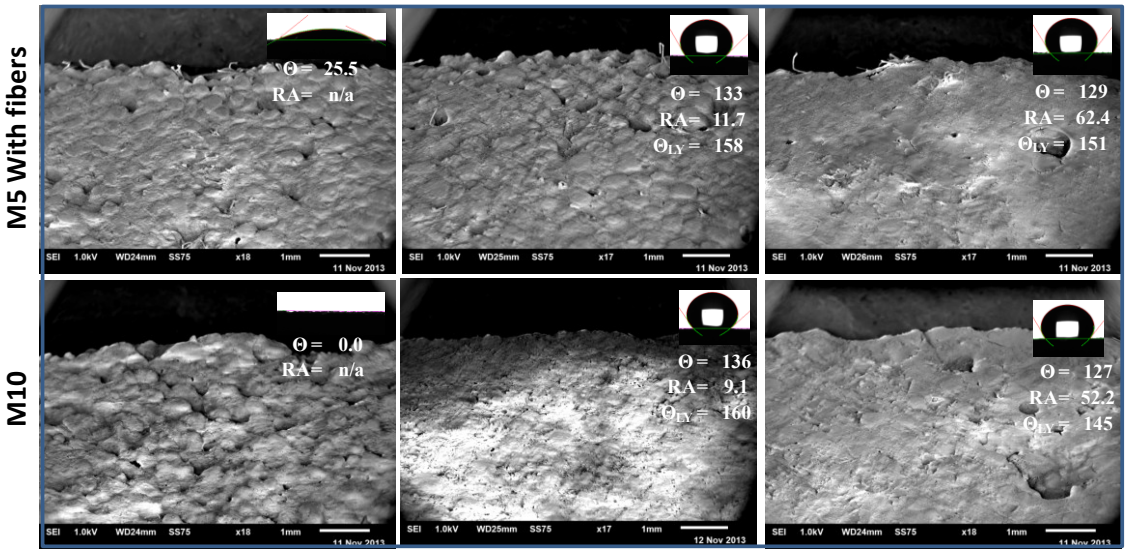

Uncoated 5% Treatment 25% Treatment

Figure 64 SEM: Sand and fiber effect s/c = 3.0

9 Discussion of contact angle fit models used in the study

Krüss software was used to determine contact angles (Θ_L left, Θ_R right, and Θ_M mean) using drop images. Contact angle determination requires definition of the baseline and detection of the drop profile in the vicinity of the drop base. For this project, in all cases, the baseline was selected manually, because automatic detection often gave nonsensical results. The Krüss Drop Shape Analysis software used had four drop profile detection options available, as shown in Table 8 above. The circular arc method (CIR) pertains to low contact angles, less than 20 degrees, and was used in some cases for untreated tiles. Tangent-1 (T-1) considers the whole drop profile in the image and finds the best conic section fit (ellipse); a symmetrical drop is not required and the fitted ellipse may appear rotated relative to the baseline. Tangent-2 (T-2) examines the drop profile in the vicinity of the drop base and finds the best polynomial fit, giving separate fits for left and right contact angle. The remaining profile detection model available, Laplace-Young (L-Y), detects the drop surface contour and uses mathematical modeling to consider the sagging that occurs in a droplet due to its inherent weight.

For each measurement made, the quality of the profile fit and the computed contact angle was assessed by visually examining the result – upon analysis, the software reports depiction of the result superimposed on the drop image. In most all cases, T-1 and T-2 gave the most valid results. In a few cases, the L-Y fits were interesting, at times giving compelling droplet profile fits in the vicinity of the base. Figure 65 shows the raw image along with analysis results for tile M05 with 5% treatment.

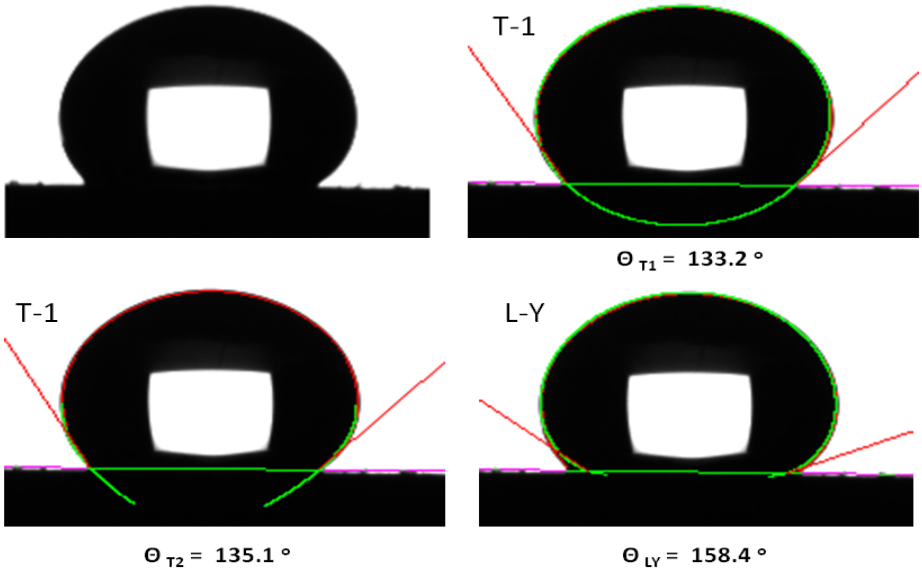

Figure 65 Droplet profile fits and contact angle results for M05 with 5% treatment

Partly due to the lack of symmetry in this drop, the L-Y profile fit looks reasonable for the right, but does not look good for the left side; the right contact angle seems slightly high, but the left is clearly higher than it should be. In addition to the drop and tile geometries, image quality along with the software algorithm's fitting capability play a role in the quality of the computed tangent line. Taking a closer look at the same drop, using T-1 and T-2, Θ_R appears to be valid, while Θ_L appears to be slightly low (Figure 66.)

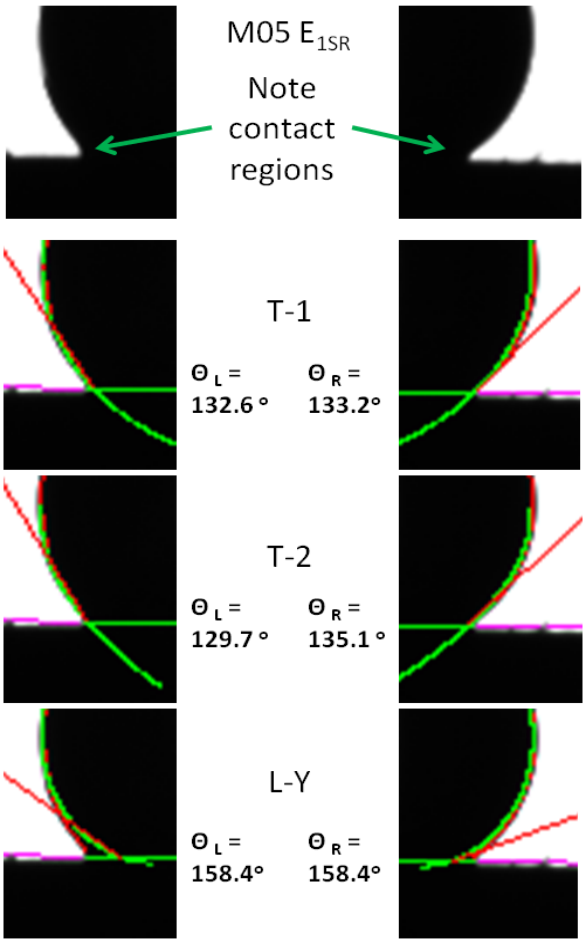

Figure 66 Zoomed contact angle results for M05 5% treatment

Figure 67 shows the corresponding zoomed images for M08 with 5% treatment. The assessments for T-1 and T-2 are similar to M05 with 5% treatment, and Θ_R appears to be valid, while Θ_L appears to be slightly low. L-Y with a contact angle of 165.6^o appears to be close on the left and overstated on the right.

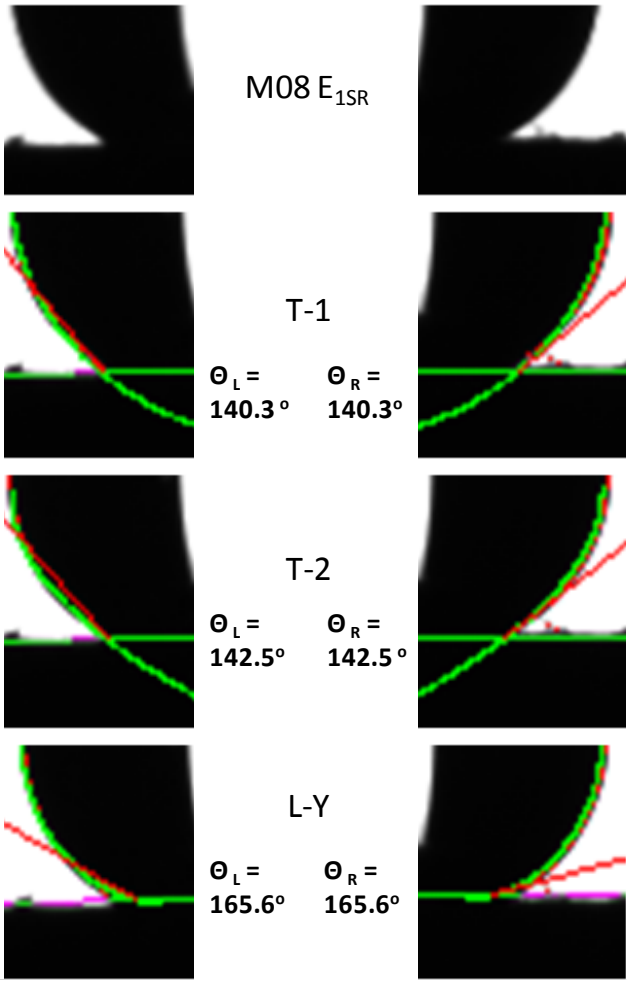

Figure 67 Zoomed contact angle results for M08 5% treatment

These tile results are presented as an example of fit challenges faced throughout the study. There were a number of tiles with high end contact angles for which the T-1 and T-2 fits used did not visually look sufficiently high. In the interest of reporting conservative values, none of the values or averages used the L-Y fit results, though in some cases an argument could have been made to include them. If they were included, some of the visually valid L-Y fits would have taken contact angle average values over 150 degrees and into the superhydrophobic category.

10 Conclusions

1. Material effectiveness and achieving superhydrophobicity

For ordinary emulsions and solutions, PMHS PVA emulsion and sodium methyl siliconate solution showed good performance for ice loss and contact angle. In screening without particles, though PMHS in isopropanol consistently gave better contact angles (by approximately 15 degrees) it gave statistically the same ice loss values relative to its PMHS PVA emulsion counterpart; the use of PMHS in emulsion form remains viable. Furthermore, in separate hydrophobicity screening on standard mortar tiles, a 5% PMHS PVA shell emulsion with silica fume particulates increased the average contact angle by 10° over simple and core emulsions and showed equivalent improvement in roll-off angle. The PMHS molecular structure has multiple -Si-H sites that can bond to sites on concrete and this material may form a better attached film.

According to Dow Corning, the sodium methyl siliconate "reacts with moisture and carbon dioxide in the air to form an insoluble water-resistant resin."[30] No mechanism was provided for the reaction, but polymerization probably occurs because the $Si\text{-}O^-$ group is quite polar and "kinetically very reactive under ionic conditions." [69]. Given its compact size, SMS likely has excellent mobility and is suited to function like a crosslinking monomer, with potential to react at its ionic site (-ONa) and its hydroxyl sites.

Dow IE-6683 (SADTE/octyltriethoxysilane mixture) may be a candidate worth pursuing, but it did not have any compelling properties over and above PMHS PVA emulsion and sodium methyl siliconate.

Examining the structures of PMHS and SMS, and IE-6683 components, it is apparent that these materials are better suited for bonding to cementitious materials and potentially crosslinking than some of the other materials evaluated. The structure for methoxy-terminated aminosilsesquioxanes appears to bulky, regardless of what isomeric form is in valid (Figure 23) and the unknown number of functional sites for bonding and film-forming could be low, so steric hindrance may play a large role in its poor performance. Hexamethyldisilazane is likely mobile, like SMS, but once the S-N site has reacted, the relatively inert silicon-methyl sites are left, essentially eliminating a crosslinked film-forming effect. It appears that the other silane type materials did not perform too well, by inference possibly because their –Si-alkoxy sites are not as reactive as -ONa, -Si-H, and $–SiO_3$ on SMS, PMHS, and SADTE, respectively. In terms of crosslinking, the alkene on vinyltrimethoxysilane is suited to polymerize under the correct conditions, but is unlikely to react with cementitious materials in the conditions used in this study.

But none of the treatments achieved superhydrophobicity in terms of contact angle but the shell emulsions were close, reaching 145 degrees. The contact angle computation via image analysis can contribute to the numerical value, positively or negatively, by several degrees. Use of the Laplace-Young fit can result in higher contact angle values. 20 µl drops were used in this study - Figure 68 shows analyses performed on a single 60

µl drop image. T-1 and T-2 fits give 136^0 and 147^0, respectively using the same baseline, while using the L-Y fit and same baseline gives 172^0. Adjusting the baseline upwards (Figure 68 e and f) gives L-Y fits that look more reasonable, ranging from 161^0 to 165^0.

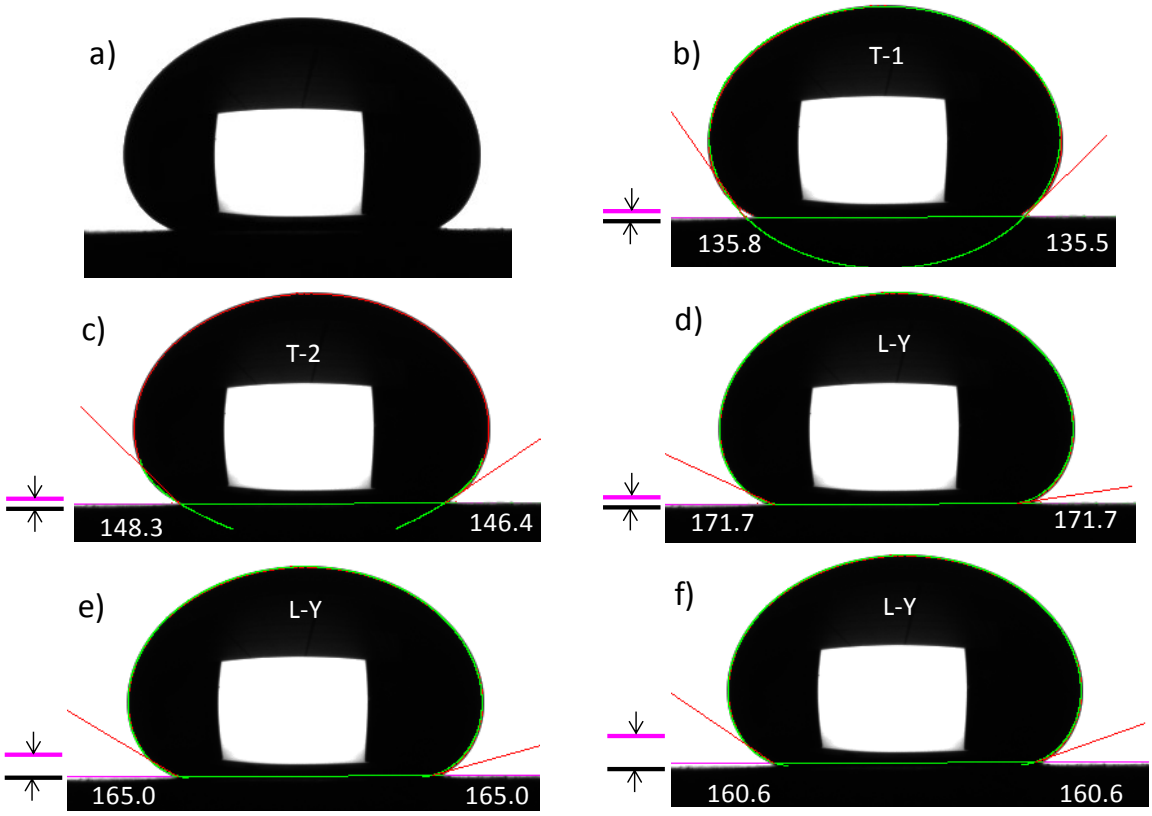

Figure 68 Contact angle fit dependency on the model and baseline selected using a 60 µl drop: a) raw image; b-d) fixed baseline varying models; e-f) increasing baseline

Presumably, the higher drop volume of 60 µl experiences a higher gravitational sagging effect, making the L-Y fit visually better. Use of different drop volumes and other drop analysis tools may have given different results.

2. Quantification of icephobicity and the correlation to hydrophobicity

The falling rod impact test for icephobicity gave fairly consistent results and appears to be a reasonable tool for screening materials or testing small samples. The standard tiles treated with PMHS isopropanol solution were evaluated in separate test sets in this report and on different days; the results were found to be quite repeatable, with contact angle values of 131 ^{o}, 135 ^{o}, and 134^{o} and corresponding ice loss values of 77%, 82%, and 78%, respectively.

The % ice loss on impact vs. contact angle plot showed a strong general relationship between icephobicity and hydrophobicity, with a correlation coefficient of 0.93 for the materials used (40 grit tiles treated with solutions). At least for concrete, this indicates that hydrophobicity can generally be predictor for icephobicity, as measured by the falling rod ice impact.

A good correlation was seen between icephobicity and hydrophobicity for the PMHS/silica fume shell emulsions on mortar mixes with varying sand and fiber content: % ice loss increased with increasing contact angle and also increased with decreasing roll off angle.

However, all studies showed clustered and poorly correlated data within subsets of contact angles greater than 100 degrees. This points to an insufficient sensitivity in the falling rod ice impact test at high % ice loss, possible error in the contact angle

computations or the influence of other factors, such as roughness and surface morphology.

3. Roughness and surface morphology

If roughness and surface morphology parameters were quantified, the clustered data at contact angles greater than 100 degrees could perhaps be better understood. Rankings for Ice loss values for the various treatments differed depending on what grit was used, but on the 120 grit smooth tiles, it became more difficult to differentiate between PHMS, sodium methyl siliconate, and IE-6683 (SADTE/octyltriethoxysilane mixture), indicating roughness is a factor.

At the levels studied, water, sand and fiber content had negligible or marginal effects on hydrophobicity and % ice loss for treated tiles.

Future work

Topics for future work that warrant consideration:

- Better characterization of surface morphology and roughness.
- Examination of the contact angle fit models, including the influence of droplet size, influence of the image baseline, camera elevation and angular perspective on the droplet, and image quality.
- Emulsion formulations that can be handled and applied in winter
- Examination of the coating reactions: film-forming and cementitious bonding.

References

[1] "Icy Road Safety, www.icyroadsafety.com," [Online].

[2] R. Robinson and S. Jones, "Ice detection and avoidance," *International Oil Spill Conference, IOSC 2005,* pp. 9570-9573, 2005.

[3] R. R. Blackburn, K. M. Bauer, D. E. Amsler, S. E. Boselly and A. D. McElroy, "Snow and Ice Control: Guidelines for Materials and Methods," *NCHRP REPORT 526, Transportation Research Board,* 2004.

[4] S. A. Ketcham, L. D. Minsk, R. R. Blackburn and E. J. Fleege, Manual of Practice for an Effective Anti-Icing Program-Guide for Highway Winter Maintenance Personnel, US Army Cold Regions Research and Engineering Laboratory Corps of Engineers, 1996.

[5] E. Cuelho, J. Harwood, M. Akin and E. Adams, "Establishing Best Practices of Removing Snow and Ice from California Roadways," *Report No. CA10-1101, Western Transportation Institute - Montana State University,* December 2010.

[6] Wisconsin Transportation, "Using Salt and Sand for Winter Road Maintenance Wisconsin Transportation Bulletin No. 6," *http://epdfiles.engr.wisc.edu/pdf_web_files/tic/bulletins/Bltn_006_SaltNSand.pdf,* August 2005.

[7] K. Sobolev, *Properties of Concrete, Civ Eng 731 class handouts, Unversity of Wisconsin - Milwaukee,* 2011.

[8] L. Zhuravlev, "The surface chemistry of amorphous silica. Zhuravlev model," *Colloids and Surfaces A: Physicochemical and Engineering Aspects ,* no. 173, p. 1–38, 2000.

[9] N. Yaroslavsky, *Dissertation, Cand. Phys.-Math. Sc., GOI, Leningrad, 1948.*

[10] N. Yaroslavsky, *Zh. Fiz. Khim. 24 (1950) 68..*

[11] G. N. L.N. Kurbatov, *Dokl. Akad. Nauk SSSR 68 (1949) 34.*

[12] Y. Liu, "Super-hydrophobic surfaces from a simple coating method: A bionic nanoengineering appoach," *Nanotechnology,* vol. 17, pp. 3259-3263, 2006.

[13] M. Nosonovsky, "Multiscale roughness and stability of superhydrophobic biomimetic interfaces," *Langmuir,* vol. 23, no. 6, pp. 3157-3161, 2007.

[14] I. Flores-Vivian, V. Hejazi, M. Nosonovsky and K. Sobolev, "Self-assembling particle-siloxane coatings for superhydrophobic concrete," *ACS Applied Materials & Interfaces,* no. Submitted, 2013.

[15] M. Nosonovsky and B. Bhushan, "Hierarchical roughness makes superhydrophobic states stable," *Microelectronic Engineering,* vol. 84, no. 3, pp. 382-386, 2007.

[16] K. Sobolev and M. Ferrada-Gutiérrez, "How Nanotechnology Can Change the Concrete World: Part 2," *American Ceramic Society Bulletin,* vol. 11, pp. 16-19, 2005.

[17] K. Sobolev and V. Batrakov, "The effect of "PEHSO" on the durability of concrete with supplementary cementitious material; Nanomaterials and nanotechnology for high-performance cement composites (SP-254-8), Nanotechnology of Concrete: Recent Developments and Future Perspectives, K. Sobolev & S. Shah (Eds.), Farmington Hills, MI, USA," *ASCE Journal of Materials in Civil Engineering,* vol. 19(10), pp. 809-819; 93-120, 2007; 2008.

[18] B. Poole, *Biomimetics: Borrowing from biology,* http://www.thenakedscientists.com/HTML/articles/article/biomimeticsborrowingfrombiology/,

[19] M. Nosonovsky, "Slippery when wetted," *Nature,* vol. 477, pp. 412-413, 2011.

[20] M. Nosonovsky and B. Bhushan, "Superhydrophobic Surfaces and Emerging Applications: Non-adhesion, Energy, Green Engineering," *Current Opinion in Colloid & Interface Science,* vol. 14, no. 4, pp. 270-280, 2009.

[21] G. Moriconi and F. Tittareli, "Effectiveness of surface or bulk hydrophobic treatments in cementitious materials," *Protection of Historical Buildings, PROHITECH,ÿ09,* pp. 1071-107, 2009.

[22] M. Raupach and L. Wolff, "Investigations on long-term durability of hydrophobic treatment on concrete," *Surface Coatings International Part B: Coatings Transactions,* vol. 99(2), pp. 127-133, 2005.

[23] S. Popovics, *Fundamentals of portland cement concrete, Vol. 1: Fresh Concrete, John Wiley and Sons Inc.,*

[24] E. E. Hekal and M. Abd-El-Khalek, "Mechanical and physico-chemical properties of hardened portland cement pastes containing hydrophobic admixtures part 1: Compressive strength and hydration kinetics.Ã," *Zkg International,* vol. 52(12), pp. 697-700, 1999.

[25] E. E. Hekal and M. Abd-El-Khalek, "Mechanical and physico-chemical properties of hardened portland cement pastes containing hydrophobic admixtures part2: Physical properties and micro-structure," *Zkg International,* vol. 53(3), pp. 152-158, 2000.

[26] W. Silicones, *Concrete protection for concrete advantages,* Wacker Silicones,

[27] I. De Vries and R. B. Polder, "Hydrophobic treatment of concrete," *Construction and Building Materials,* vol. 11(4), pp. 259-265, 1995.

[28] G. Xiaojian and Z. Ying, "Influence of Silane Treatment on the Freeze-Thaw Resistance of Concrete," *Advanced Materials Research,* vol. 250, pp. 565-568, 2011.

[29] V. G. Batrakov, Modified Concrete Theory and Practice, 2nd Ed revised and expanded 1998, Moscow, Russia: Stroyizdat,

[30] D. Corning, *Dow and Xiameter technical sheets and MSDSs for OFS-6124, OFS-6341, OFS-0772, OFS-6070, OFS-2306, OFS-6697, 1-6184, IE-6683,* Dow Corning https://www.xiameter.com/en/Pages/SelectorGuides.aspx.

[31] Rust-Oleum, *Rust-Oleum Neverwet™ TDS,* http://www.homedepot.com/catalog/pdfImages/9d/9d28a478-3317-4f42-8418-9e000bdbdfe6.pdf.

[32] Cabot, *Cabot® Waterproofing Crystal Clear #1000 brochure,* http://www.cabotstain.com/pdf/Cabot-Waterproofing.pdf.

[33] K. Sobolev, H. Tabatabai, J. Zhao, I. Flores-Vivian, R. Rivero, S. Muzenski, M. G. Oliva and R. Rauf, "Superhydrophobic Engineered Cementitious Composites for Highway Bridge Applications: Phase I; National Center for Freight & Infrastructure Research & Education; CFIRE 04-09; University of Wisconsin-Milwaukee, University of Wisconsin-Madison; May 2013. htt".

[34] S. Muzenski, I. Flores-Vivian and K. Sobolev, "Freeze-Thaw Resistance of Fiber Reinforced Composites with Superhydrophobic Admixtures," in *Concreep9 @ MIT*, September 24th, 2013.

[35] K. Sobolev, "Anti-Icing and De-Icing Superhydrophobic Concrete to Improve the Safety on Critical Elements of Roadway Pavements," http://www.wistrans.org/cfire/research/, Submitted 2013.

[36] P. A. M. Basheer and L. Basheer et al, "Surface treatments for concrete: Assessment methods and reported performance," *Construction and Building Materials,* Vols. 11(7-8), pp. 413-429, 1997.

[37] NCHRP, "The National Cooperative Highway Research Program (NCHRP) report 244".

[38] P. Grubl and M. Ruhl, "German Committee for Reinforced Concrete (DAfStb)-Code: Concrete with Recycled Aggregates," in *In sustainable construction: use of recycled concrete aggregate-proceedings of the international symposium held at department of trade and industry conference centre*, London, UK, November 1998..

[39] M. Ibrahim and A. S. Al-Gahtani, "Use of surface treatment materials to improve concrete durability," *Journal of Materials in Civil Engineering,* vol. 11(1), pp. 36-40, 1999.

[40] F. Tittarelli, "Influence of silane-based hydrophobic admixture on oxygen diffusion through concrete cement matrix," *Proceedings of the Sixth CANMET/ACI International Conference,* Vols. SP-195, pp. 431-445, 2000.

[41] R. Fratesi, G. Moriconi, R. Tittarelli and M. Collepardi, "The influence of hydrophobized concrete on the corrosion of rebars, superplasticizers and other chemical admixtures in concrete," *Proceedings Fifth CANMET/ACI International Conference,* pp. 105-122, 1997.

[42] K. S. M. N. V. Hejazi, "From superhydrophobicity to icephobicity: forces and interaction analysis," *Nature's Scientific Reports,* no. 3, p. 2194, 2013.

[43] R. Menini and M. Farzaneh, "Advanced Icephobic Coatings," *Journal of adhesion science and technology ,* vol. 25, no. 9, pp. 971-992, (2011.

[44] N. D. Mulherin and R. B. Haehnel, "Ice Engineering Technical Note, 03-4," 2003.

[45] M. A. Sarshar and e. al., "Effects of Contact Angle Hysteresis on Ice Adhesion and Growth over Superhydrophobic Surfaces under Dynamic Flow Conditions," *Journal of Adhesion Science and Technology 290.15 (2012).,* vol. 290, no. 15, 2012.

[46] S. Farhadi, M. Farzaneh and S. Kulinich, "Anti-icing performance of superhydrophobic surfaces," *Applied Surface Science,* vol. 257, no. 14, pp. 6264-6269, 2011.

[47] S. A. Kulinich and e. al., "Superhydrophobic surfaces: are they really ice-repellent?," *Langmuir,* vol. 27, no. 1, pp. 25-29, 2010.

[48] M. He and e. al., "Super-hydrophobic film retards frost formation," *Soft Matter,* vol. 6, no. 11, pp. 2396-2399.

[49] P. Guo and e. al., "Icephobic/Anti-Icing Properties of Micro/Nanostructured Surfaces," *Advanced Materials,* vol. 24, no. 19, pp. 2642-2648., 2012.

[50] S. A. Kulinich and M. Farzaneh, "Ice adhesion on super-hydrophobic surfaces," *Applied Surface Science,* vol. 255, no. 19, pp. 8153-8157, 2009.

[51] L. Cao and e. al., "Anti-icing superhydrophobic coatings," *Langmuir,* vol. 25, no. 21, pp. 12444-12448, 2009.

[52] C. Laforte and A. Beisswenger, "Icephobic material centrifuge adhesion test," in *Proc 11th International Workshop on Atmospheric Icing of Structures*, Montréal, 2005.

[53] M. Zou and e. al., "Effects of surface roughness and energy on ice adhesion strength," *Applied Surface Science,* vol. 257, no. 8, pp. 3786-3792, 2011.

[54] A. C. International, *Standard specification of standard sand; ASTM C778; 2013; 4.01.,* 2013.

[55] A. C. International, *Standard Practice for Mechanical Mixing of Hydraulic Cement Pastes and Mortars of Plastic Consistency ASTM C305,*

[56] A. C. International, *Standard Test Method for Compressive Strength of Hydraulic Cement Mortars (Using 2-in or 50-mm Cube Specimens); ASTM C109,*

[57] StructureN3, *Structure of N-(3-(Trimethoxysilyl)propyl)ethylenediamine adatped from http://www.inchem.org/documents/sids/sids/1760243.pdf.*

[58] StructurePMHS, *http://www.sigmaaldrich.com/catalog/product/aldrich/176206?lang=en&region=US.*

[59] M. A. Brook, Silicone in Organic, Organometallic, and Polymer Chemistry, (ISBN 0-471-19658-4) p194-204, John Wiley and Sons, 2000.

[60] F. Deyhimi and J. Munoz, "Surface resistivity of different silylated glasses," *Journal of Applied Electrochemistry,* vol. 14, no. 6, pp. 803-806, November 1984.

[61] M. L. Hair and W. Hertl, "Reaction of hexamethyldisilazane with silica," *Journal of Physical Chemistry,* vol. 75, no. 14, p. 2181–2185, 1971.

[62] M. A. Brook, Silicone in Organic, Organometallic, and Polymer Chemistry, (ISBN 0-471-19658-4) p322-323, John Wiley and Sons, 2000.

[63] StructureSILSQ, *Adapted from http://www.sigmaaldrich.com/etc/medialib/docs/Aldrich/Brochure/al_pp_poss.Par.0001.File.tmp/al_pp_poss.pdf.*

[64] StructureSILICIC1, *http://www.guidechem.com/cas-216/216689-57-5.html.*

[65] J. H. Kim and R. E. Robertson, "Structure and properties of poly(vinyl alcohol)-modified mortar and concrete," *Cement and Concrete Research,* vol. 29(3), pp. 407-415, 1999.

[66] StructurePVA, *http://www.sigmaaldrich.com/catalog/product/aldrich/363170?lang=en&region=US.*

[67] I. Flores-Vivian, *Courtesy of Dr. Ismael Flores-Vivian, University of Wisconsin - Milwaukee, Department of Civil Engineering.*

[68] Krüss, *Krüss DSA4 Software for Drop Shape Analysis User manual part 1, V1.0-02, Kruss GmbH, Hamburg 2004-2012, page 48-49.*

[69] M. A. Brook, Silicone in Organic, Organometallic, and Polymer Chemistry, (ISBN 0-471-19658-4), John Wiley and Sons, 2000 , p. 29.

[70] A. C. International, *Standard Test Method for Electrical Indication of Concretes Ability to Resist Chloride Ion Penetration. ASTM C1202,*

[71] A. C.-9. International, *Standard Test Method for Flexural Strength of Hydraulic-Cement Mortars. ASTM C348-97,*

[72] A. C. /. C. International, *Standard Test Method for Resistance of Concrete to Rapid Freezing and Thawing. ASTM C666 / C666M,*

Appendix: Images for ice loss on impact for M series tiles

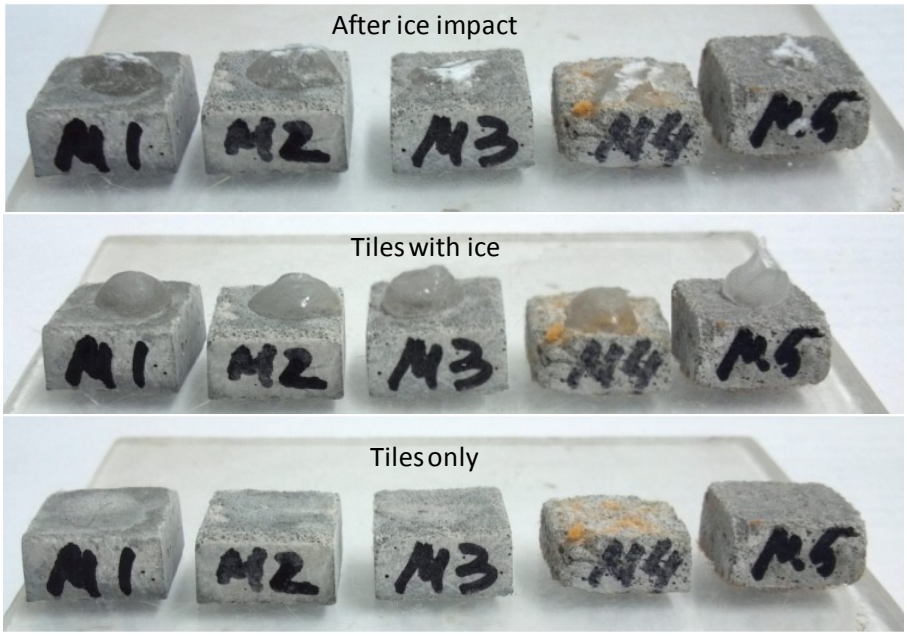

Untreated M01-M05 with fibers

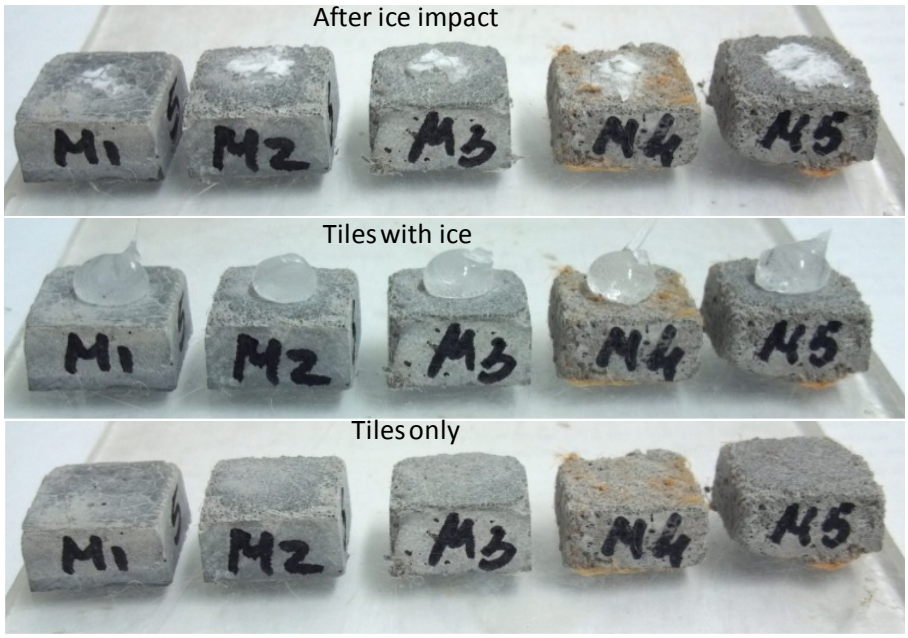

5% M01-M05 with fibers

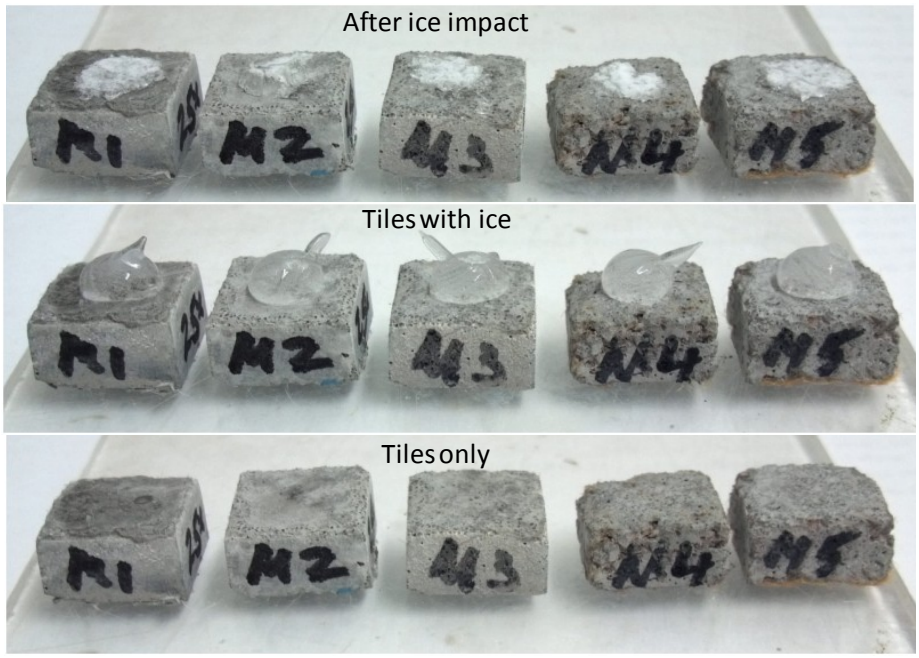

25% M01-M05 with fibers

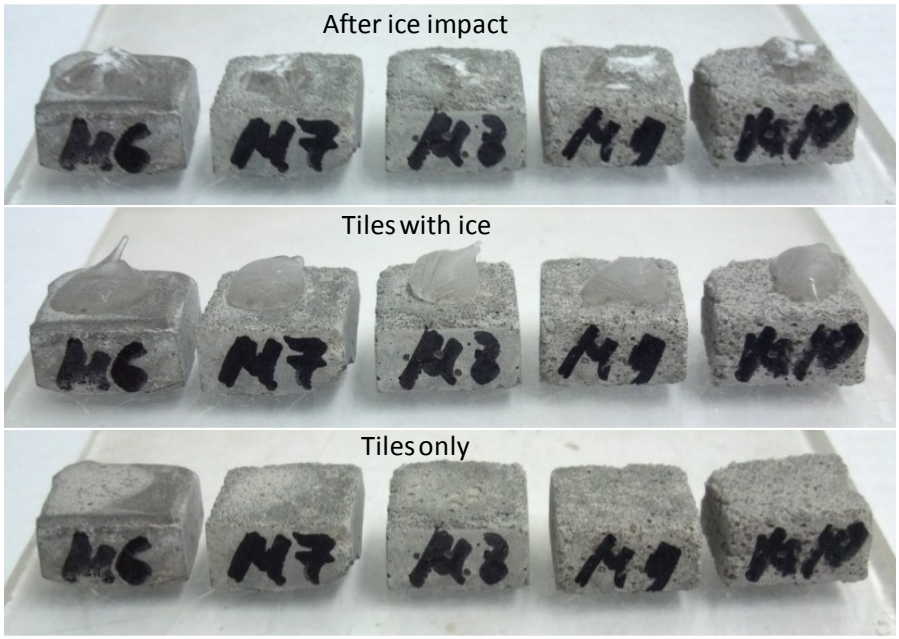

Untreated M06-M10

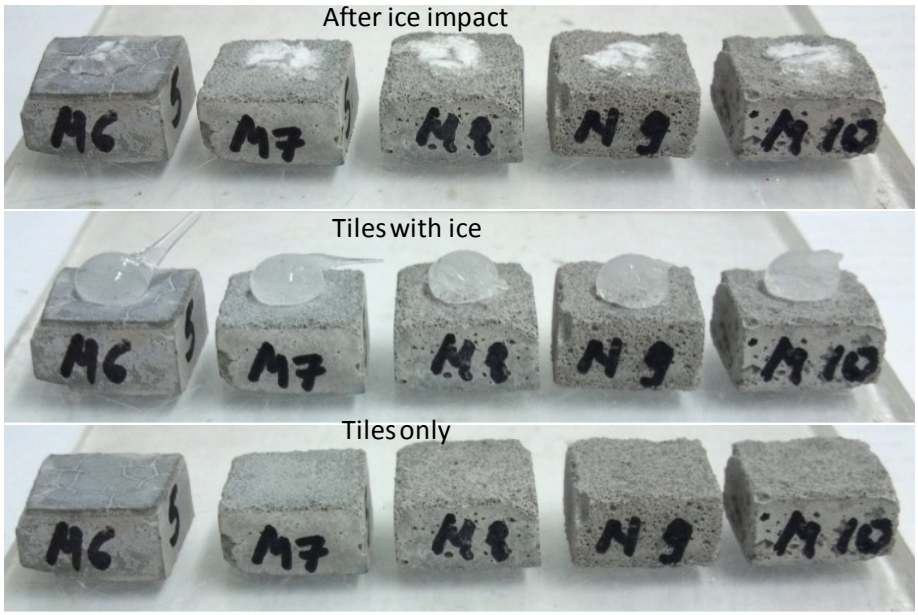

5% M06-M10

25% M06-M10